# Biomimetic Poly(ethylene glycol)-based Hydrogels as a 3D Tumor Model for Evaluation of Tumor Stromal Cell and Matrix Influences on Tissue Vascularization

by

Saniya Ali

Department of Biomedical Engineering
Duke University

Date:_____

Approved:

_____
Jennifer L. West, Supervisor

_____
Brenton D. Hoffman

_____
Bruce Klitzman

_____
William M. Reichert

_____
George A. Truskey

Dissertation submitted in partial fulfillment of
the requirements for the degree of Doctor
of Philosophy in the Department of
Biomedical Engineering in the Graduate School
of Duke University

2015

ABSTRACT

Biomimetic Poly(ethylene glycol)-based Hydrogels as a 3D Tumor Model for Evaluation of Tumor Stromal Cell and Matrix Influences on Tissue Vascularization

by

Saniya Ali

Department of Biomedical Engineering
Duke University

Date:_____

Approved:

_____
Jennifer L. West, Supervisor

_____
Brenton D. Hoffman

_____
Bruce Klitzman

_____
William M. Reichert

_____
George A. Truskey

Dissertation submitted in partial fulfillment of the requirements for the degree of Doctor of Philosophy in the Department of Biomedical Engineering in the Graduate School of Duke University

2015

# Abstract

To this day, cancer remains the leading cause of mortality worldwide[1]. A major contributor to cancer progression and metastasis is tumor angiogenesis. The formation of blood vessels around a tumor is facilitated by the complex interplay between cells in the tumor stroma and the surrounding microenvironment. Understanding this interplay and its dynamic interactions is crucial to identify promising targets for cancer therapy. Current methods in cancer research involve the use of two-dimensional (2D) monolayer cell culture. However, cell-cell and cell-ECM interactions that are important in vascularization and the three-dimensional (3D) tumor microenvironment cannot accurately be recapitulated in 2D. To obtain more biologically relevant information, it is essential to mimic the tumor microenvironment in a 3D culture system. To this end, we demonstrate the utility of poly(ethylene glycol) diacrylate (PEGDA) hydrogels modified for cell-mediated degradability and cell-adhesion to explore, in 3D, the effect of various tumor microenvironmental features such as cell-cell and cell-ECM interactions, and dimensionality on tumor vascularization and cancer cell phenotype.

In aim 1, PEG hydrogels were utilized to evaluate the effect of cells in the tumor stroma, specifically cancer associated fibroblasts (CAFs), on endothelial cells (ECs) and tumor vascularization. CAFs comprise a majority of the cells in the tumor stroma and secrete factors that may influence other cells in the vicinity such as ECs to promote the organization and formation of blood vessels. To investigate this theory, CAFs were

isolated from tumors and co-cultured with HUVECs in PEG hydrogels. CAFs co-cultured with ECs organized into vessel-like structures as early as 7 days and were different in vessel morphology and density from co-cultures with normal lung fibroblasts. In contrast to normal lung fibroblasts (LF), CAFs and ECs organized into vessel-like networks that were structurally similar to vessels found in tumors. This work provides insight on the complex crosstalk between cells in the tumor stroma and their effect on tumor angiogenesis. Controlling this complex crosstalk can provide means for developing new therapies to treat cancer.

In aim 2, degradable PEG hydrogels were utilized to explore how extracellular matrix derived peptides modulate vessel formation and angiogenesis. Specifically, integrin-binding motifs derived from laminin such as IKVAV, a peptide derived from the $\alpha$-chain of laminin and YIGSR, a peptide found in a cysteine-rich site of the laminin $\beta$ chain, were examined along with RGDS. These peptides were conjugated to heterobifunctional PEG chains and covalently incorporated in hydrogels. The EC tubule formation *in vitro* and angiogenesis *in vivo* in response to the laminin-derived motifs were evaluated.

Based on these previous aims, in aim 3, PEG hydrogels were optimized to function as a 3D lung adenocarcinoma *in vitro* model with metastasis-prone lung tumor derived CAFs, HUVECs, and human lung adenocarcinoma derived A549 tumor cells. Similar to the complex tumor microenvironment consisting of interacting malignant and

non-malignant cells, the PEG-based 3D lung adenocarcinoma model consists of both tumor and stromal cells that interact together to support vessel formation and tumor cell proliferation thereby more closely mimicking the functional properties of the tumor microenvironment. The utility of the PEG-based 3D lung adenocarcinoma model as a cancer drug screening platform is demonstrated with investigating the effects of doxorubicin, semaxanib, and cilengitide on cell apoptosis and proliferation. The results from drug screening studies using the PEG-based 3D *in vitro* lung adenocarcinoma model correlate with results reported from drug screening studies conducted *in vivo*. Thus, the PEG-based 3D *in vitro* lung adenocarcinoma model may serve as a better tool for identifying promising drug candidates than the conventional 2D monolayer culture method.

## Dedication

Bismillah hir-Rahman nir-Rahim. I would like to dedicate this thesis to my dad and mom, Dr. Amir Ali and Mrs. Shireen Ali, who have always inspired me to think outside of the box, innovate, and strive for excellence. Thank you for instilling in me good values of honesty, faith, and hard work. This would not have been possible without your support and prayers.

# Contents

# List of Figures

## Acknowledgements

My sincerest gratitude to Dr. Jennifer West for her continued guidance and mentorship. Thank you for providing opportunities to succeed and grow during my training as a scientist. It has been an honor to work with you.

Thank you to my committee members, Dr. Brenton D. Hoffman, Dr. Bruce Klitzman, Dr. William M. Reichert, and Dr. George A. Truskey for your helpful advice and guidance on my research.

Thank you to Dr. Jonathan Kurie and Dr. Jonathon Roybal from MD Anderson Cancer Center, and Dr. Mary Dickinson from Baylor College of Medicine for supporting research collaborations and providing valuable assistance.

Thank you Aakash Keswani, one of the hardest working undergraduates I have had the privilege to mentor.

Thank you to my lab colleagues who have provided invaluable time, advice, and encouragement towards my goals. Special appreciation and thanks goes to Drs. Hanin Bearat, Anita Shukla, Lynda Thomas, Jennifer Saik, Andrew Coughlin, and Melissa McHale. Special thanks to also Yan Wu and Kasie Collins for their unconditional care and friendship throughout the years.

Immense thank you to my family, especially to Shahil Rais, for showering me with so much love and for keeping me happy and positive throughout the years. I love you and thank you.

This research was supported by grants from National Institute of Health, including Center for Biomolecular and Tissue Engineering Training Grant.

# 1. Introduction and Background

Despite research advances, cancer remains the second most common cause of death, accounting for over 500,000 deaths per year in the United States[2]. Cancer arising in the lung is the second most prevalent type of cancer in both men and women[2]. With over 200,000 new cases diagnosed each year and 100,000 deaths annually in the U.S., lung cancer accounts for more deaths in men and women than any other cancer[2]. Lung cancer is most often diagnosed when the disease has progressed to stage III or IV when patients present symptoms. Once lung cancer has metastasized, the survival rate reduces significantly due to the limited treatment options that are effective[2]. Improving cancer therapies and patient outcomes requires useful research tools and models that represent the pathological environment observed in lung carcinoma. Additionally, we need more detailed knowledge of the tumor microenvironment and how its different components (i.e. different cells, extracellular matrix, etc.) regulate interactions leading to tumor invasion and metastasis.

## *1.1 Tumor microenvironment and its role in promoting tumor growth*

The tumor microenvironment is a complex connective tissue framework consisting of cellular components (i.e. fibroblasts, vascular cells, immune cells, etc.), extracellular matrix (including basement membranes), and soluble factors (cytokines, chemokines, growth factors, etc.)[3–5]. Interactions between tumor cells and the stroma can promote the transformation to and proliferation of malignant cells[3–5].

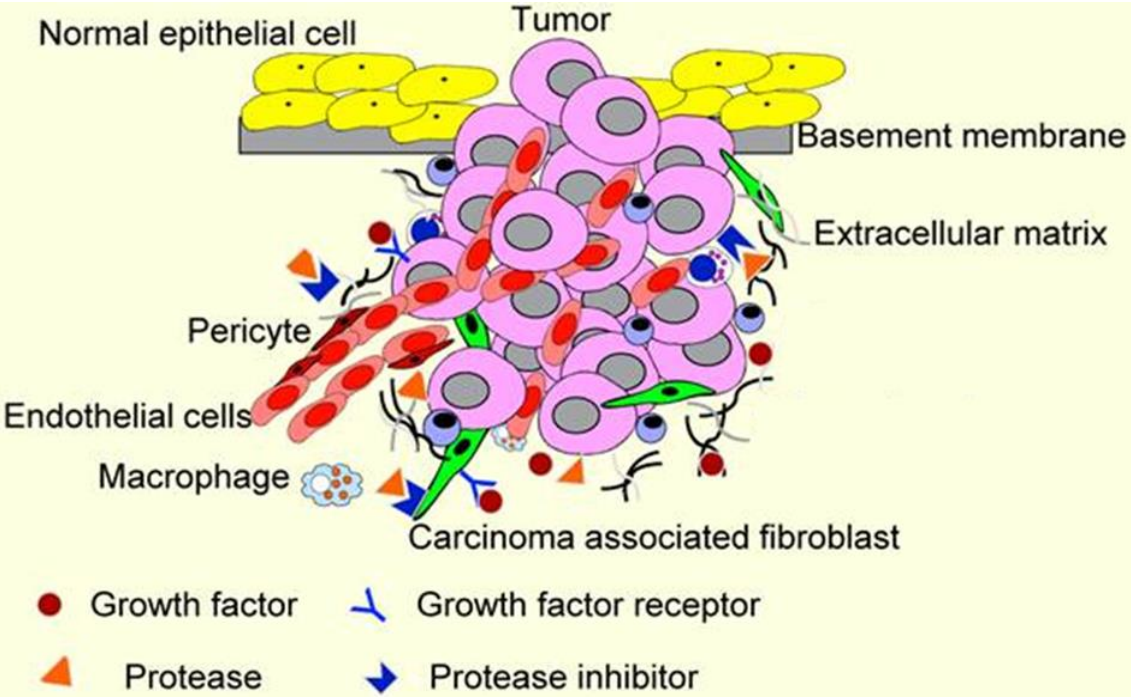


**Figure 1: Schematic of the biologic components within the tumor microenvironment. Adapted from Koontongkaew *et al*[6].**

### 1.1.1 Stromal cells

The tumor stroma consists of a variety of non-tumor cells such as cancer-associated fibroblasts (CAFs), immune cells, and cells that make up the vasculature such as endothelial cells and pericytes[5,7]. Crosstalk through direct cell-cell contacts or by secreted molecules between tumor cells and cells in the stromal compartment can lead to alterations in the stroma structure and by this means establish a more permissive and supportive environment for cancer cell invasion[8,9]. For example, stromal cells such as

CAFs and endothelial cells secrete serine proteases and matrix metalloproteinases (MMPs) which facilitate extracellular matrix (ECM) degradation enabling cancer cells to migrate and invade through the tissue matrix[10,11]. Previous studies have shown that activated stromal cells can also promote the switching of cancer cells from a pre-malignant to a malignant and invasive tumor phenotype via secretion of soluble factors such as transforming growth factor-beta (TGF-β) and epidermal growth factor (EGF) within the microenvironment[6,12–14].

Additionally, soluble factors, including fibroblast growth factor (FGF)[15], insulin growth factor-1 and -2 (IGF-1 and -2)[16], , and hepatocyte growth factor (HGF)[17,18], platelet-derived growth factor (PDGF)[19,20], can bind to receptors on cancer cells causing cell proliferation, inflammation, migration, and other tumor-promoting effects. In addition to stromal cells and their products, the evolving network of interactions between cancer cells and the ECM influence tumor transformation and progression as well[21,22].

### 1.1.2 Extracellular matrix

The ECM consists of epithelial cells and stromal cells found within the tissue matrix[23]. The ECM provides structural support for cells and facilitates cell attachment and migration[23,24]. Additionally, the ECM is also involved in controlling the diffusion of nutrients and waste, mediating cell signaling factors, and regulating a wide variety of cellular processes which include growth, proliferation, differentiation, and apoptosis[21].

These processes are regulated in part by the protein and polysaccharide composition of the ECM and the structural organization of these components.

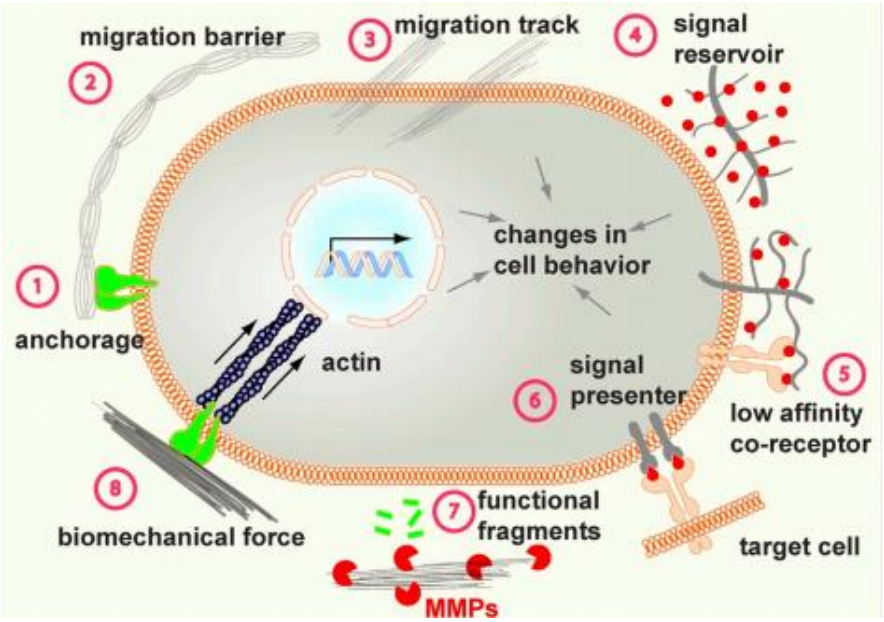


**Figure 2: Functions of the ECM include providing anchorage to the basement membrane, controlling cell migration, facilitating the binding and diffusion of growth factors, and regulating cell-cell communication. From Lu *et al*[21].**

The ECM is composed of glycosaminoglycans, proteoglycans, and fibrous proteins like collagen and elastin[22,24,25]. Collagen is the primary protein present in the ECM in most tissues. Collagen is present in different isoforms with specialized functions[22]. Cells interact with collagen molecules primarily through integrins to mediate cellular attachment[22]. Collagen molecules provide structural support to tissues and binding sites for other ECM proteins to organize the ECM network[21]. Elastin is

another structural protein in the ECM which, along with fibrillin, is responsible for tissue flexibility[21]. The ECM meshwork can affect the mechanical properties of the tissue. The tissue mechanical properties can impact a variety of cell behaviors such as cell migration for example[21].

ECM proteins and structures can govern various biological functions. One way is by presenting growth factor signals. Polysaccharides like heparin sulfate proteoglycans in the ECM can bind to numerous growth factors including angiogenic proteins like vascular endothelial growth factor (VEGF) that direct cell proliferation and migration[26,27]. Growth factors in the ECM can in turn stimulate cells to secrete ECM-digesting enzymes[28,29]. The production of proteases such as MMPs by cells can lead to ECM remodeling. MMPs can act on collagen and laminin components of the ECM[29]. The cleavage of collagen and laminin proteins by MMPs during tissue remodeling can expose cryptic cell-binding sites that promote cellular invasion and migration[30].

ECM proteins like laminin have growth-factor binding domains that control cell signaling effects with or without proteolysis. Finally, integrins and other adhesion-related receptors bind to ECM proteins like collagen, laminin, fibronectin and subsequently act as signal transduction receptors to initiate signaling pathways such as the FAK/Src and the MEK1/ERK2 pathways and thereby effect intracellular processes[31,32]. The focal adhesion kinase (FAK) pathway is activated by most integrins through interactions with cytoskeletal proteins talin and paxillin. Upon activation, FAK autophosphorylates Tyr397 which then creates a binding site for Src kinase. Src kinase in

turn phosphorylates a number of focal adhesion components that may activate other cascades such as the mitogen-activated protein kinase 1(MEK1) pathway. Activation of these protein tyrosine kinase (PTK) pathways can lead to transcription of genes regulating cell migration, differentiation, survival, and other functions. In fact, FAK–Src signaling promotes tumor angiogenesis[31]. Src phosphorylation of FAK leads to the activation of the MAPK/Erk pathway in which enhanced Erk2 phosphorylation can lead to increase VEGF gene transcription (Figure 3)[31]. Enhanced VEGF gene transcription stimulates angiogenesis and thus supports tumor growth.

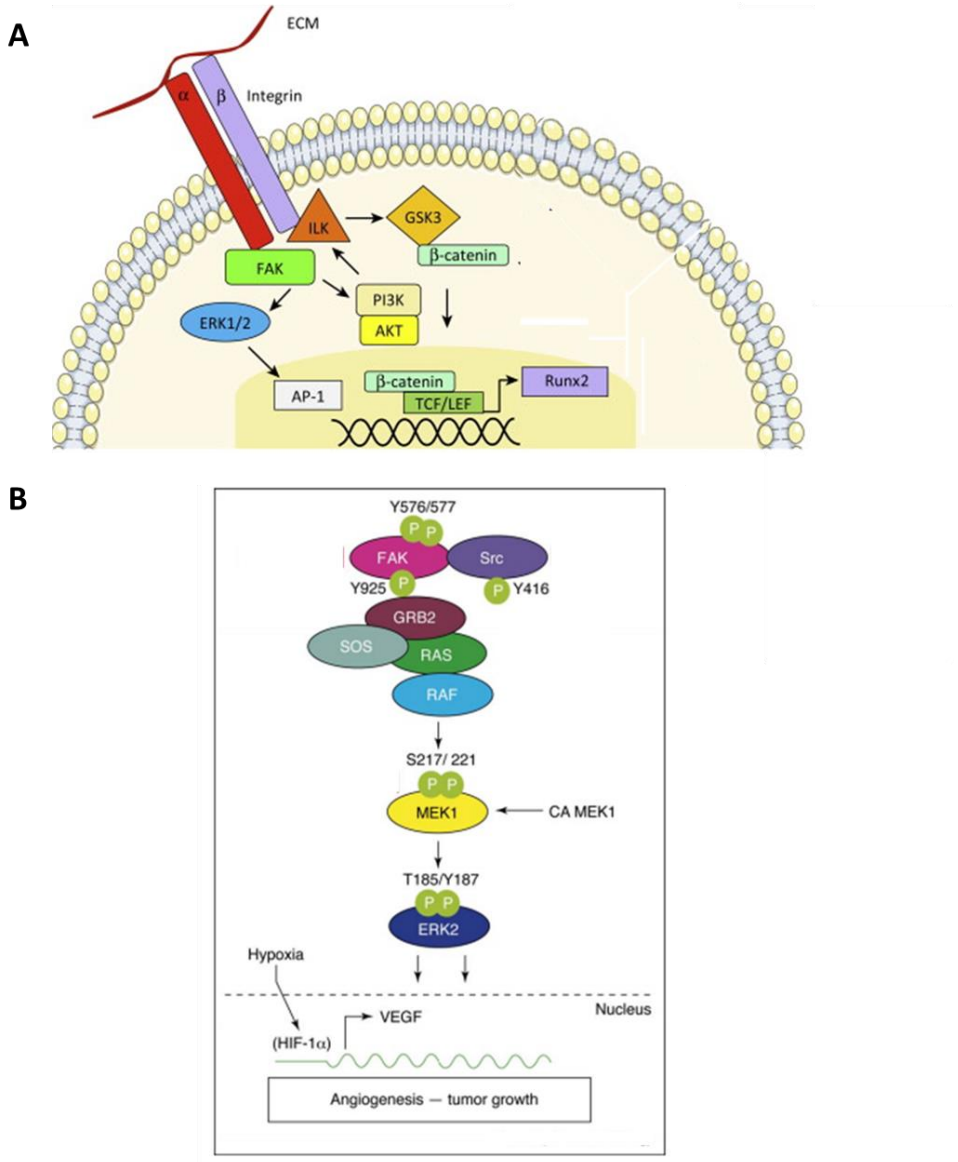


**Figure 3: Src phosphorylation of FAK promotes angiogenesis. A) Ligand-integrin binding prompts phosphorylation of FAK and activation of MEK/ERK2 pathway, leading to the activation of transcription factors that regulate cellular processes. Adapted from Marie *et al*[33]. B) FAK signaling can enhance mitogen-activated protein kinase (MEK1) phosphorylation leading to enhanced ERK2 phosphorylation. ERK2 nuclear translocation can enhance VEGF gene transcription and thereby stimulate angiogenesis. Adapted from Mitra *et al*[31].**

When assembled together, these ECM components, with their structural and functional diversity, impart unique mechanical and biochemical properties that are essential for regulating normal cell behavior and maintaining tissue homeostasis. Disorganization of ECM contributes to tumor growth and so therefore it is important to understand the changes in ECM composition and organization that occur during cancer initiation, progression, and metastasis.

## *1.2 ECM in cancer initiation, progression, and metastasis*

Given that ECM properties govern a wide variety of cellular functions and that cells are able to remodel the matrix that in turn influences cellular processes and ECM function, it is apparent that ECM-cell interactions are vital for tissue development and function. In disease processes such as cancer, ECM dynamics may become abnormal.

Abnormal ECM dynamics are well documented in clinical studies of cancer. For example, excess ECM production causes pathological tissues to be typically stiffer than normal tissue[34–36]. This increase in stiffness can be attributed to increased deposition of ECM components such as collagen I, II, III, V, and IX, and the up-regulation of lysyl oxidase (LOX) which covalently crosslinks collagens and elastins[34–36]. In fact overexpression of LOX has been observed in many cancers and is considered a poor prognostic marker[34].

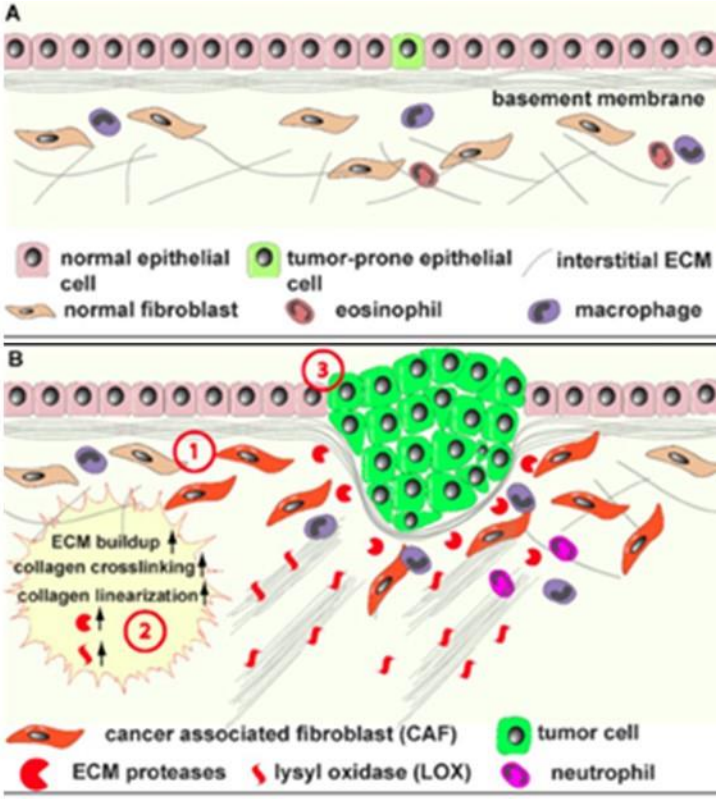


**Figure 4: Normal ECM dynamics versus ECM in cancer. (A) Normal ECM dynamics are controlled to ensure a healthy microenvironment. (B) In cancer, activated fibroblasts or CAFs initiate changes to the ECM and increase expression of ECM remodeling enzymes. Tumor stromal and cancer cells create a local metastatic niche that promotes survival, rapid growth, and expansion of the malignant cells. Adapted from Lu *et al*[21].**

Alterations to the ECM can facilitate tumor invasion and the formation of a metastatic microenvironment[37]. Cancer cell metastasis is a multistep process consisting of local invasion, survival in the circulation, and extravasation and colonization at distant sites[38]. These processes are supported by components of the ECM. For example secreted membrane type-matrix metalloproteinases (MT-MMPs) localize in tumor regions by binding to integrins or through interactions with heparin sulfate

proteoglycans or collagen type IV[21,39,40]. This localization of MT-MMPs promotes matrix degradation to enhance tumor growth, cancer cell migration and invasion, and angiogenesis[39]. MMPs enhance these effects not only by cleaving structural components of the ECM but also by the release of growth-factor binding proteins, cell-adhesion molecules, and tyrosine kinase receptors[40]. MMP and other protease activity (cathepsins, elastases, etc.) are increased in most tumors and more so in more invasive tumors[41,42].

Abnormal ECM can not only affect cancer cells but also contribute to changes in stromal cell behavior, leading to tumor-promoting angiogenesis by endothelial cells[43]. ECM fragments such as endostatin, tumstatin, arresten, and hexastatin, which are protein fragments cleaved from collagens type IV and XVIII by proteases like MMPs, cathepsin-L, and elastase, have potent inhibitory or stimulatory effects on endothelial cells during vessel formation[44]. Stromal cells such as CAFs constitute a major portion of the reactive tumor stroma and are actively involved in both degradation and synthesis of ECM[18]. As such, it is necessary to take a closer look on the role of CAFs in cancer progression and metastasis.

## *1.3 Cancer-associated fibroblasts*

Cancer-associated fibroblasts (CAFs) are distinctly different from their normal counterparts. Unlike normal fibroblasts, CAFs either reside within the tumor margins or infiltrate the tumor mass, and are believed to facilitate cancer transformation and progression[45]. One mechanism by which CAFs may contribute to tumor growth and

migration through secretion of growth factors[18,46]. CAFs secrete a range of growth factors which enhance oncogenic potential [18]. For example, CAFs secret insulin-like growth factor 1 (IGF1) and hepatocyte growth factor (HGF) which promote tumor cell survival and migration[18,47]. Other growth factors secreted by CAFs such as VEGF and FGF2 signal vascular cells and can stimulate angiogenesis[13,18].

In addition to secreting growth factors, CAFs are also involved in remodeling the ECM to generate a microenvironment more conducive to tumor growth[48–50]. For example, CAFs synthesize many of the constituents of the ECM such as collagens I, III, and V, as well as fibronectin[7,18]. Moreover, CAFs secrete increased levels of ECM-degrading proteases such as MMP 2 and MMP 9, which aid in tumor cell invasion[40,42,51].

Several studies allude to the contribution of CAFs in supporting tumor growth and facilitating metastatic dissemination. Cunha and colleagues compared the effect of CAFs isolated from primary prostate tumors with normal fibroblasts cultured in combination with BPH-1 prostatic epithelial cells. The study showed that when prostatic epithelial cells were subcutaneously transplanted in combination with CAFs, massive tumors of greater than 1,300 mg in weight developed *in vivo* after 3 months, whereas tumor growth was meager (less than 10 mg in weight) in the presence of normal fibroblasts and BPH-1 cells. This indicates that CAFs create a niche that promotes cancer cell proliferation and tumor growth. Similarly, metastatic Ras-transformed human MCF-7 breast cancer cells were co-injected subcutaneously in suspension with CAFs or normal fibroblasts in mice[13]. The mice that were injected subcutaneously with CAFs in

combination with MCF-7 breast cancer cells developed tumors that were 2-fold larger in tumor volume (~600 $mm^3$ after 50 d) than tumors that developed in the presence of normal fibroblasts with MCF-7 breast cancer cells (~325 $mm^3$ in tumor volume). The enhanced growth in tumor size was attributed to increased cancer cell proliferation and tumor vascularization[13].

## *1.4 Tumor angiogenesis and vascularization*

Tumors face the increasing demand for nutrients and oxygen as they increase in size. This demand drives rapid angiogenesis, the process whereby new blood vessels sprout from the existing vasculature[13]. Moreover, tumor vasculature is the main route through which cancer cells migrate through the basement membrane and metastasize[52].

### 1.4.1 The Structure and formation of the microvasculature

Capillaries are tubes composed of a monolayer of endothelial cells with an underlying specializing ECM structure, the basement membrane, and then supporting mural cells referred to as pericytes. Endothelial cells adhere together through cell-cell junctions to form a selectively permeable barrier. Pericytes or mural cells which are contractile surround the endothelial cells and the binding components of the intervening basement membrane (Figure 5). Additionally, pericyte cytoplasmic fingers are inserted into the introversions within the endothelium to form peg-and-socket type contacts[53,54]. These junctions are important for regulating vessel contractility and tone, permeability to metabolites, and stabilization for maturation [53].

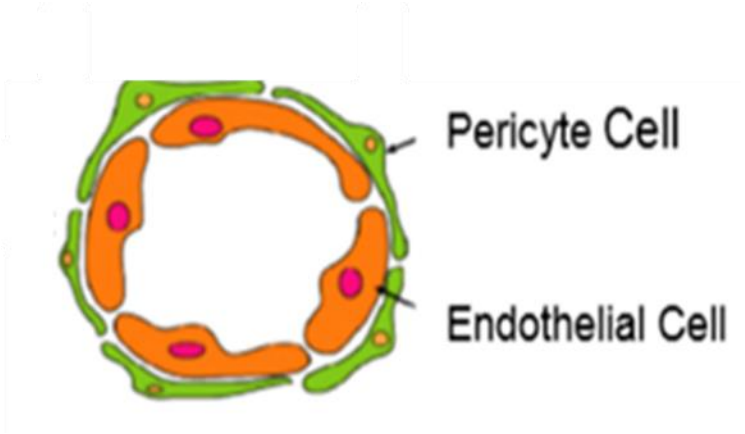


**Figure 5: New blood vessels form with endothelial cells organizing into lumens and tubules. The resulting immature capillaries are stabilized by pericytes. From Moon *et al*[55].**

## 1.4.2 The process of angiogenesis

Angiogenesis is an important factor in the progression of cancer and a well-controlled process. The process of angiogenesis is triggered by exacerbated oxygen deprivation during rapid tumor growth. In response to hypoxia, hypoxia inducible factor 1 alpha (HIF1$\alpha$) is overexpressed which turns on expression of VEGF by cells within the tumor microenvironment leading to a VEGF gradient as shown in Figure 6. Endothelial cells respond to the VEGF gradient by becoming activated. In order to migrate, endothelial cells release MMPs, specifically MMP-2 and MMP-9[55]. MMPs degrade and loosen the matrix. Release of MMPs and the subsequent matrix degradation allows tumor cells to migrate and invade. In response to the released proteins, activated endothelial cells or tip cells extend filapodia and migrate in the interstitial space[56,57]. A cord of endothelial cells known as, stalk cells, follow tip cells.

These cells proliferate and form connections to neighboring vessels. Subsequently, vacuoles form and merge to form tubules with hollow lumen. The formation of lumen and the start of blood flow help to reinforce vessel connections and junctions[56,57]. Following after, pericytes migrate to the newly formed vessel structures and position themselves at the budding front of the endothelial sprouts. Pericytes closely associate with endothelial cells and thereby stabilize the newly formed vessels[56].

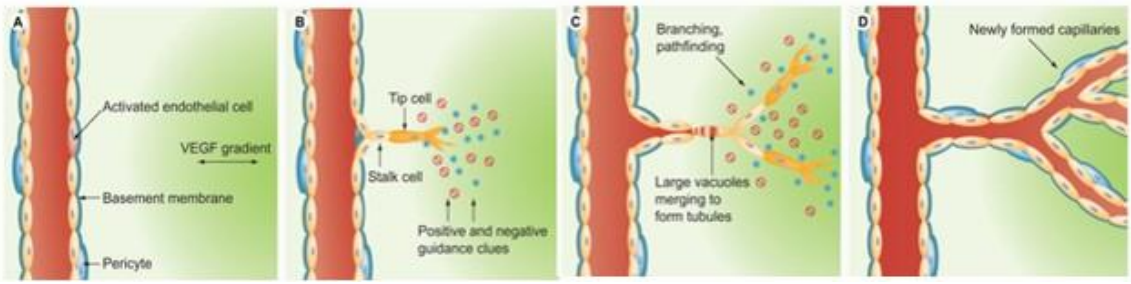


**Figure 6: Angiogenic Process. (A) Endothelial cells activate in response to VEGF gradient. (B) Tip cells migrate and secret proteinases to degrade the matrix. (C) Stalk cells proliferate, form large vacuoles, and merge to make tubules. (D) Pericytes migrate to the area of sprouting and deposit basement membrane to stabilize the newly formed vessels[57].**

Gap junctions provide direct connections between the cytoplasm of pericytes and endothelial cells and enable the exchange of molecules. Pericytes are functionally significant in regulating capillary blood flow and maintenance of vessel formation and maturation. Loss of pericyte coverage on vessels results in hyper-dilated and leaky vasculature[58]. Reports suggest that tumor vasculature is irregularly covered by pericytes which may contribute to vessels in the tumor being immature and leaky[59,60]. The amount of pericyte coverage is lower in breast[60,61] and lung carcinoma[59,62] than in corresponding normal tissues. The low degree of pericyte invasion and association with endothelial

cells observed with breast and lung carcinomas raises the possibility of the involvement of alternative mural cells in the tumor stroma replacing critical functions of pericytes[61]. In the last step of angiogenesis, new ECM is deposited to form basement membrane to surround blood vessels. The basement membrane of the tumor vasculature is more porous and leaky than normal which further facilitates tumor cell metastasis[61].

## *1.5 Engineering approaches to modeling the tumor microenvironment*

To obtain a more complete understanding of the biochemical and stromal cellular factors that promote tumor angiogenesis, *in vitro* culture platforms that model the tumor microenvironment can be utilized. There are several important design principles and functions to consider in engineering a tumor mimicking culture system. Ideally these platforms would mimic the physical properties of the natural ECM found in tissues and provide adequate physical support for both tumor and vessel growth. The scaffold should also allow the diffusion of nutrients and growth factors and provide a means of incorporating cells within the structure. Additionally, the scaffold should also be degradable and permit cell migration. To engineer systems that meet these requirements, both 2D and 3D culture substrates made from natural or synthetic materials have been utilized which will be reviewed in the following sections.

### 1.5.1 Differences in 2D versus 3D for modeling the tumor microenvironment

The majority of cancer studies have been conducted with 2D monolayer cultures, where cells are usually grown on a flat polystyrene (PS) or glass surface with or without cell-adhesive protein coatings[63]. Although 2D monolayer culture models have provided extensive fundamental knowledge on cancer cell biology, recent studies conducted in 3D culture platforms have emphasized some of the shortcomings of 2D culture models. Differences in cell morphology[64,65], proliferation[66], and drug metabolism[67] have been noted between cells grown as 2D monolayers and in 3D culture environments in which cells in 3D display behaviors more closely to what is observed *in vivo*. Weaver and colleagues showed that both malignant and non-malignant HMT-3522 breast cells appeared similar in morphology under 2D culture conditions. However, cells behaved very differently when cultured in 3D[65]. Non-malignant HMT-3522 breast cells grown in 3D using Matrigel™ (MG) organized into polarized, acini structures that are analogous in morphology to those found in healthy breast tissue *in vivo*. In contrast to non-malignant cells, the malignant HMT-3522 breast type cells formed disorganized, abnormal masses that resembled tumor cell aggregates *in vivo*. Treatment of these malignant cell aggregates with a β1 integrin function inhibiting antibody in 3D culture caused the cells to lose their abnormal structure and revert to a normal phenotype and morphology analogous to non-malignant cells[65]. When non-malignant breast cells were treated with the same inhibiting antibody in 3D, the cells underwent apoptosis. This sort

of differential response between malignant and non-malignant cells was not observed under 2D culture conditions. Both cell types grown in 2D underwent apoptosis upon treatment with β1 integrin function inhibiting antibody. This study emphasizes that the extracellular cues in a 3D microenvironment differ from 2D and how cells respond to these cues can trigger different cellular functions and interactions.

In addition to cell morphology, profound differences in the proliferative properties of cells cultured in 2D as opposed to a 3D microenvironment have also been reported. For example, Jeanes and colleagues showed that primary mammary epithelial cells (MECs) cultured on 2D surface have a poor growth response showing a burst of proliferation initially after which proliferation halts with cells either undergoing apoptosis or becoming senescent after only 2 or 3 days in culture[66]. In comparison to 2D culture conditions, MECs cultured in a 3D basement membrane matrix derived from Engelbreth-Holm-Swarm mouse sarcoma formed spherical acini and proliferated steadily over a period of 8 to 10 days[66]. This steady proliferation of MECs in 3D mimics more closely to the steady growth of mammary cells in the body.

Apart from differences in the cell morphology and proliferation, cells grown in 3D culture have exhibited differences in resistance to cancer therapeutic agents when compared to 2D controls. Tung and colleagues showed that A431 human epithelial carcinoma cells grown as 3D cell aggregates in comparison to cells cultured in 2D responded differently when treated with the same concentration of a common chemotherapeutic called 5-fluorouracil (5- FU)[67]. Following a 96-hour treatment with 10

mM of 5-FU, cells in 2D were reduced to less than 5% viability whereas cells treated with the same concentration in 3D persisted at ~75% viability. Results indicate that the 3D A431 cancer cell spheroids were more resistant to the apoptotic effects of 5-FU[67]. According to the authors, one means by which cell spheroids in 3D display higher resistance to drugs as compared to cells in 2D could be explained by the diffusive blockade of drugs caused by the multiple layers of cells in a tumor spheroid structure. Tumor spheroids consist of multi-layers of interacting cells whereas cells in 2D culture conditions form a monolayer of cells spread out on a surface. The distance that anti-cancer drugs need to diffuse through a 2D monolayer is much shorter than cells in 3D. In 2D, the drug only needs to diffuse through the cell membrane to have an effect whereas in 3D a drug needs to diffuse across multi-layers of cells before reaching cells in the inner core of the spheroid. Additionally, scaffolds for culturing cells in 3D can also serve as a barrier for drug diffusion, especially in the case of hydrophobic drugs such as paclitaxel that can potentially adsorb to the scaffold material. The diffusion across multi-layers of cells or across the thickness of a 3D scaffold more closely mimics the situation in the body in which a cancer therapeutic needs to diffuse through multiple layers of cells or tissues to reach target tumor cells. Results of studies discussed above indicate that cells grown in 3D are more analogous to their existence *in vivo* and as such may be exploited as valid testing platforms for anti-cancer drug candidates.

Furthermore, by utilizing tissue engineering techniques, 3D cell culture platforms can potentially be engineered to simulate an environment that better mirrors

tumors in the body by regulation of matrix composition, density, stiffness and selective incorporation of adhesion molecules and signaling factors. As a well-defined environment, 3D culture platforms can allow more control over experimental manipulations to test different hypotheses. By recapitulating the properties of the tumor microenvironment, 3D *in vitro* culture systems can provide more biologically relevant information, allow for better evaluation of anti-cancer drug candidates, and overall provide a better understanding of the molecular mechanisms underlying tumor progression and drug metabolism. To engineer microenvironments for supporting tumor growth, both natural and synthetic materials have been employed which will be reviewed in the following section.

### 1.5.2 Natural biomaterials for tumor microenvironment engineering

Natural materials such as MG, collagen, hyaluronate, and fibrin are most commonly used since they are the components or similar to the components of ECM[68]. Overall, these natural ECM-based matrices can provide abundant integrin binding sites and growth factors that naturally support and promote cell adhesion and interactions. Furthermore, natural materials like MG and collagen can be degraded by cells to permit migration and cell infiltration into the surrounding environment. Finally, mechanical properties of collagen and MG can be easily manipulated or tailored to specific matrix elasticities with the addition of chemical cross-linkers or collagen.

MG has been widely used in cancer studies as a 3D culture system to support cell adhesion and migration. MG is reconstituted basement membrane extracted from Englebreth-Holm-Swarm (EHS) mouse tumor cells and contains a high amount of laminin in addition to other matrix protein and growth factors[69]. Bissell and colleagues have utilized MG to recapitulate *in vivo* characteristics of breast cancer through 3D culture of human breast cancer cells[70]. MG has also been widely used to study angiogenesis. For example, using MG Mukai and colleagues showed the formation of vessel-like structures by umbilical cord blood EPCs and by human umbilical vein endothelial cells (HUVECs)[71]. The abundance of growth factors and ECM protein inherent in MG signals endothelial cells to migrate and organize into capillary-like networks. Haralabopoulos *et al.* tested the effect of thrombin on endothelial cell tubule formation *in vitro* and angiogenesis *in vivo* using MG[72]. In *in vitro* studies using MG, thrombin was shown to induce differentiation of endothelial cells into capillary structures with this effect dependent on the dose of thrombin. Studies *in vitro* showed that thrombin at a concentration of 0.3 IU/mL increased the formation of capillary-like structures in MG by 70%. Studies *in vivo* showed a 10-fold increase in endothelial cell infiltration in response to thrombin in MG injected subcutaneously[72]. MG has also been used in studies evaluating angiogenic inhibitors as potential cancer therapies. For example, Khoo and colleagues tested angiogenic inhibitors, SU6668 and suramin, with endothelial colony-forming cells (ECFCs) in MG to evaluate the effect of drugs in reducing tubule formation[73]. Although the use of MG has resulted in important findings,

there are certain drawbacks that need to be considered. MG allows little experimental control over matrix bioactivity and makes comparing studies difficult due to its batch to batch variability and unknown amounts and identities of growth factors.

Collagen is one of the most abundant proteins found in the ECM of most tissues and is the most widely used tissue-derived natural material. Similar to MG, The natural proteolytic degradation of collagen allows cells to easily infiltrate the material thereby promoting interaction with neighboring cells. Also, collagen abundantly presents the short amino acid sequence, RGD (Arg-Gly-Asp)[74], which binds to receptors on cell surfaces and facilitates cells to adhere to the matrix. Endothelial cells have been shown to organize into branching tubules with lumens that resemble capillary networks found *in vivo* when cultured in a 3D collagen matrices[75]. The mechanical properties of collagen-based gels can be altered with the addition of collagen during formation for studies examining cellular response to matrix stiffness[76]. Reinhart-King and colleagues investigated the use of collagen I substrates for evaluating matrix stiffness on endothelial cell tubule network formation where compliant substrates (E=200 Pa) were able to support endothelial cell migration and organization into vessel-like networks as compared to stiff substrates (E=10,000 Pa)[76]. The use of collagen hydrogels has also been demonstrated in cancer research. Rylander and colleagues demonstrated the use of collagen type I hydrogels to study tumor biology. They showed that MDA-MB-231 breast cancer cells cultured in collagen formed 3D cancer spheroids with a necrotic core similar to what is usually observed *in vivo*[77]. Though collagen meets certain scaffold

design criteria and provides a more defined environment that MG, there are some limitations to using collagen for engineering the tumor microenvironment. One of the methods by which the mechanical properties of collagen are altered is by changing the concentration of collagen in the matrix. Changing the concentration of collagen to alter mechanical properties in turn alters the concentration of sites bound by integrin adhesion receptors, the proteolytic degradation rate, and porosity. Controlling matrix stiffness without changing the matrix density is difficult with collagen-based constructs. Additionally, collagen has a limited range of mechanical properties (E = 0.1 - 10 kPa) and is potentially immunogenic[78–80]. Similar to MG, collagen matrices permit limited experimental control over bioactivity with variable bioactivity from material batch-to-batch resulting in inconsistencies in cellular response.

Like collagen, hyaluronate is also degraded by enzymes, specifically, hyaluornidase which is produce by many types of cells. Hyaluronate is a glycosaminoglycan component in the natural ECM and has been shown to promote cell communication and organization of vessel-like structures[81]. Ratliff *et al.* encapsulated endothelial progenitor cells in hyaluronate hydrogels and demonstrated the formation of vessel networks[82]. Gurski and colleagues have synthesized hyaluronic acid-based 3D matrices to generate a tumor model for anti-cancer drug screening with prostate tumor cells[83]. Their studies showed that prostate tumor cells residing in the hyaluronic acid-based 3D matrix formed distinct cell clusters which grew, resembling tumors *in vivo* and

underwent apoptosis to a higher degree than cells in 2D in response to anti-cancer drug treatment[83].

The use of fibrinogen, a plasma glycoprotein, that is enzymatically converted to fibrin gel via interaction with thrombin[68,81], to form cell culture substrates has also been thoroughly investigated. A study conducted by Liu *et al.* demonstrated the use of fibrin hydrogels to investigate effects of hydrogel stiffness on cancer cell behavior[84]. They encapsulated murine B16-F1 melanoma cells within fibrin hydrogels with mechanical stiffness ranging from 90 to 1050 Pa and evaluated changes in cell morphology[84]. The mechanical stiffness of fibrin gels was altered via modulating the concentration of fibrin where gels with 1, 4, 8 mg/mL fibrin corresponded to 90, 420, 1,050 Pa in elastic stiffness. Despite the potential increase in the presentation of integrin ligands and slower proteolytic degradation as a result of increasing fibrin concentration, the results of the study indicated that fibrin gels of 90 Pa were optimal for cancer cell proliferation and spheroid formation. Hall *et al*. demonstrated the use of fibrin hydrogels with covalently immobilized VEGF-A and FGF-2 to probe the effect of pro-angiogenic growth factors on endothelial cells[85]. As endothelial cells infiltrated into the 3D fibrin based scaffold and degraded it, immobilized growth factors were released thereby inducing the formation of vessels and promoting angiogenesis[85]. Growth factor release from fibrin gels was controlled by using different fibrin concentrations and various cross-linking densities[81]. Fibrin has certain drawbacks that limit its use as a well-defined 3D tumor microenvironment. Fibrin, unlike collagen, is not an ECM protein but instead represents

the provisional matrix at the earliest stages of wound healing. Similar to collagen, controlling matrix stiffness of fibrin gels without altering cell adhesion peptide density is challenging. As with other natural materials, the inherent batch-to batch variability can limit repeatability of results and the scope at which conclusions can be translated to actual *in vivo* processes.

### 1.5.3 Synthetic biomaterials for tumor microenvironment engineering

Synthetic materials are often chosen for engineering microenvironments since they allow for more control over modification of mechanical and sometimes biochemical properties of the material. Unlike natural materials that possess a high degree of batch to batch variability and are potentially immunogenic, synthetic materials can be a safer alternative that can be readily produced consistently. With the numerous advantages that synthetic materials offer, synthetic polymer scaffolds can be designed to mimic aspects of the tumor microenvironment in an effort to guide and support cancer studies. Some of the most commonly used synthetic biomaterials include poly(lactic-co-glycolic acid) (PLGA), polycaprolactone (PCL), and poly(ethylene glycol) (PEG).

PLGA is a highly porous material that degrades by hydrolysis of ester bonds in the polymer backbone. The utility of PLGA scaffolds as a 3D microenvironment for creating *de novo* engineered vasculature has been demonstrated[78,81]. Endothelial-progenitor cells from human umbilical cord blood along with human smooth muscle cells seeded on PLGA scaffolds formed capillary-like structures throughout the

scaffold[86]. Due to its pliability and slower degradation, PCL also serves as a useful candidate for fabricating scaffolds to model tumor angiogenesis *in vitro*. Previous work has shown that PCL has the ability to support EC proliferation and differentiation. Chung *et al.* in 2005 demonstrated that in contrast to unmodified PCL substrate, PCL modified with RGD peptide on the surface enhanced the growth and proliferation of human endothelial cells and induced tubule formation[87]. It is important to note that synthetic materials like PLGA and PCL innately lack bioactivity and therefore resist cell adhesion. To improve cell affinity, functionalization of these synthetic materials is required which typically involves nonspecific physical adsorption of peptides and growth factors. In some cases, additional processing of PLGA or PCL constructs is required for functionalization which can involve solvent casting and chemical leaching. These methods allow very little control in the amount and orientation of biomolecules immobilized in the material making it difficult to study the mechanistic effects of specific ECM components or signaling molecules on tumor growth dynamics. Additionally, PLGA has limited mechanical range (E = 0.5—2 MPa) that may not be typical of cancerous tissue (E = 1-100 kPa)[88,89]. Also PLGA tends to lose its mechanical integrity quickly between 2 to 4 weeks due to its rapid degradation in aqueous solutions[88,90]. These drawbacks of PLGA limit its use for tissue engineering applications.

Unlike PCL and PLGA constructs, poly(ethylene glycol) (PEG) based scaffolds can be easily modified with peptides and proteins with high control over covalent immobilization, orientation, and presentation of biomolecules to investigate cellular

processes and functions[91–94]. Additionally, the mechanical properties of PEG based scaffolds are tunable via varying polymer chain length or percent weight polymer. PEG hydrogels have been developed and tested for promoting vascularization and morphogenesis of endothelial cells[91,92,94]. PEG-based scaffolds offer special advantages for engineering 3D tumor microenvironments that will be discussed in detail in the next section.

### 1.5.4 Poly(ethylene glycol)-based hydrogel matrices

Poly(ethylene glycol) diacrylate (PEGDA) is an FDA approved polymer that intrinsically exhibits high hydrophilicity and therefore strong affinity with water molecules. This hydrophilic nature of PEGDA prevents interaction with the hydrophobic domains of proteins causing PEGDA to be resistant to protein adsorption and consequently nonspecific cell adhesion[95,96]. As such, PEGDA acts as a ‘‘blank slate” into which bioactivity can be incorporated by covalent attachment of proteins and peptides thereby creating a controlled microenvironment where cell interactions are driven primarily by the incorporated biomolecules[55]. The mechanism by which hydrogels are formed dictates how biomolecules and cells are incorporated into a scaffold.

One mechanism of forming PEGDA hydrogels is photopolymerization. Key advantages of fabricating hydrogels via photopolymerization are that the process is rapid, spatiotemporally controllable and mild enough to be carried out in the presence

of cells[78,97]. Free radicals, created by cleaving photoinitator molecules upon light exposure, initiate addition polymerization of the acrylate termini of liquid PEGDA macromers to form hydrogels[97]. In this work, a visible light sensitive photoinitator, eosin Y, was utilized due to its high biocompatibility and stability. Eosin Y is excited to a triplet state upon illumination with visible light at ~525 nm and participates in a single electron redox reaction with an electron donor from triethanolamine (TEOA)[98]. The radicals from TEOA then initiate a rapid addition polymerization of PEG macromers. These mild photocrosslinking conditions permit cellular encapsulation within PEGDA hydrogels while maintaining high cell viability[99].

Photopolymerizable PEGDA hydrogels can be modified to be bioactive with the incorporation of peptides and proteins that elicit a cellular response. For example, the peptide Argininin-Glycine-Aspartic Acid-Serine (abbreviated as RGDS), which serves as an integrin binding motif for cells, can be covalently crosslinked and immobilized into a PEG hydrogel network to promote cell adhesion and spreading. The chemistry for incorporating peptides or proteins simply involves reacting a hetero-bifunctional acrylate PEG to a free amine or terminal carboxyl group on proteins or peptides to form acrylol-PEG-biomolecule which then can be incorporated into the hydrogel matrix as it is crosslinked. Following this chemistry, PEGDA hydrogels can also be rendered degradable through the incorporation of a cleavable subunit with reactive amines on both ends of the peptide into the polymeric backbone[100]. To form a hydrogel, cells of interest can be combined with PEG conjugated moieties and a photoinitator to form a

hydrogel precursor solution. Upon exposure to light, acrylate groups at the ends of the PEG are covalently cross-linked leading to the formation of a hydrogel with immobilized cell-responsive cues that enable cell adhesion and proteolytic degradation of the matrix.

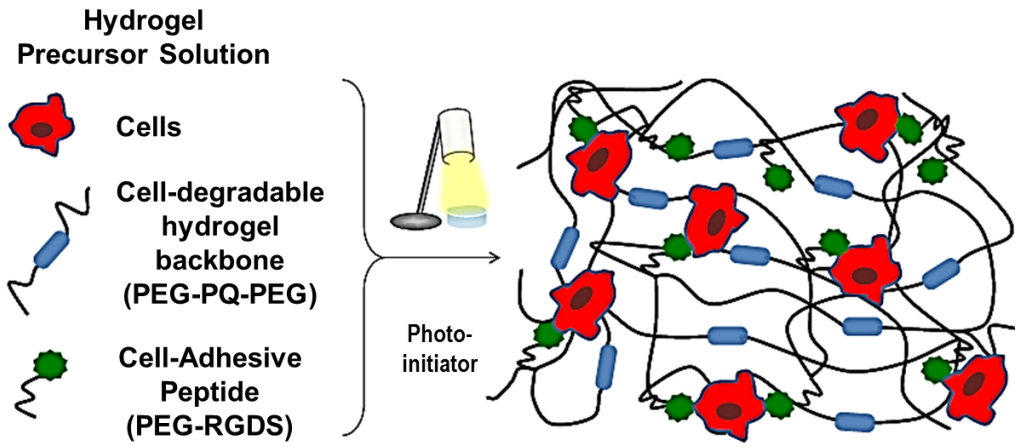


**Figure 7: In the presence of a photoinitiator and activating light, cells of interest can be encapsulated in PEG based hydrogels. Cell-responsive cues like PEG-RGDS for cell adhesion and PEG-PQ-PEG for matrix degradation can also be incorporated into the hydrogel backbone via covalent crosslinking of acrylate groups at the PEG terminus.**

Degradation of the hydrogel matrix is necessary to allow cell migration and tissue remodeling. By controlling degradation, the release of bioactive molecules and tissue infiltration can essentially be controlled[100]. Ideally, degradation kinetics can be controlled to follow the rate of tissue formation. The mechanisms by which photopolymerizable hydrogels can be made to degrade include hydrolysis of ester

linkages or enzymatic cleavage. Enzymatically degradable hydrogels can be degraded naturally by cell secreted enzymes like MMPs and hyaluronidase[68,78]. The rate of degradation will be dependent on the number of substrates per polymer chain and the affinity of enzymes for the degradable substrate. Additionally, the concentration of enzymes and inhibitors in the environment and permeability of matrix to enzymes will also affect degradation kinetics.

The incorporation of peptides that are susceptible to degradation by cellular proteolytic enzymes in PEGDA hydrogels has been demonstrated in previous studies[91,100–102]. Raeber and colleagues demonstrated the use of protease-sensitive PEG hydrogels to evaluate migration of dermal fibroblasts. Cell migration of dermal fibroblasts in PEG hydrogels functionalized with a MMP-sensitive peptide was compared with natural materials like collagen matrix in the presence of both a MMP inhibitor and inducer. In their study, Raeber and colleagues showed that fibroblast cells in PEG-based hydrogels were more sensitive to the MMP modulators, as compared to natural materials, where a MMP inducer increased the number of migrating cells significantly and a MMP inhibitor suppressed cell migration[102]. In an effort to study angiogenesis, Moon *et al.* incorporated protease sensitive peptide sequence GGGPQGIWGQGK (abbreviated PQ) in the polymer backbone. The PQ peptide sequence is sensitive to cleavage by cell secreted MMP2 and MMP9[91]. Moon *et al.* showed that endothelial cells encapsulated in protease sensitive PEG hydrogels with

covalently immobilized RGDS organized into stable tubule networks within 7 d in culture[91].

In addition to control over bioactivity and degradation kinetics, PEG hydrogels allow for tuning mechanical properties. Unlike natural materials, matrix stiffness of synthetic PEG hydrogels can be precisely tuned by changing the molecular weight of the PEG polymer chain where the use of higher molecular weight PEG chain can produce more compliant substrates due to lower crosslinking densities. Matrix stiffness can also be tuned by altering the concentration of PEG in a hydrogel where higher percentage of polymer weight by volume will yield more stiff substrates. Unlike natural materials such as collagen and fibrin, PEG is inert and thus changing the hydrogel stiffness by altering the concentration of PEG does not alter the bioactivity of the matrix. By these methods, the mechanical properties of PEG hydrogels can be tuned over a broad range and designed to mimic the mechanical stiffness of malignant tissue. A study conducted by Nemir *et al*. demonstrated the capability of tuning matrix elasticity of PEG hydrogels[103]. By controlled mixing of low and high molecular weight PEG polymers during polymerization, Nemir and colleagues were able to produce hydrogels with an elasticity gradient varying in a linear range from 2 to 100 kPa[103]. Additionally, a photomask was employed during photo-polymerization to pattern specific regions of 3.4 kDa polymer chain length PEGDA within 20 kDa PEG hydrogel thereby demonstrating that varying stiffness can be spatially patterned within hydrogels[103].

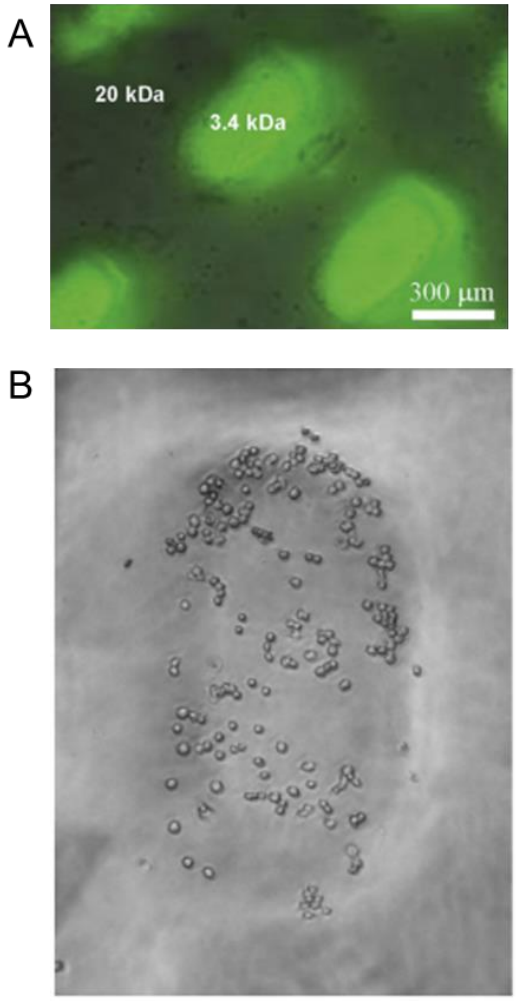


**Figure 8: A) 3.4 kDa PEG with acrylated fluorescein (green) was immobilized in specific areas with spatial control over location within 20 kDa PEG hydrogel. B) PEG gels with an elasticity gradient were utilized to show that RAW 264.7 macrophages preferentially adhere to stiff regions after 48 h. From Nemir *et al*[103].**

These patterned hydrogels can be utilized to study the influence of matrix rigidity on cellular behavior. Nemir *et al.* showed that when RAW 264.7 macrophages were seeded on gradient hydrogels, the cells preferentially attached to stiffer areas of the hydrogel after 48 h post seeding (Figure 8). Overall, PEG hydrogels can provide supportive framework, maintain high cell viability, and present both biochemical and

mechanical stimuli to direct the formation of various tissues and allow for studying cellular mechanisms and functions. Due to its versatility and advantages, the PEGDA based hydrogel system was utilized in this work to closely mimic the vascularized tumor microenvironment.

# 2. Function and role of cancer-associated fibroblasts in tumor vascularization in an *in vitro* 3D biomimetic hydrogel matrix

## *2.1 Introduction*

Blood vessels consist of two types of interacting cells, endothelial cells, which form the inner lumen of the vessel, and mural cells such as pericytes that envelop the surface of the vessel[53]. Pericytes, which are contractile cells located adjacent to the basement membrane of normal capillaries, stabilize vessel walls and are required for endothelial cell proliferation and survival[61]. During normal tissue development and angiogenesis, newly formed vessels supported by pericytes mature, stabilize, and cease to proliferate. In contrast to angiogenesis in normal tissue, blood vessel formation in tumors is not as tightly regulated and continue to proliferate[58]. Reports also suggest that the amount of pericyte coverage on vessels is lower in pathological tissue, such as breast and lung carcinoma, than in normal tissue[61]. The low degree of pericyte invasion and association with endothelial cells observed in tumors raises the possibility of the involvement of alternative mural cells in the tumor stroma replacing critical functions of pericytes and supporting vessel formation in tumors[61]. There are reports suggesting that CAFs have the potential to create a milieu that can promote the formation of blood vessels and thereby support cancer cell growth, invasion, and metastasis[104–106]. CAFs express a number of factors such as VEGF and FGF-2 that regulate angiogenesis and endothelial cell proliferation, migration, and behavior[104]. Based on these functions, we

postulate that CAFs may play a direct role in influencing ECs to form vessels and function like pericytes to stabilize vessel networks in tumors.

To explore this hypothesis, a lung adenocarcinoma mouse model developed by Gibbons *et al.* with defined metastatic potential was utilized. Mice expressing a K-ras mutation develop lung adenocarcinomas that become locally advanced but do not metastasize[47,107,108]. However, mice that express the same K-ras mutation along with a p53 mutation ($p53^{R172H}$) produce primary lung adenocarcinoma with widespread metastatic disease[47,107,108]. Previous studies on these K-ras and p53 mutant mice have revealed that their lung tumors mimic the transcriptional features of tumors from patients with lung adenocarcinoma with poor-prognoseses[108]. CAFs were isolated from the tumor stroma of lungs of $Kras^{LA1/+}$ mice (CAFkras) and from mice expressing both the Kras mutation and p53 mutation (CAFp53kras). As a comparison, normal mouse lung fibroblasts (LF) were isolated from wild-type littermates. The role of fibroblasts from metastasis and non-metastasis prone lung tumors in promoting vascular formation has not been fully elucidated. CAF cells have the potential to influence the tumor microenvironment by release of growth factors and MMPs, and production of ECM to create a cancer cell growth promoting niche[7,18,46,47]. Unlike non-invasive tumors, metastatic tumors are active and dynamic. The connective tissue and the ECM are continually remodeled through dynamic processes such as ECM degradation and production by MMPs[4]. The ECM turnover at metastatic sites is unrestrained. Studies suggest that at the site of metastatic tumors, through interactions with each other and

directly or indirectly with cancer cells, CAF cells become distinct from normal fibroblasts in that they display uncontrolled growth, increased proliferation potential, abnormal migratory behavior, and higher contractility[4,49]. This altered function results in increased secretion of ECM proteins and growth factors such as insulin-like growth factor 1 (IGF1) and hepatocyte growth factor (HGF) which contribute to tumor cell survival and migration[18,47]. Taken together, these functions of CAFs have led us to believe that such metastasis-associated fibroblasts could represent a variant of fibroblasts that have a more active role in supporting cancer growth and may be functionally and phenotypically distinct from normal fibroblasts amnd fibroblasts from benign tumor sites. To date, the functional properties and differences between metastasis associated and non-metastasis associated tumor-derived CAFs have not been characterized and remain an area to be investigated.

The goal of our study is to understand some of the intrinsic properties and behavior of CAFs from K-ras and p53 mutant mice that may regulate blood vessel structure and formation. Previous work investigating the role of CAFs in tumors has provided tremendous amount of information to understanding CAFs; however work thus far has been restricted to two-dimensional culture[109,110]. There are several limitations to 2D cell culture to consider in investigating the tumor stroma. A major limitation of 2D cell culture is its lack of ECM architecture. The ECM in tissues *in vivo* is 3D, complex and dynamic in its composition and stiffness. Through mechanical forces and interactions with cell integrins, the ECM provides signaling cues to cells which in turn induce a

cascade of molecular and cellular events such as changes in cell shape, motility, and proliferation and affect the morphogenesis of cellular structures. By their ability to resemble more closely to the *in vivo* environment, 3D cell culture studies can provide information on cell function and behavior that is more relevant to actual *in vivo* physiological processes. Therefore, it is important to use a 3D *in vitro* cell culture microenvironment. We utilized 3D degradable poly(ethylene glycol) diacrylate (PEGDA) hydrogels described in the previous section and depicted in Figure 9 to culture endothelial cells with CAFs and LFs to evaluate the influence of CAFs on endothelial cell-cell interactions and the formation of vessel networks.

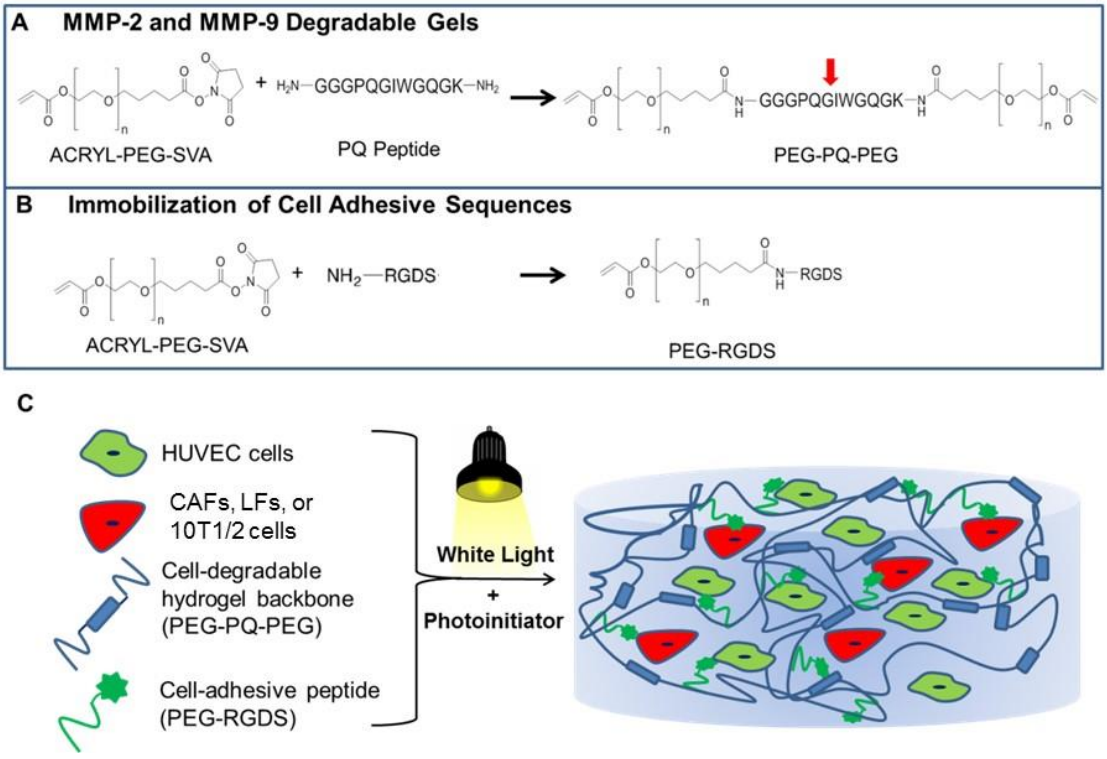


**Figure 9: Bioactivity can be incorporated in hydrogels with the addition of peptides. A) The collagenase-sensitive sequence GGGPQGIWGQGK (PQ) is conjugated to acrylate PEG-succinimidyl valerate (PEG-SVA) chain via the N-**

**terminus and the amine group of the lysine at the C-terminus of the PQ peptide yielding PEG-PQ-PEG which serves as the polymer backbone. Cell-mediated degradation at the cleavage site (indicated by red arrow) occurs by cell-secreted matrix metalloproteinases (MMPs) 2 and 9. B) The cell-adhesive ligand, RGDS, is conjugated to acrylate-PEG via the N-terminus to form PEG-RGDS. PEG-RGDS permits cell adhesion to the matrix. C) PEG-PQ-PEG and PEG-RGDS are mixed along with cells and eosin Y photoinitiator to form a hydrogel precursor solution. Upon exposure to light, the acrylate groups are covalently cross-linked leading to the formation of a three-dimensional, biomimetic hydrogel.**

In numerous published studies, we have utilized MMP-2 and MMP-9 sensitive, RGD-modified PEGDA hydrogels depicted in Figure 9 as 3D scaffolds to grow microvascular networks[91,92,94]. Prior work utilizing this system has shown that ECs co-cultured with mural cells in PEGDA-based hydrogels organize into tubules[91]. A common source for ECs is the human umbilical vein endothelial cells (HUVECs). HUVECs have the ability to form primitive tubule structures. However, for these primitive tubules to mature and stabilize over longer periods of time, they require interaction with mural cell types such as pericytes or smooth muscle cells (SMCs)[91]. 10T1/2 cells are mouse MSCs known to be precursors to pericytes and smooth muscle cells and were utilized in co-culture with HUVECs in this work. Upon interaction with ECs, 10T1/2 cells up-regulate alpha smooth muscle actin, express basement membrane components such as collagen IV and laminin[91,94]. Previously, we have shown that HUVEC cells, when co-cultured with 10T1/2 cells in 3D hydrogels, organize into stable, lumenized tubule networks that are similar in structure and function to microvascular networks *in vivo*[91,92,94]. These

tubule networks are stable for at least 28 d in culture, whereas tubule structures formed by HUVECs alone regress in 6 d[91,94].

The purpose of this study is to probe the function and contribution of CAFs to vascularization. To obtain more biologically relevant information, 3D PEG-based hydrogels were utilized to culture ECs with either metastasis-associated CAFs or non-metastasis-associated CAFs. For comparison, normal lung fibroblasts were co-cultured with ECs. ECs cultured with 10T1/2 cells served as a positive control group. In addition to vessel structure, the ability of CAFs to interact with ECs, support newly formed endothelial-tubule networks, and remodel the extracellular matrix was evaluated.

## *2.2 Materials & Methods*

### 2.2.1 Isolation of Primary Lung Fibroblasts

Prior to initiation, all mouse experiments were approved by the University of Texas MD Anderson Cancer Center Institutional Animal Care and Use Committee (IACUC). Cell lines were derived as previously published[107]. Prior to initiation, all mouse experiments were approved by the University of Texas MD Anderson Cancer Center Institutional Animal Care and Use Committee (IACUC). Cell lines were derived as previously published[107]. Normal lung fibroblasts or cancer-associated fibroblasts were isolated from the lungs of syngeneic WT 129/SV mice, $Kras^{LA1}$, and $Kras^{LA1/+;}p53^{R172HDG/+}$ mice. Briefly, a 20 mm incision was made on the left side of the anesthetized mouse. 344SQ cells (a metastatic lung cancer cell line), described previously[47,107] as expressing

the miR-200b-200a-429 gene cluster, were injected subcutaneously in a single-cell suspension of 1 million cells in phosphate-buffered saline (PBS) in the posterior flank. After surgery, mice were monitored daily for three weeks and then were euthanized and examined for visible metastases.

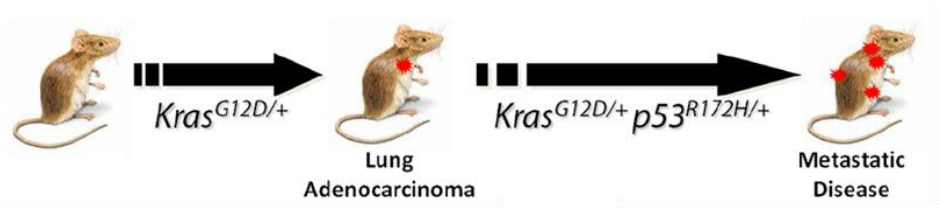


**Figure 10: Mice with somatically activated K-ras formed primary lung adenocarcinomas with no metastatic disease. When mated with mice with a p53 mutation, the heterozygous mutations induced formation of lung adenocarcinoma with widespread metastatic disease. Adapted from Roybal *et al*[47].**

Cells were harvested from lung tumor tissues from mice[47]. Lung tissues from mice were dissociated into single cell suspensions using both enzymatic digestion (3 mg/mL collagenase and 1.6 mg/mL dispase II) and mechanical separation using a GentleMacs Dissociator (Miltenyi Biotec, Lung_01 and Lung_02 programs). Cells were centrifuged and washed with Hanks Buffer Salt Solution (HBSS) containing 2% fetal bovine serum (FBS) and subjected to red blood cell lysis buffer according the manufacturer's directions (BioLegend). Remaining cells were washed with HBSS-FBS and passed through 30 and 40 μm filters to create a single cell suspension. Viability and cell number were determined using the Invitrogen Countess. Magnetic beads (Dynal;

Invitrogen) were conjugated to antibodies targeting for different cell-type receptors: anti-CD45 and anti-CD68 (Leukocytes), anti-PECAM (endothelial cells), anti-Epithelial cell adhesion molecule (EpCAM) (epithelial cells), and anti-F4/80 (macrophages). Cells were mixed with each antibody-conjugated magnetic bead suspension and the beads were pelleted by magnet to clear the bound cells and to collect the remaining unbound cells. Unbound cells were subjected to magnetic beads conjugated with anti-Thy-1. Thymocyte antigen-1 (Thy-1), a marker expressed by primary fibroblasts[111]. Thy-1 positive cells were collected and eluted off the beads using HBSS-FBS with 0.5% bovine serum albumin (BSA) and 2 mM Ethylenediaminetetraacetic acid (EDTA).

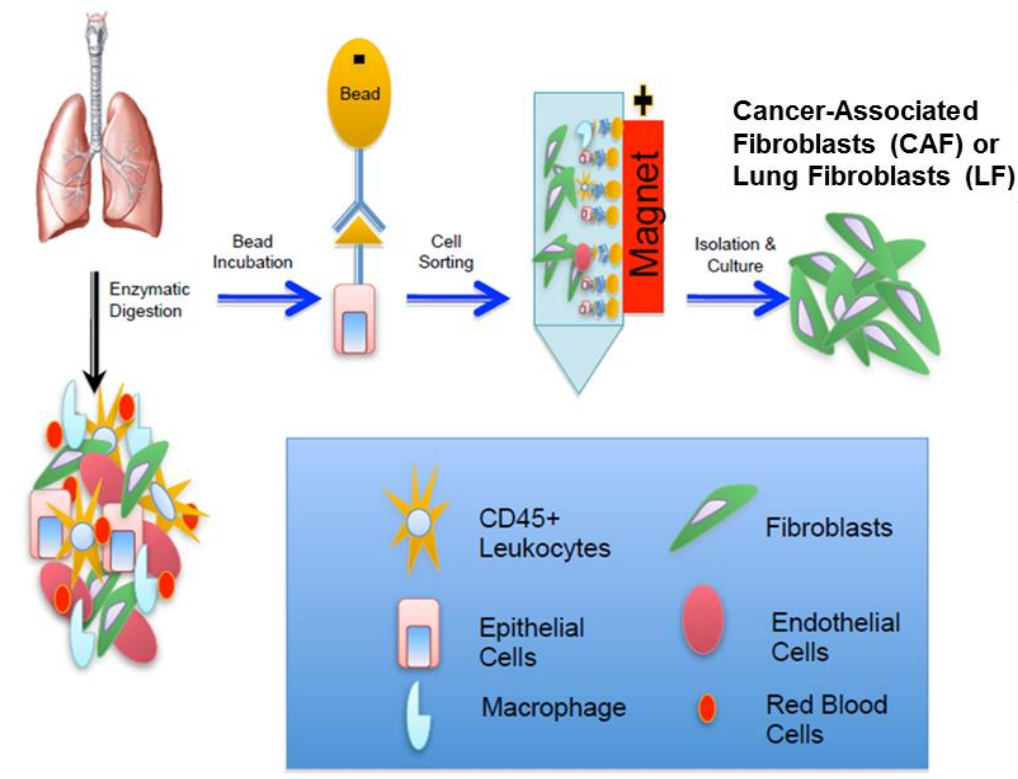


**Figure 11: Lung tissue isolated from Kras$^{LA1}$, Krasp53, and wild type mice littermates were mechanically and enzymatically digested to acquire a cell suspension. The suspension was then incubated with Dynal magnetic beads conjugated with various antibodies to recognize cell surface receptors for certain cell types. After incubation with beads, the cell suspension was placed on a magnet to remove unwanted cells and to acquire fibroblasts. From Roybal *et al*[47].**

Cells collected from beads were centrifuged, washed with HBSS-FBS, and plated in Alpha-MEM Medium (Cell-Gro, Corning) containing 20% FBS, 1 mM sodium pyruvate (Gibco), 2 mM L-glutamine (Gibco), and 100 mg/100 U penicillin-streptomycin (Gibco). Wild-type mice (WT129/SV mice) did not develop tumors, and therefore fibroblasts derived from lungs of WT129/SV mice are designated as normal lung fibroblasts or LF. Fibroblasts derived from Kras$^{LA1}$ mice are labeled as CAFkras and fibroblasts derived from Kras$^{LA1/+;\ p53R172HDG/+}$ mice are labeled CAFp53kras.

### 2.2.2 Cell Maintenance

CAFp53kras, CAFkras, and LF were cultured in Minimum Essential Medium Eagle Alpha Modification (Gibco, North Andover, MA) with 20% FBS (Lonza, Walkersville, MD). HUVECs (Lonza) were grown in endothelial basal medium (EBM), supplemented with an EGM-2 BulletKit™ containing ascorbic acid, human fibroblast growth factor-B (h-FGFb), heparin, hydrocortisone, VEGF, insulin-like growth factor, GA-1000 (gentamicin, amphotericin-B), and 2% fetal bovine serum (Lonza). 10T1/2 pericyte precursor cells (American Type Culture Collection, Manassas, VA) were cultured in Dulbecco's Modified Eagle's Medium (DMEM; Gibco) supplemented with 10% fetal bovine serum and 2 mM L-glutamine, 1000 U/mL penicillin, and 100 mg/L streptomycin (Sigma, St. Louis, MO). Experiments were conducted with CAFp53kras, CAFkras, and LF cells from passages to 2 to 9. HUVEC cells were used from passages 2 to 8, and 10T1/2 cells were used from passages 15 to 18. All cells were incubated at 37°C and 5% $CO_2$, and medium was changed every other day.

### 2.2.3 αSMA and S100A4 Expression

Expression of alpha smooth muscle actin and the calcium-binding protein S100A4 was assessed via immunohistochemistry. Alpha smooth muscle actin ($\alpha$SMA) is a differentiation marker of smooth muscle cells and S100A4 is a protein shown to be upregulated in metastatic cells and involved in regulating cell proliferation, migration, and extracellular transduction[112]. Cells seeded at 8,500 cells/cm$^2$ on polystyrene plates

were fixed with 4% paraformaldehyde for 20 min at room temperature and then rinsed with PBS three times at room temperature. After fixation, cells were then permeabilized with 0.125% Triton-X in PBS for 10 min, rinsed three times with PBS, and then incubated with 5% BSA for 30 min. After blocking, cells were incubated with primary antibodies at room temperature for 1 hour. The primary antibodies were mouse anti-$\alpha$SMA (1:500 in PBS with 0.1% BSA, Abcam, Cambridge, UK) and rabbit anti-S100A4 (1:250 in PBS with 0.1% BSA, Abcam). Cells were rinsed in PBS three times and then incubated with Alexa Fluor 647 donkey anti-mouse IgG (1:500 in in PBS with 0.1% BSA, Invitrogen) for $\alpha$SMA expression or Alexa Fluor 488 donkey anti-rabbit IgG (1:500 in in PBS with 0.1% BSA, Invitrogen) for S100A4 expression for 1 hr at room temperature to visualize the binding of the primary antibodies. Following another PBS wash, cells were finally exposed to 2 μM 4',6-diamidino-2-phenylindole (DAPI) in HBS with 0.1% BSA for 30 min to visualize cell nuclei and imaged using a Zeiss Axio Observer widefield fluorescence microscope with a 20x objective (Carl Zeiss Microscopy, Jena, Germany).The excitation/emission wavelengths used for observing Alexa Flour 488 were 488 nm/519 nm, for Alexa Fluor 647 was 633 nm/665 nm, and for DAPI were 405 nm/421 nm.

### 2.2.4 Synthesis of PEG-RGDS and PEG-PQ-PEG

The cell-adhesive peptide RGDS (American Peptide, Sunnyvale, CA) was conjugated to acryloyl-PEG-succinimidyl valerate (PEG-SVA, 3400 Da, Laysan Bio Inc., Arab, AL) to form PEG-RGDS (Figure 9 ). The RGDS peptide was first dissolved in

anhydrous dimethyl sulfoxide (DMSO) with 2 mol diisopropylethylamine (DIPEA) and then added dropwise to dry acryloyl-PEG-SVA at a molar ratio of 1:1.2 (PEG:RGDS). The resulting product was then purified via dialysis against ultrapure water in a regenerated cellulose membrane (MWCO 3,500; Spectrum Laboratories, Inc., Rancho Dominguez, CA) and lyophilized. PEG-PQ-PEG was synthesized by reacting PEG-SVA with the MMP 2 and MMP 9 sensitive peptide sequence GGGPQGIWGQGK (PQ) at a molar ratio of 2:1 (PEG:PQ). MMP-2 and MMP-9, secreted by ECs, cleave the PQ peptide in the polymer backbone resulting in the degradation of PEG hydrogel[91,92]. The PQ peptide was synthesized on an APEX 396 solid phase peptide synthesizer (Aapptec, Louisville, KY) using standard Fmoc chemistry and characterized via matrix-assisted laser desorption/ionization-time-of-flight mass spectrometry (MALDI-ToF; Bruker Daltonics, Billerica, MA). Conjugation of PQ to PEG was achieved in process similar to that for PEG-RGDS but with a PEG-SVA:PQ peptide molar ratio of 2:1 generating an MMP-degradable segment attached to PEG at the N-terminus and at the lysine residue at the C-terminus (PEG-PQ-PEG) (Figure 9). Successful conjugation of the peptide to PEG was confirmed via gel permeation chromatography (GPC) with UV-VIS and evaporative light scattering detectors (GPC, Polymer Laboratories, Amherst, MA).

### 2.2.5 Encapsulation of Cells in Degradable Hydrogels

In order to elucidate how CAFs influence ECs in the formation, stability, and proliferation of microvascular networks, HUVECs were encapsulated in 5 μL

degradable hydrogels with either 10T1/2 cells, CAFp53kras, CAFkras, or LF at a ratio of 4:1 (HUVECs:CAFs) with a total cell density of 30,000 cells/μL. Hydrogels were formed from a pre-polymer solution composed of 10% (w/v) PEG-PQ-PEG and 3.5 mM PEG-RGDS in sterile HEPES-buffered saline (HBS) containing 1.5% (v/v) triethanolamine, 1 mM eosin Y, and 3.5 μL/mL N-vinyl-2-pyrrolidone (NVP). The test groups for this study were the following: (1) HUVEC cells with CAFp53kras, (2) HUVEC cells with CAFkras, and (3) HUVEC cells with LF (control) and (4) HUVEC cells with 10T1/2 (positive control). Previous work has shown that HUVECs and 10T1/2 cells, pericyte precursors, encapsulated in degradable hydrogels undergo tubule network formation by 7 d[91,94]; therefore, this co-culture was utilized as a positive control group. All cells were detached from plates using 0.05% trypsin-EDTA and pelleted by centrifuging at 700 x g for 4 min. The cell pellets were then re-suspended in the pre-polymer solution to concentrations of 30,000 cells/μL (24,000 cells/μL of HUVECs to 6,000 cell/μL of CAFs, LFs, or 10T1/2 cells). 5 μL droplets of cell-laden polymer were sandwiched between a Sigmacote® functionalized (a hydrophobic surface treatment prepared as described below, Sigma, St. Louis, MO) glass slide and a methacrylate-modified cover glass (a surface treatment that mediates covalent attachment of the hydrogel to glass prepared as described below) separated by a 380 μm polydimethylsiloxane (PDMS) spacer. Sigmacoted glass slides were prepared by washing each glass slide in 70% ethanol and then submerging the slide in Sigmacote® for 1 min before washing the slide with 70% ethanol. Sigmacote® is a clear, colorless solution of a chlorinated organopolysiloxane in

heptane that reacts with surface silanol groups on glass to produce a hydrophobic, water-repellant thin film. Methacrylate-modified coverslips were prepared by first cleaning round 12 mm diameter coverslips in a piranha solution consisting of 30 mL of sulfuric acid and 13 mL of hydrogen peroxide. After 1 hr in piranha solution, coverslips were washed thoroughly with DI water three times, then with 200 proof ethanol three times, and then with 190 proof ethanol for three times. Following washing, the coverslips were incubated overnight at room temperature in a solution containing 2% 3(trimethoxysilyl) propyl methacrylate in 95% ethanol. The methacrylate-modified coverslips were then washed with 70% ethanol, dried, and stored in a clean flask under argon at 4°C until ready for use. The pre-polymer solutions were cross-linked under white light at a power of 200 mW/cm$^2$ for 35 s to form hydrogels that were then immersed in EGM-2 media (Lonza) and incubated at 37°C in a 5% $CO_2$ environment for up to 7 d. Media was replenished every other day.

### 2.2.6 Angiogenic Protein Secretion in Cell Medium

The amounts of angiogenic proteins secreted by cells in the media were quantified using a VEGF-A ELISA kit (R&D Systems, Minneapolis, MN), PDGF-BB ELISA kit (R&D), and FGF-2 ELISA kit (Abcam) according to the manufacturers' instructions. Medium was collected from gels with encapsulated cells in culture for 24 hr and 72 hr. VEGF-A, FGF-2, and PDGF-BB measured from EGM-2 media controls was subtracted from the measured protein content collected from hydrogel samples.

### 2.2.7 Assessment of Vessel Assembly & Morphology

Hydrogels were fixed in 4% paraformaldehyde for 20 min and then washed with PBS. Encapsulated cells were permeabilized with 0.5% Triton-X for 30 min and then washed with PBS. Afterwards, nonspecific binding was blocked by incubation with 1% BSA overnight. Hydrogels were then incubated with a 1:200 dilution of goat anti-platelet endothelial cell adhesion molecule-1 (PECAM-1) (Santa Cruz Biotechnology, Dallas, Texas) and 1:100 dilution of mouse anti-$\alpha$SMA (Abcam, Cambridge, UK) in HBS with 0.1% BSA overnight on a rocker table at 4°C to stain endothelial cells and cells with a mural cell phenotype, respectively. Hydrogels were rinsed in PBS 5 times at 1 hr intervals and then incubated with a 1:400 dilution of Alexa Fluor 532 donkey anti-goat IgG (Invitrogen) and Alexa Fluor 647 donkey anti-mouse IgG (Invitrogen) overnight at 4°C to visualize the primary antibodies. Samples were then rinsed with PBS and exposed to 2 μM DAPI in HBS for 30 min to stain cell nuclei. The hydrogels were visualized using a confocal microscope (Zeiss 5-LIVE, Plan-Apochromat 20x objective with 0.8 NA) with a z-stack depth of 20 μm with 1 μm thick slices. Imaris software (Bitplane Inc., South Windsor, CT) was used to trace and measure tubule length and tubule diameter, and count vessel branch points in three fields of view for each hydrogel (n = 3-4 hydrogels per experimental group, FOV =318 μm x 318 μm). The colocalization function in the Imaris analysis software was utilized to assess percent of tubules covered by $\alpha$SMA positive cells. Vessel density was quantified from images of anti-PECAM staining of endothelial cell intercellular junctions as previously described[113]. Briefly, vessel

density is measured using the anti-PECAM channel image and counting the number of pixels that contain part of the vessel image and dividing these by the total number of pixels for a given image[113]. This measurement provides information on the fraction of the image area occupied by the vessels.

### 2.2.8 Collagen IV and Laminin Deposition

Basement membrane deposition was assessed via immunohistochemical staining for collagen IV and laminin. Hydrogels were first fixed in 4% paraformaldehyde for 20 min and then washed with PBS 3 times. After fixation, 0.5% Triton-X was for 30 min added to permeabilize cells, followed by a PBS wash. Blocking of nonspecific binding was accomplished by incubating with 1% BSA overnight on a rocker at 4°C and then washing with PBS. Hydrogels were then incubated with primary antibodies on a rocker table at 4°C overnight. For these studies, primary antibodies were rabbit anti-collagen IV (1:200 in PBS with 0.1% BSA, Abcam, Cambridge, MA) and chicken anti-laminin (1:200 in PBS with 0.1% BSA, Sigma, St. Louis, MO). Hydrogels were rinsed in PBS five times at one-hour intervals and then incubated with a 1:400 dilution of Alexa Fluor 488 donkey anti-rabbit IgG (Invitrogen) or Alexa Fluor 488 goat anti-chicken IgG (Invitrogen) overnight at 4 °C on the rocker to visualize the primary antibodies. Subsequently, samples were rinsed with PBS and then imaged using a Zeiss 510 inverted confocal microscope under a 20x objective with a z-stack depth of 20 μm with 1 μm thick slices. Relative amounts of laminin and collagen IV production around tubules were

determined by measuring Alexa Fluor 488 pixel intensity in ImageJ (National Institutes of Health, Bethesda, MD) and normalizing to cell number using the DAPI pixel intensity.

### 2.2.9 Treatment with VEGF-A, FGF-2, and PDGF-BB Neutralizing Antibodies

To inhibit VEGF-A and FGF-2 activity in conditioned EGM-2 media, the effect of neutralizing antibodies against VEGF-A and FGF-2 antibodies on HUVEC metabolic activity was assessed using a colorimetric assay kit based on the reduction of 3-(4,5-dimethylthiazol-2-yl)-5-(3-carboxymethoxyphenyl)-2-(4-sulfophenyl)-2H-tetrazolium, inner salt; MTS] to formazan by NAD(P)H-dependent cellular oxidoreductase enzymes. For the assay, HUVECs were seeded on 96-well tissue-culture treated dishes at a concentration of 15,625 cells/$cm^2$ and cultured in EGM-2 media at 37°C and 5% $CO_2$. After 1 day of culture, neutralizing VEGF-A and FGF-2 antibodies were added to the wells. Both goat polyclonal anti-VEGFA and goat polyclonal anti-FGF-2 (R&D Systems, Minneapolis, Minnesota) were added at concentrations ranging from 0 to 100 nM for up to 3 d. The use of these antibodies for blocking VEGFA and FGF-2 binding and signaling have been demonstrated in previous studies with HUVECs[114,115]. A goat polyclonal anti-PDGF-BB antibody (Abcam, Cambridge, UK), demonstrated as a blocking antibody previously[116], was tested with 10T1/2 at a concentration ranging from 0 to 100 nM. After 3 d of treatment with neutralizing antibodies, 20 μL of MTS reagent (Promega, Madison, WI, USA) was added for every 100 μL media in each well, mixed, and incubated for 3 hr

at 37°C and 5% $CO_2$. To measure the amount of soluble formazan produced by cellular reduction of MTS, the well plate was read at an absorbance of 490 nm. Similarly, the effect of a PDGF-BB neutralizing antibody on 10T1/2 cell proliferation was assessed via the same MTS assay.

To assess the effect of inhibiting VEGF-A, FGF-2, and PDGF-BB on the formation of microvascular networks, exogenous VEGF-A, FGF-2, and PDGF-BB were neutralized by the addition of 100 nM anti-VEGF-A, anti-basic FGF, and anti-PDGF-β neutralizing antibodies in the hydrogel precursor solution before photo-polymerization and additionally added in the EGM-2 media for 7 d. This concentration was selected based on the 2D monoculture dose response studies. Media supplemented with the appropriate neutralizing antibody was replenished every day. An isotype-matched goat IgG was used as a control. Tubule formation was assessed after treatment with each of the neutralizing antibodies for the following co-culture test groups: (1) HUVEC cells with CAFp53kras, (2) HUVEC cells with CAFkras, and (3) HUVEC cells with LF and (4) HUVEC cells with 10T1/2. Tubule formation was evaluated by measuring vessel density after staining for PECAM and DAPI as described in previous sections.

### 2.2.10 Statistical Analysis

Single factor ANOVA and subsequent *post hoc* Tukey test were used to analyze vessel formation and ECM production. For each analysis, $p<0.05$ was considered to be significant. All data is presented as mean ± standard deviation.

## *2.3 Results*

### 2.3.1 Characterization of PEG-RGDS and PEG-PQ-PEG

The protease sensitive sequence GGGPQGIWGQGK (abbreviated PQ) was incorporated into the polymer backbone to render hydrogels degradable by cell secreted MMP-2 and MMP-9. The protease sensitive sequence was synthesized and its molecular weight was confirmed at 1141 grams/mol via matrix-assisted laser desorption/ionization-time-of-flight mass spectrometry (MALDI-ToF; Bruker Daltonics, Billerica, MA) shown in Figure 12.

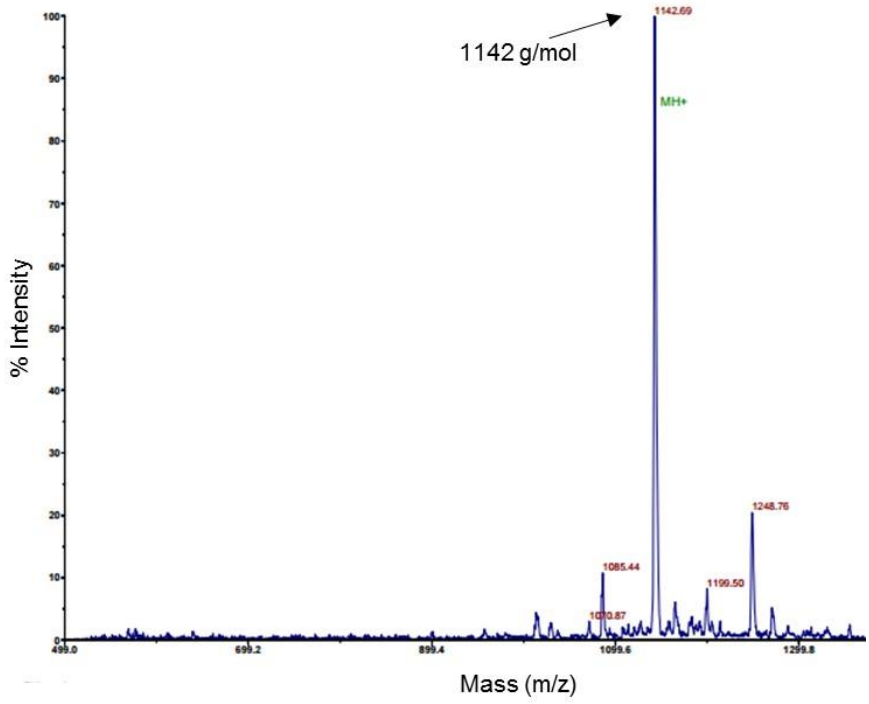


**Figure 12: MALDI-ToF conformation of PQ molecular weight at 1141 grams/mol.**

Conjugation of the MMP-sensitive peptide PQ and cell adhesive peptide RGDS to PEG-SVA was confirmed via GPC. Figure 13 shows GPC analysis of PEG-PQ-PEG with the blue line representing PEG-SMC, the red line representing PEG-PQ-PEG. Figure 14 shows GPC analysis of PEG-RGDS in which the blue peak represents the PEG-RGDS and red peak represents unreacted PEG-SVA.

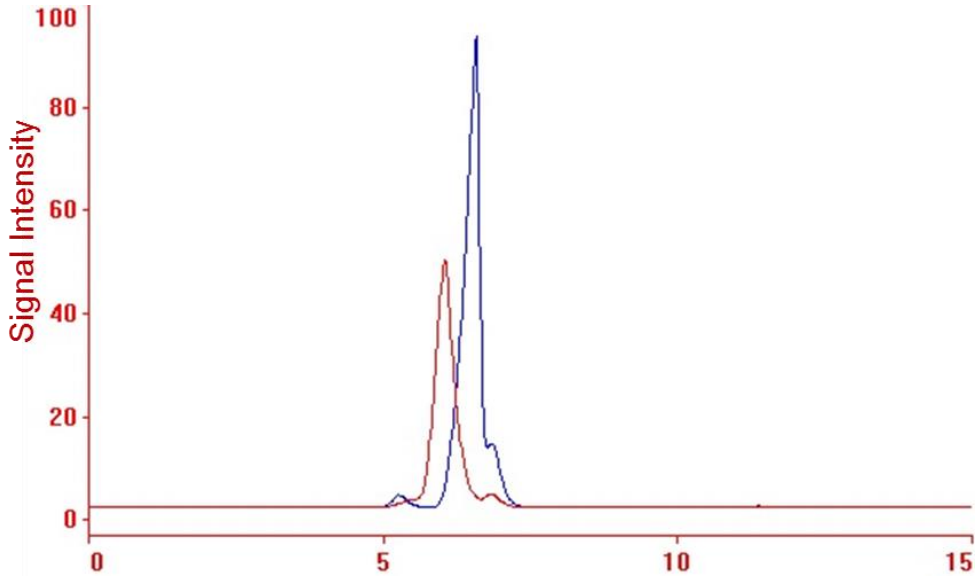


**Figure 13: GPC analysis of PEG-PQ-PEG with the blue line representing PEG-SVA, the red line representing PEG-PQ-PEG.**

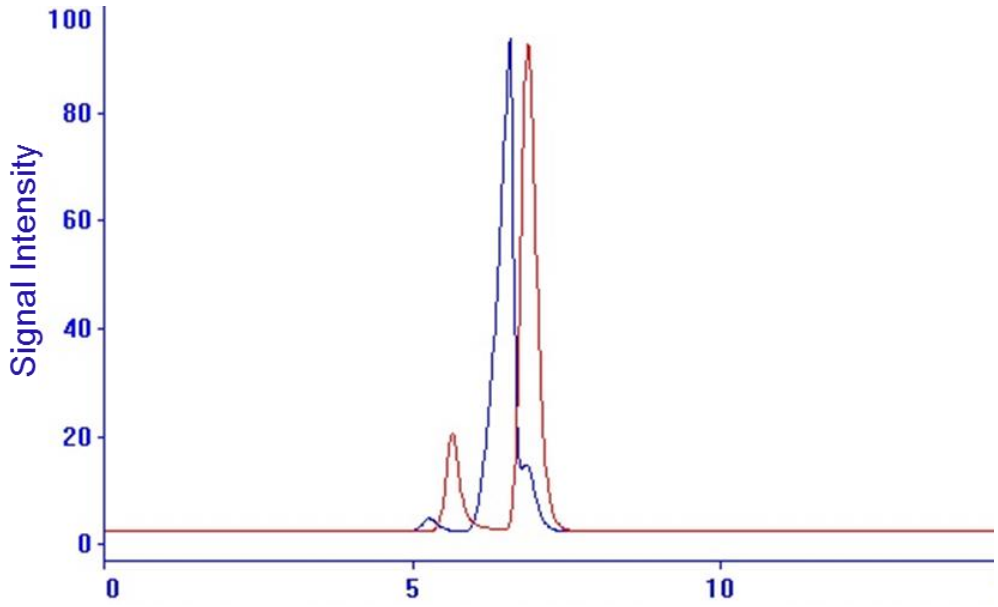


**Figure 14: GPC analysis of PEG-RGDS in which blue peak represents the PEG-RGDS and red peak represents unreacted PEG-SVA.**

### 2.3.2 αSMA and S100A4 protein expression

Examination of CAFs and LFs in culture revealed clear differences in cell morphology, spreading, and expression of $\alpha$SMA and S100A4 protein (Figure 15). CAFkras cells displayed a more rounded morphology similar to LF and had fewer cellular projections than CAFp53kras cells. As opposed to LF, CAFp53kras and CAFkras cells appear to be more elongated with greater cellular projections. Moreover, CAFp53kras cells appear to express $\alpha$SMA and S100A4 protein at higher levels than LFs and CAFkras cells.

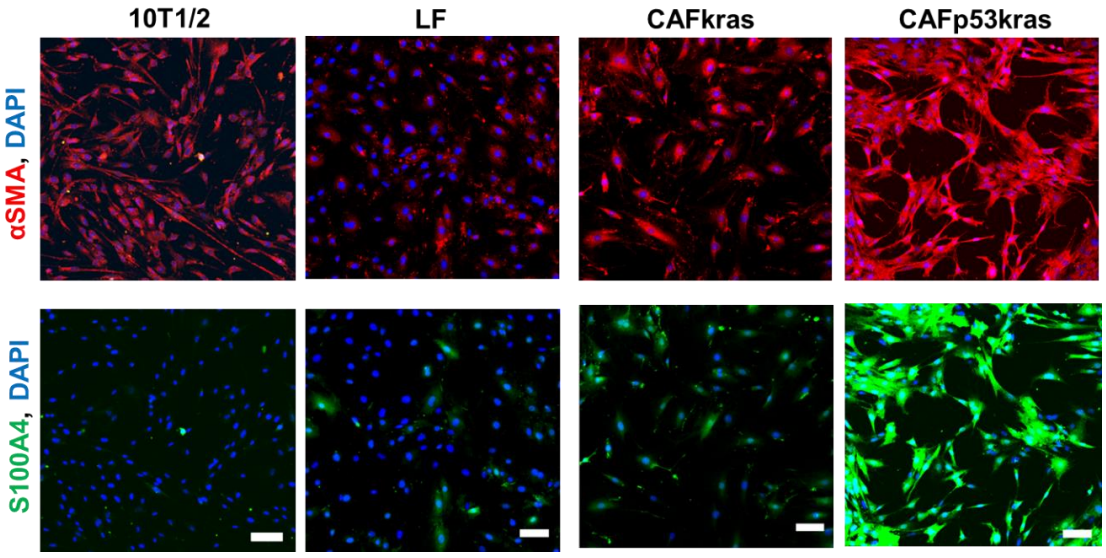


**Figure 15: Expression of $\alpha$SMA and S100A4. Differences in cell morphology and expression of $\alpha$SMA and the calcium-binding protein S100A4 amongst the distinct cell lines tested were evaluated via immunostaining. Staining of cells with $\alpha$SMA (shown in red) displays differences in cell morphology where 10T1/2 cells and normal lung fibroblasts (LF) have fewer cellular projections than the CAF cells. Minimal level of $\alpha$SMA actin staining was observed in normal lung fibroblasts. As compared to normal lung fibroblasts, CAFs expressed higher levels of $\alpha$SMA and S100A4. Scale Bar = 50 μm.**

### 2.3.3 CAFs enhance vessel formation

We hypothesis that secreted molecules produced by CAFs enhance tumor vascularization, modify vessel structure, and regulate basement membrane assembly. All of these functions can subsequently enhance cancer cell invasion and metastasis. To test this hypothesis, ECs were co-cultured with CAFs and LFs in 3D in PEGDA hydrogels. HUVECs with CAFs, LFs, or 10T1/2s encapsulated in degradable PEGDA hydrogels underwent vascular network formation, with the extent of this response dependent upon the metastatic potential of the CAFs. The vessel-like networks were

visualized as early as 7 d after encapsulation by staining for cell nuclei via DAPI and endothelial cell intracellular junctions via PECAM-1 staining (Figure 16). To quantify the tubule formation response, average tubule diameter, total tubule length, branch points, and vessel density were calculated.

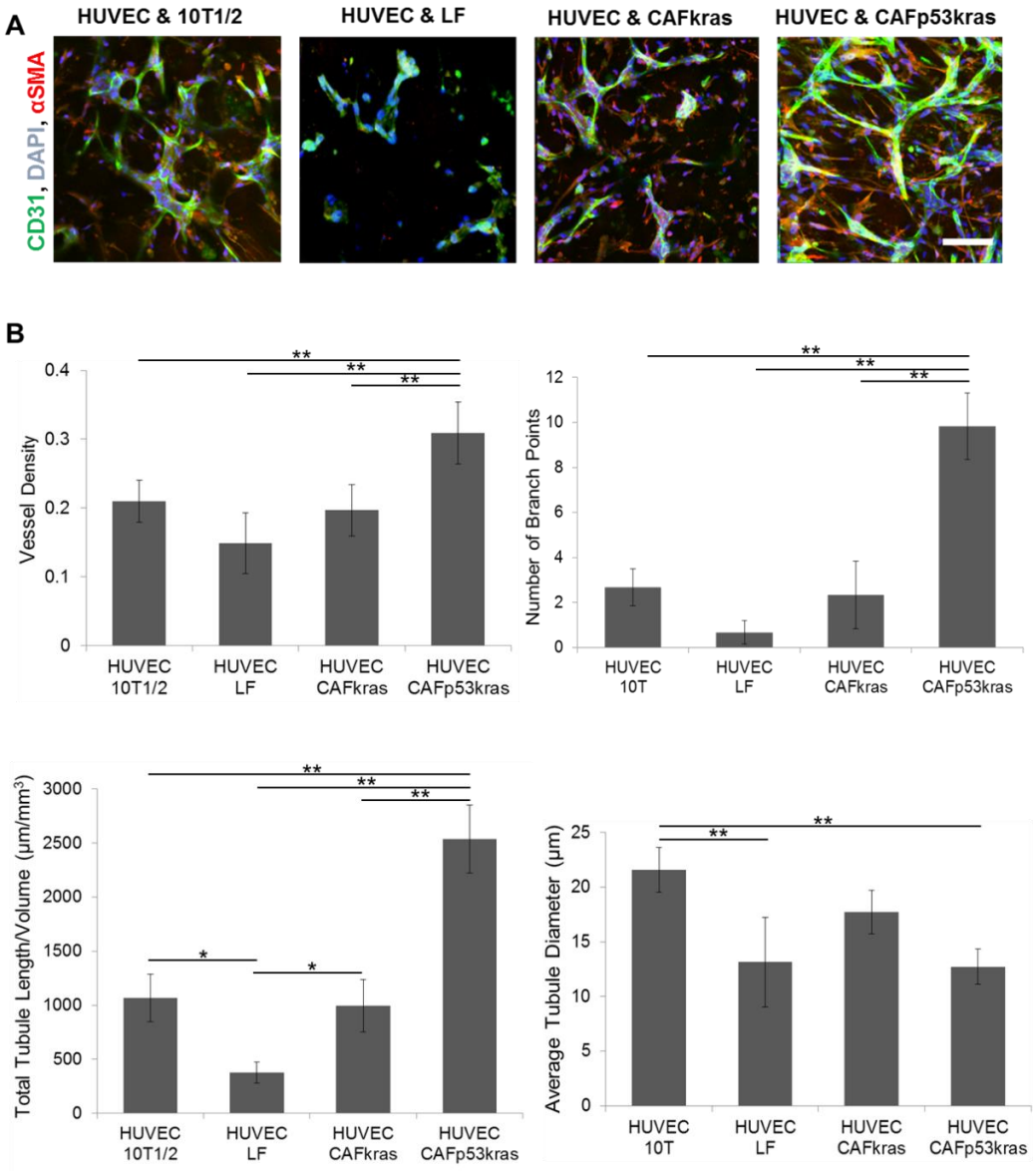


**Figure 16: HUVEC cells with CAFs, LF, or 10T1/2 encapsulated in degradable PEG hydrogels underwent vascular network formation. A) The vessel-like networks**

**were visualized as early as seven d after encapsulation by staining for cell nuclei via DAPI (indicated in blue) and endothelial cell intracellular junctions via PECAM-1 staining (indicated in green). B) To quantify the tubule formation response, average tubule diameter, total tubule length, branch points, and vessel density were evaluated. Scale Bar = 100 μm.**

ECs co-cultured with CAFp53kras had a significantly higher total tubule length per volume and vessel density when compared with all other groups ($p<0.01$). Total tubule length per volume for vessels formed by ECs co-cultured with CAFp53kras was about 2.5 fold higher than vessels formed by ECs co-cultured with CAFkras or 10T1/2. Additionally, vessel-like networks formed with the co-encapsulation of CAFp53kras cells with ECs were significantly more branched than all other groups ($p<0.01$). The number of branch points for vessel structures in hydrogels with HUVECs and CAFp53kras was about 5-fold higher than the average number of branch points for vessels consisting of HUVECs and 10T1/2.

### 2.3.4 CAFs exhibit pericyte cell-like functions

Interactions between endothelial cells and mural cells like pericytes are crucial for vascular formation and stabilization. Similar to the 10T1/2 pericyte precursor cells, CAFs also appear to express αSMA. This observation led us to hypothesis that CAFs may be acting like pericytes in the tumor. To test this hypothesis, we evaluated CAFs with endothelial cells co-cultured in 3D in PEG hydrogels and quantified percent of tubule coverage by αSMA positive cells. The percent of tubules covered by αSMA positive CAFs was compared with percent of tubules covered by 10T1/2 pericyte cells.

Higher magnification images focused in on vessel-like networks (Figure 17) clearly show that CAFs expressing $\alpha$SMA (indicated in red) are closely associating with endothelial cells.

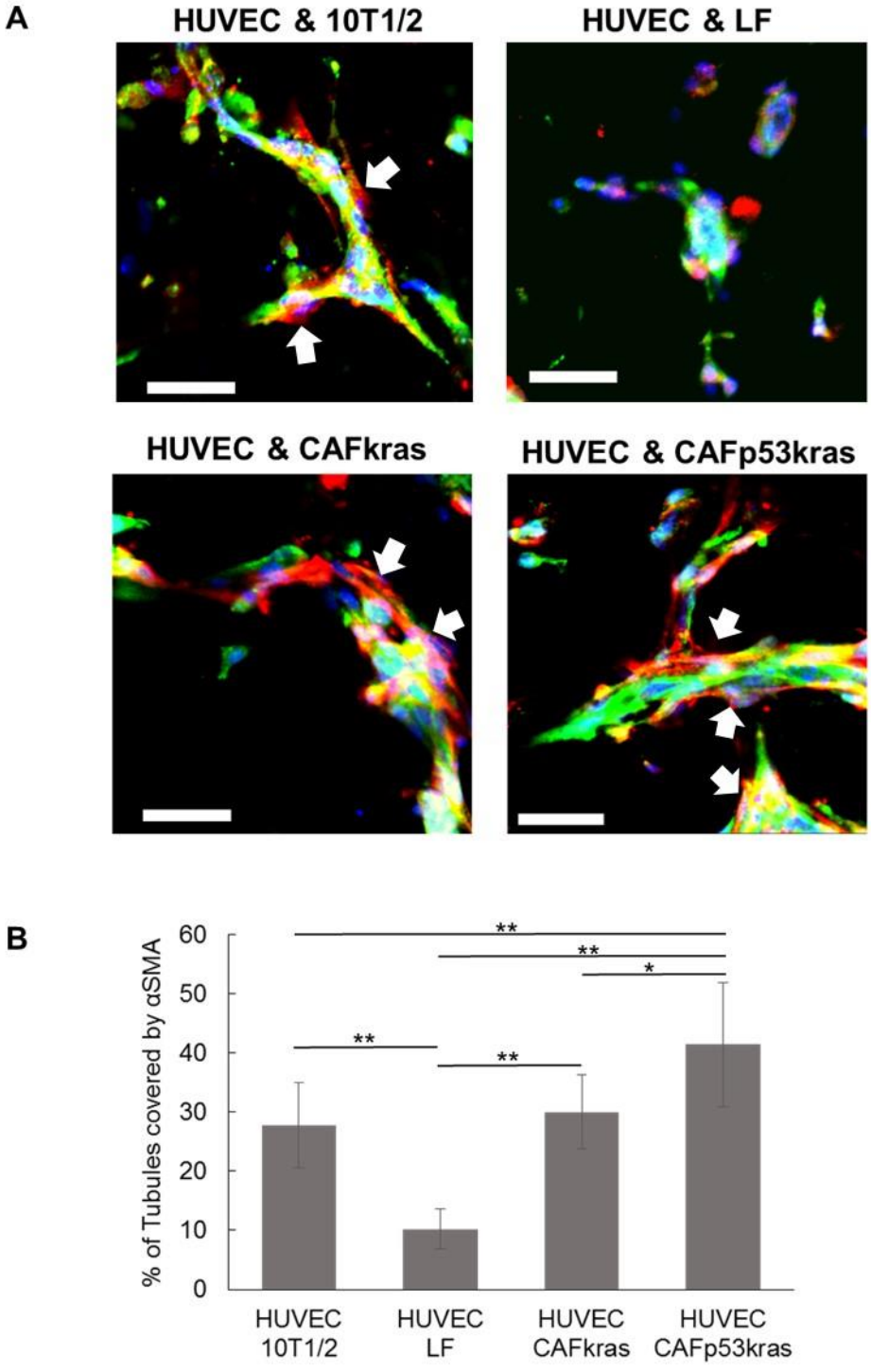


**Figure 17: Colocalization of αSMA around tubule networks. A) αSMA, a differentiation marker of smooth muscle cells shown in red, is present in pericyte-precursor 10T1/2 cells closely associating with EC tubule networks indicated by**

**white arrows. Similarly, CAFs also express αSMA and wrap PECAM-1 positive (green) ECs (pointed out in white arrows). B) Quantitative analysis on the percent of tubules covered by αSMA reveals significantly higher colocalization of αSMA positive with tubules supported by CAFp53kras cells than 10T1/2, LF, and CAFkras cells (**p<0.01). Scale Bar = 50 μm.**

Similar to the function of pericytes *in vivo*, CAFs cover the endothelial tubule network (indicated with white arrows) and thereby provide support and stabilization to the newly-formed tubules. The percent of tubules covered by αSMA positive 10T1/2 and CAF cells was quantified. The 10T1/2 pericyte cell coverage of the endothelium vessel area is partial, ranging from 20% to 35%. The highest αSMA coverage around microvessels is found in networks formed by endothelial cells supported by CAFp53kras cells. The percent of tubule networks covered by CAFp53kras cells ranges from 35% to 55% and is significantly higher than all other co-culture groups.

### 2.3.5 CAFs regulate basement membrane assembly

To determine if CAFs regulate ECM deposition, immunohistochemistry was performed visualize collagen IV and laminin in the hydrogels. Relative amounts of laminin and collagen IV were determined by measuring Alexa Fluor 488 pixel intensity and normalizing against DAPI pixel intensity. ECM proteins, such as collagen IV and laminin, are secreted during vascular development, and provide structural support to newly formed capillaries[91]. Areas of tubule structures in hydrogels were found to correspond to high amounts of collagen IV and laminin deposition (Figure 18).

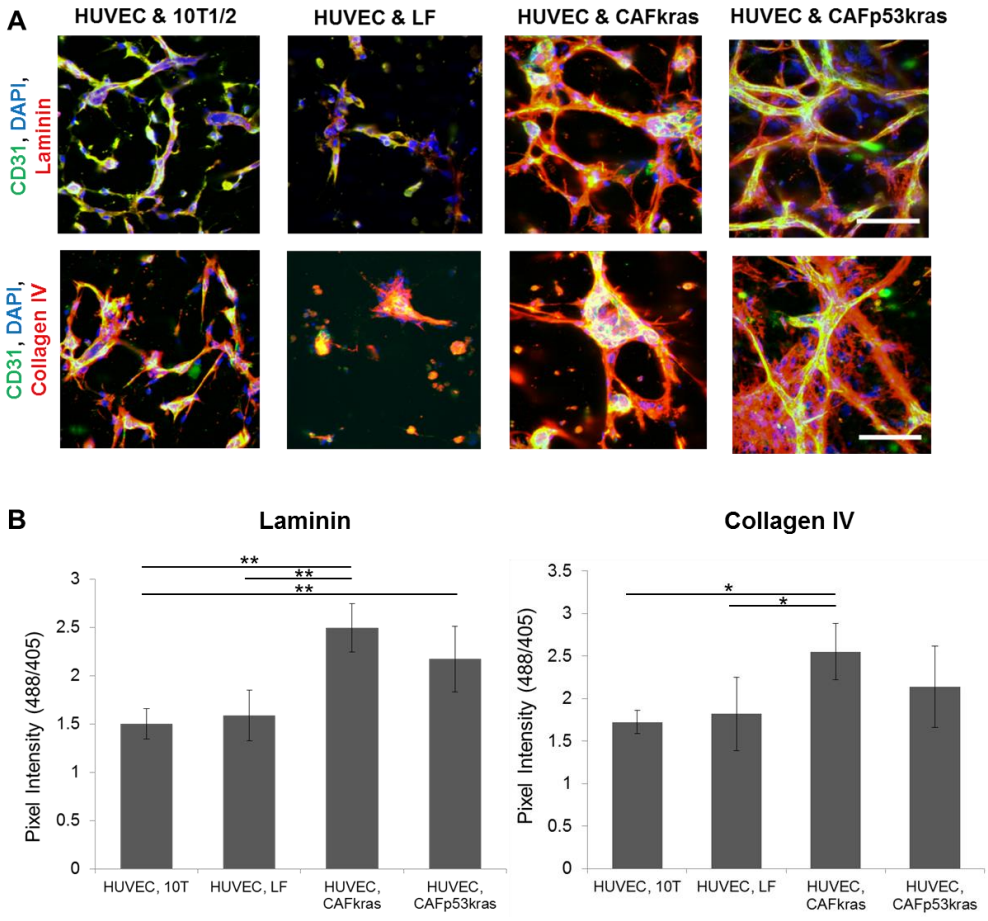


**Figure 18: Basement Membrane Assembly. A) Immunohistochemistry was performed to visualize laminin and collagen IV around tubules formed in the hydrogels. B) Areas of tubule structures in hydrogels were found to correspond to high amounts of collagen IV and laminin deposition. Laminin production was significantly higher (*p<0.05, ** p<0.01) in the co-culture of HUVEC cells with CAFp53kras in hydrogels as compared to HUVECs with LFs or 10T1/2 cells. Collagen IV production by cells was significantly higher in hydrogels with CAFkras co-cultured with HUVECs compared to the control groups. Scale Bar = 100 μm.**

Laminin production was significantly higher ($p<0.05$) in the co-culture of HUVECs with CAFp53kras in hydrogels as compared to HUVECs with 10T1/2 cells.

Collagen IV production by cells was significantly higher in hydrogels with CAFkras co-cultured with HUVECs compared to the control groups. The amount of collagen production in hydrogels with CAFkras and HUVECs was 32% greater than with LFs encapsulated with HUVECs. Moreover, laminin and collagen IV accumulation was visualized on the periphery of the tubules (Figure 18).

### 2.3.6 Secreted angiogenic proteins are required for induction of tubule formation

Growth factors play an important role in tumor growth and angiogenesis by their influence on tumor cell proliferation and neovascularization. To determine if CAFs secrete growth factors that are known to regulate the formation and stability of EC tubule networks, we screened all co-cultures with HUVECs in hydrogels VEGF-A, FGF-2, and PDGF-BB production. (Figure 19). VEGF-A and FGF-2, which stimulate endothelial cells to migrate and proliferate and are up-regulated in tissues undergoing vascularization,[117] were significantly higher in co-cultures with CAFp53kras cells. In contrast to the expression of FGF-2 and VEGF, PDGF-BB in the culture medium (Figure 19) was approximately 50% less for CAFs than for the 10T1/2 pericyte cells.

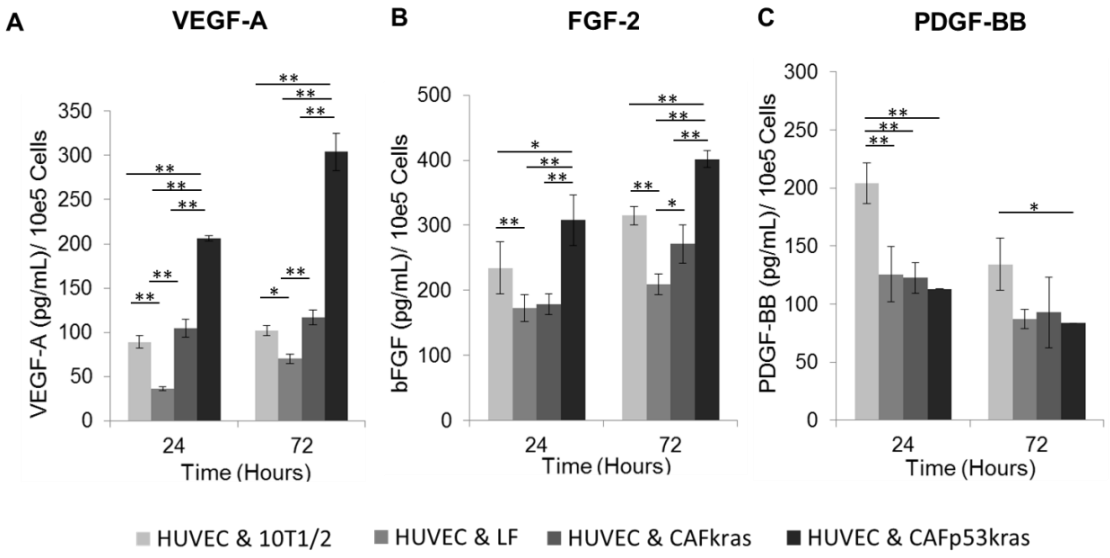


**Figure 19: Secretion of Angiogenic Proteins. A) VEGF-A, B) FGF-2, and C) PDGF-BB proteins in culture supernatant taken from co-culture of HUVEC cells with 10T1/2, normal LF, CAFkras, and CAFp53kras encapsulated in PEG hydrogels were quantified by sampling at 24 and 72 hr and evaluated using ELISA. VEGF-A and FGF-2, which are up-regulated in tissues undergoing vascularization, were expressed significantly higher in co-cultures with CAFp53kras cells at both 24 and 72 hr after placement in the hydrogels (**p<0.01). In contrast, secretion of PDGF-BB by CAFs was approximately 50% less than by the pericyte precursor 10T1/2 cells. Statistical significance performed using single factor ANOVA with a subsequent post hoc Tukey test (n=3; **p< 0.01, *p<0.05).**

The ability of HUVECs to form capillary-like structures in the presence or absence of neutralizing antibodies against VEGF-A, FGF-2, and PDGF-BB was also evaluated. The neutralization capabilities of these antibodies at a range of concentrations were first tested via a metabolic activity assay with HUVEC and 10T1/2 cells. Because VEGF-A and FGF-2 are known to stimulate endothelial cell proliferation, neutralizing antibodies against VEGF-A and FGF-2 were tested with HUVECs. Neutralizing antibody

against PDGF-BB was tested with 10T1/2 cells. Results in Figure 20 indicate that metabolic activity of HUVECs is significantly reduced upon treatment with either neutralizing antibody against VEGF-A or FGF-2 at 1 nM concentration.

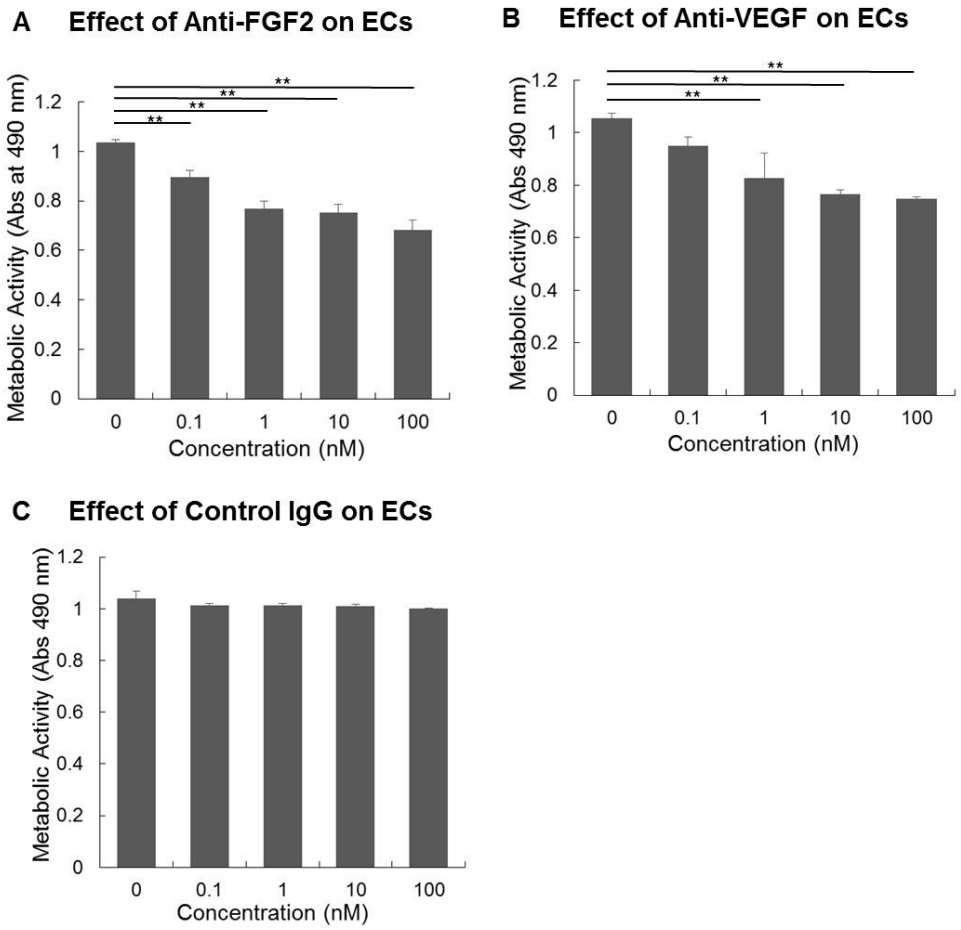


**Figure 20: A) & B) The ability of neutralizing antibodies against FGF-2 and VEGF in blocking cell metabolic activity was assessed via MTS assay with HUVECs. C) Metabolic activity of cells was also evaluated in the presence and absence of IgG isotype control antibody. Statistical significance performed using single factor ANOVA with a subsequent post hoc Tukey test (n=6; **p< 0.01, *p<0.05).**

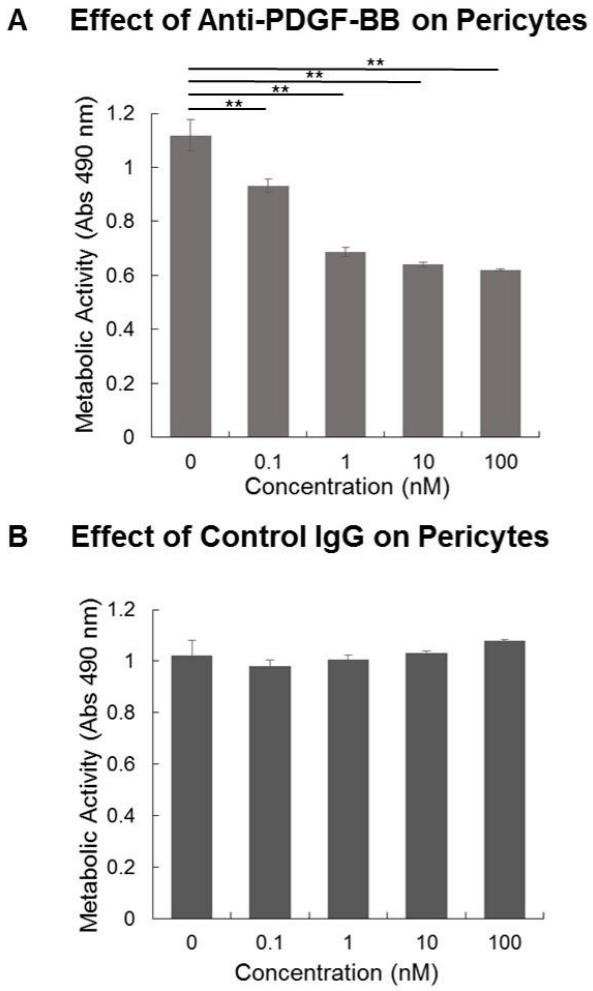


**Figure 21: Effect of neutralizing antibodies against PDGF-BB on the metabolic activity of pericytes. A) To validate the bioactivity of neutralizing antibody against PDGF-BB, metabolic activity of 10T1/2 cells in the absence or presence of neutralizing antibody was assessed via MTS assay. B) Cells were also evaluated in the presence and absence of IgG isotype control antibody. Statistical significance performed using single factor ANOVA with a subsequent post hoc Tukey test (n=6; **p< 0.01, *p<0.05).**

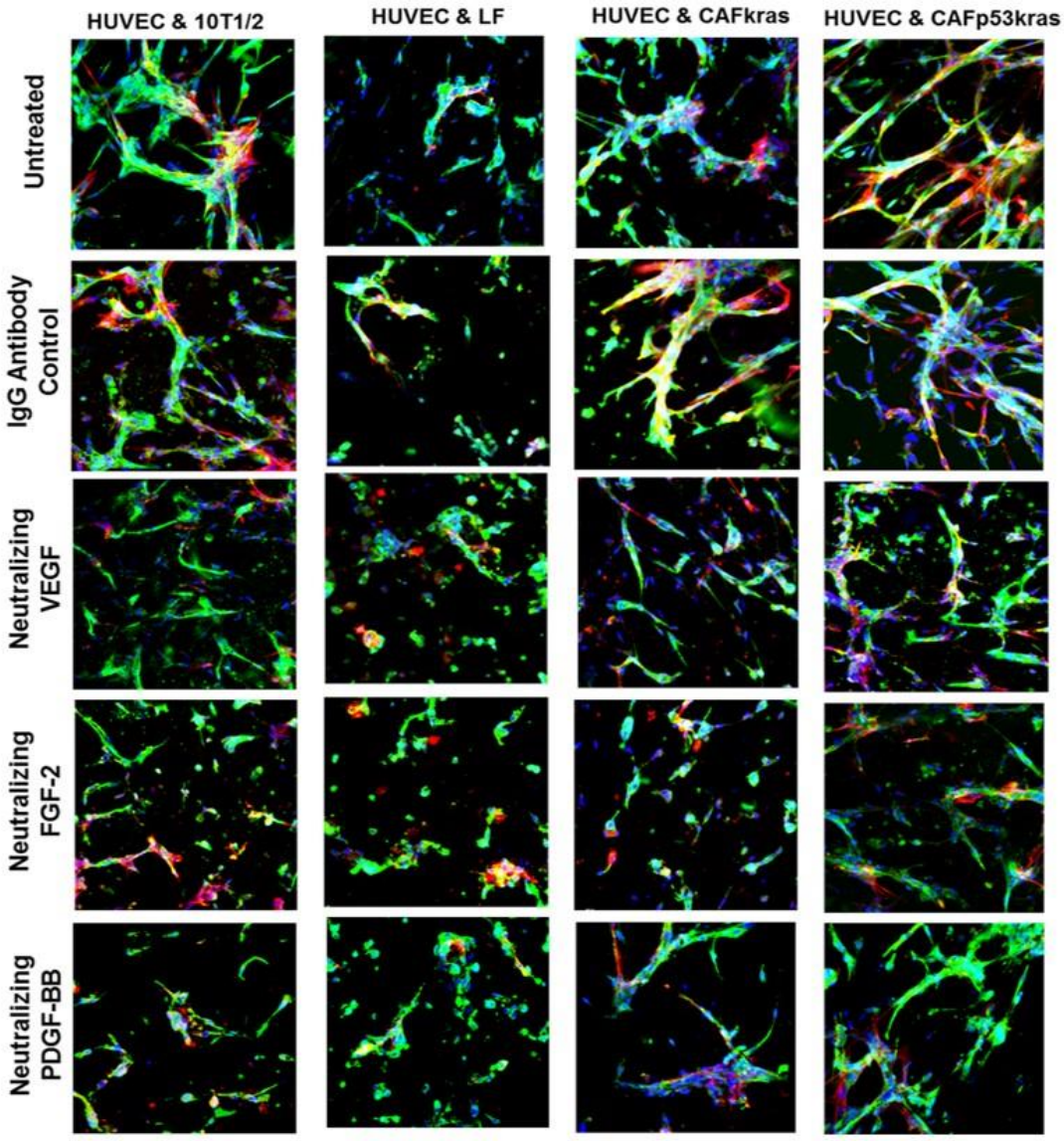


**Figure 22: Effect of neutralizing antibodies against VEGF, FGF-2, and PDGF-BB on tubule formation. HUVECs were co-cultured with 10T1/2, LF, CAFkras or CAFp53kras cells in the presence or absence of neutralizing antibodies at 100 nM concentration in both hydrogel and cultured media for 7 d. Effect of neutralizing antibodies on tubule formation was observed by immunostaining PECAM-1 (shown in green) for ECs, $\alpha$SMA (shown in red) for 10T1/2 cells or fibroblasts, and DAPI (shown in blue) for cell nuclei.**

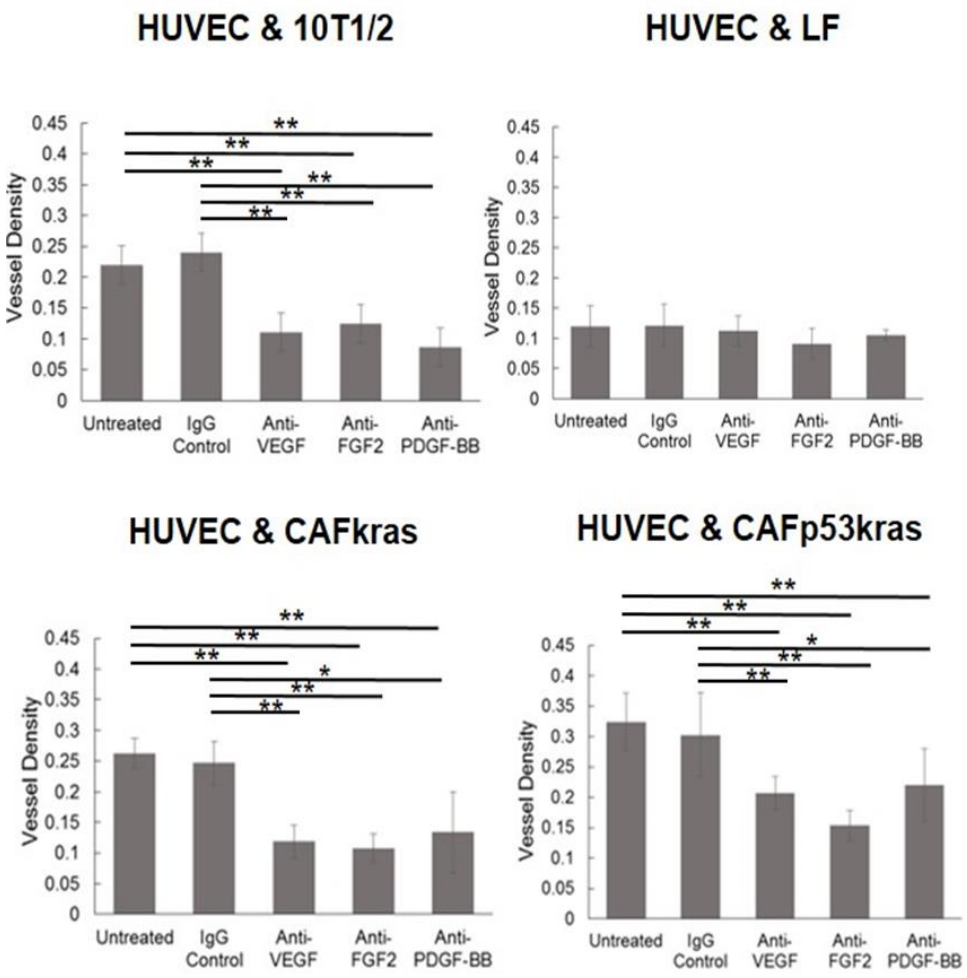


**Figure 23 : Tubule formation response to neutralizing antibodies was evaluated by quantifying vessel density in treated and untreated groups. Addition of neutralizing antibodies for FGF-2 and VEGF significantly reduced vessel formation in hydrogels with 10T1/2, CAFkras, and CAFp53kras (**p<0.01). The influence of each individual growth factor on vessel network formation was abrogated with the addition of the corresponding neutralizing antibody. Unlike the other co-culture groups, the addition of neutralizing antibodies for FGF-2, VEGF, and PDGF-BB had very little to no effect in the HUVEC & LF co-culture group. Statistical significance performed using single factor ANOVA with a subsequent post hoc Tukey test (n=8; **p< 0.01, *p<0.05).**

Similarly, metabolic activity of 10T1/2 cells measured via MTT assay was significantly blocked by neutralizing antibody against PDGF-BB at concentrations of 1 nM or higher ($p<0.01$). The initial assessment of neutralizing antibodies against VEGF and FGF-2 on HUVECs and neutralizing antibody against PDGF-BB on 10T1/2 cells showed that the metabolic activity of cells was significantly reduced at a 100 nM concentration of each of the neutralizing antibodies. Therefore, in subsequent studies, we used neutralizing antibodies blocking all three growth factors at a concentration of 100 nM. Blocking VEGF-A, FGF-2, and PDGF-BB was also tested for their effect on tubule formation. Tubule formation in the presence or absence of neutralizing antibodies against angiogenic growth factors was assessed via staining for PECAM-1 for ECs, $\alpha$SMA for 10T1/2 or CAFs, and DAPI for nuclei. Interestingly, tubules formed in co-cultures of HUVECs with 10T1/2, LF, or CAFkras cells seemed to be more affected by neutralizing antibodies than co-culture groups with CAFp53kras cells. As shown in Figure 22, the addition of neutralizing antibodies for FGF-2 and VEGF-A significantly abrogated tubule formation in hydrogels containing 10T1/2, CAFkras, and CAFp53kras cells ($p<0.01$). In contrast to cells untreated or treated with IgG control antibody, ECs and CAF cells exposed to neutralizing antibody against PDGF-BB significantly decreased the formation of branch, capillary networks ($p<0.05$).

## 2.4 Discussion

We have utilized a unique PEG hydrogel system to study the influence of important cell constituents from the tumor microenvironment on vascular development in 3D. Specifically we investigated CAFs which abundantly populate the tumor stroma and have the potential to impact the surrounding cells and the environment by secretion of various growth factors[21]. We hypothesized that the secreted molecules produced by CAFs could enhance tumor vascularization and modify vessel development. To test this hypothesis, CAFs were isolated from non-metastasis associated lung tumors of Kras-mutant mice (CAFkras) and from metastasis associated tumors of mice expressing both the Kras and p53 mutations (CAFp53kras). CAFs were tested and compared with normal lung fibroblasts and pericyte-precursor 10T1/2 cells. First, differences in $\alpha$SMA and S100A4 expression amongst the different lung-derived cells was assessed by immunofluorescence staining. There were less $\alpha$SMA positive normal lung fibroblasts as compared to CAFp53kras cells. In contrast to normal lung fibroblasts, CAFs appeared to express higher levels of $\alpha$SMA. S100A4 is a protein shown to be elevated in growth stimulated tumor cells during morphogenic conversion from an epithelial to mesenchymal phenotype[118]. Additionally, S100A4 expression levels are up-regulated during oncogenic transformation from benign to metastatic tumors[118]. Similar to $\alpha$SMA, S100A4 protein also appeared to be expressed more in CAFp53kras cells as compared with normal lung fibroblasts and CAFkras cells.

The phenotype dissimilarities amongst the non-metastatic prone versus metastatic prone CAFs and normal lung fibroblasts and 10T1/2 cells led us to question if these cells have varying capabilities in inducing endothelial cell (ECs) organization into vessel-like networks. Visible differences in the formation of vessel-like networks were observed when ECs were co-cultured with CAFs and normal lung fibroblasts in 3D in PEGDA hydrogels. The degree of vessel network formation varied with the metastatic potential of the CAFs. For example, CAFs from lung tumors in p53 and Kras mutant mice induced vessel formation with a particularly heightened response compared to CAFs from mice that express the K-ras$^{G12D}$ allele alone, which develop lung adenocarcinomas that do not metastasize. In comparison with all other co-culture groups, CAFp53kras cells in association with ECs arranged in tubule networks with significantly greater total tubule length per volume and vessel density. Heterogeneity in the degree of vessel formation in lung tumors varying in metastatic potential is consistent with previous findings[59,119]. Tubule networks formed by HUVECs and CAFp53kras were dissimilar to tubules formed by HUVECs and 10T1/2 cells. Tubule networks generated by ECs co-cultured with CAFp53kras cells exhibited more extensive branching. Quantitative analysis of changes in vessel architecture and formation also revealed differences in tubule diameter between the groups tested. Tubules generated by ECs co-cultured with CAFp53kras cells were significantly smaller in diameter than tubules formed by HUVECs and 10T1/2. Extensive branching and smaller diameter are characteristics of vessels found in tumors as opposed to vessels in normal tissues[61]. The

endothelial tubular structures formed by HUVECs and 10T1/2 cells are more similar to capillary structures in their cellular organizations and morphology found in healthy, non-pathological tissues *in vivo*[55,91].

Similar to the 10T1/2 pericyte cells, CAFs also express αSMA and make specific focal contacts with endothelial cells. The close association of mural cells like pericytes with endothelial cells in the blood vessel wall is a crucial behavior for vessel maturation, stabilization, and maintenance. One of the causes for abnormal vascular morphogenesis is the lack of pericytes wrapping the vessel endothelium, leading to abnormal junctions and vascular leakage. By wrapping around endothelial cells and providing support to newly formed vessel-like structures, CAFs exhibit at least some of the functions and properties of mural cells or pericytes. The percent of tubule coverage by αSMA-positive CAF cells was quantified and compared with 10T1/2 pericyte cells. Significantly higher αSMA coverage around microvessels is found in networks formed by endothelial cells supported by CAFp53kras cells. The heterogeneity in αSMA coverage observed between the co-culture groups may reflect the variation in the morphology between CAFs and pericytes in that CAFs are elongated with multiple cytoplasmic processes encircling the capillary endothelium and covering a large vessel area whereas the 10T1/2 pericyte cells are more compact.

Another mechanism by which CAFs stabilize tubule formation may be related to the production of basement membrane proteins such as collagen IV and laminin[7,10,120]. As shown, both laminin and collagen IV accumulated in the center and close periphery of

tubules. Amount of deposition of both collagen IV and laminin was dependent on the type of cells co-cultured with the HUVEC cells. Collagen IV and laminin deposition was greater in co-cultures with CAFs and significantly higher in co-cultures with CAFkras cells as compared to the control groups. Increase in laminin is an indication of maturation of vessels while collagen IV deposition influences the structural integrity and stiffness of the basement membrane[121,122]. Previous studies suggest that the varied composition and structural organization of some ECM proteins, such as collagen, can alter ECM stiffness which in turn enhances cell growth and survival and promotes migration[123]. Furthermore, increase in collagen and laminin deposition, and enhanced MMP activity are behaviors implicated in tumor progression[51]. ECM deposition and increased tissue stiffness have been noted to enhance tumor progression through altering integrin signaling, focal adhesions, and Rho/Rho associated protein kinase pathway activation[120,124,125]. The Rho/Rho associated protein kinase pathway activation leads to beta-catenin activation, which in turn induces tumor growth, enhances endothelial cell-cell contact, and consequently, vessel formation[126].

The process of regulating vascularization requires the precise coordination of various signaling molecules to form stable and functional vessels[117,127,128]. The balance of growth factors determines whether ECs remain in a state of homeostasis or whether they proceed to the state of hyper-vascularization instigating tumor growth and metastasis[10]. CAFs found predominately in the reactive tumor stroma have been implicated to play a crucial role in tumor progression by producing specific growth factors that regulate

angiogenesis[104–106]. The aforementioned reasons led us to investigate if angiogenic growth factors secreted by CAFs could potentially correlate with proliferation and vascularization in invasive lung adenocarcinoma. We have studied the expression of a panel of angiogenic growth factors, specifically FGF-2, VEGF-A, and PDGF-BB, derived from a co-culture of HUVECs with CAFs in hydrogels. Primary CAFkras and CAFp53kras cells were evaluated in comparison with LFs. VEGF-A, which stimulates ECs to migrate and proliferate and is up-regulated in tissues undergoing vascularization[117], was expressed significantly higher in co-cultures with CAFp53kras cells at both 24 and 72 hr after placement in the hydrogels. This finding suggests that metastatic prone lung adenocarcinoma derived CAFs could signal ECs to migrate into lung tumors and interact with CAFs to form vessels.

Similar to VEGF-A, the expression of FGF-2 was significantly higher in co-cultures with CAFp53kras cells than all other groups. FGF-2 is involved in a wide range of activities that includes promotion of angiogenesis, chemotaxis, cellular differentiation and tissue repair[129,130]. Tumor expression of both VEGF-A and FGF-2 is associated with poor survival and metastatic prone outcomes[131]. In a study involved in evaluating concentration of FGF-2 and VEGF-A in serum samples from cancer patients with metastatic carcinomas, investigators observed a positive correlation between the progression rate of metastatic lesions and tumor microvessel density with a higher expression of both growth factors[131]. Imbalanced production of angiogenic growth factors, for instance high levels of VEGF-A expression, may explain the unusual features

found in tumor blood vessels. The tumor vasculature usually consists of unstable, disorganized, leaky, and premature blood vessels that provide a structural basis for cancer invasion and metastasis[132].

In contrast to the expression of FGF-2 and VEGF-A, secretion of PDGF-BB by CAFs was approximately 50% less than by the pericyte precursor 10T1/2 cells. PDGF-BB growth factor affects mural cells including pericytes and PDGFR-expressing smooth muscle cells, but not ECs[133,134]. Release of PDGF-BB induces the recruitment of pericytes and/or SMCs to support and stabilize blood vessels formed by ECs[135,136]. The decreased expression of PDGF-BB observed in co-cultures with CAFs and ECs in our study could explain why progressive tumors are manifested with high degree of disorganized primitive blood vessels. These primitive vessels may be poorly coated with pericytes, or perhaps the pericytes are displaced by CAFs. Previous studies have found that deletion of PDGF-BB in mice leads to the formation of leaky and hemorrhagic blood vessels due to the lack of pericytes and vascular SMCs supporting and stabilizing nascent vessel structures[137].

Our results suggest that survival of ECs and enhancement of vessel sprouting is dependent upon exogenous angiogenic-specific growth factors. To support this idea, we tested the effects of blocking antibodies directed at VEGF-A, FGF-2, and PDGF-BB. Neutralizing antibodies bind to soluble VEGF-A, FGF-2, and PDGF-BB growth factors secreted by cells and thereby prevent their binding to cell receptors and downstream signaling. Blocking antibodies directed at VEGF-A, FGF-2, and PDGF-BB were added to

HUVEC co-cultures with CAFs, LFs, and 10T1/2 cells in hydrogels and to the culture supernatant for up to 7 d. The effect of neutralizing antibodies on tubule formation was quantified via vessel density. As a control, hydrogels were also treated with an IgG isotype antibody with no relevant specificity for any of the target proteins. Treatment with neutralizing antibodies against VEGF, FGF-2, or PDGF-BB significantly inhibited vessel formation. Strikingly, blocking VEGF and FGF-2 had a dramatic effect on ECs. Treatment with neutralizing antibodies to VEGF-A and FGF-2 disrupted endothelial cell tubule formation. Tubule structures appeared isolated or assembled in clumps of rounded cells or short, unbranched tubule cords. Hydrogels treated with neutralizing antibody against PDGF-BB exhibited a significant reduction in vessel density as compared with IgG treated hydrogels. This could be due to 10T1/2 pericyte cursor cells making less focal contacts with ECs and thereby not providing the necessary support for stable tubule networks. These studies reflect the dominant contribution of exogenous VEGF-A, FGF-2, and PDGF-BB signaling during endothelial cell tubule formation but does not exclude the involvement of other growth factors, which may vary depending on culture conditions. It is important to keep in mind that other signaling factors for ECs can be produced by tumor cells or other stromal cells. These results indicate that a mechanism by which CAFs signal endothelial cells to assemble into tubule structures is via secretion of VEGF, FGF-2, and PDGF-BB. Our results also emphasize the role that VEGF-A, FGF-2, and PDGF-BB may have as a therapeutic target of the tumor

microenvironment, specifically in stromal-infiltrating cells such as ECs and CAFs that contribute to tumor vascularization.

## *2.5 Conclusion*

The current work focused on CAFs derived from lung adenocarcinomas with varying metastatic potential and their involvement in the formation, stability, and proliferation of microvascular networks. Several findings presented in this study complement a growing body of evidence that the contribution of CAFs to tumor cell proliferation and motility include several secreted factors with various biological functions that drive the formation of tumor vessels and modulate vessel assembly. In this study conducted in 3D biomimetic hydrogel, we showed that CAFs express $\alpha$SMA and closely associate with vessel cells in a fashion similar to pericytes. These findings support our underlying hypothesis that CAFs may be pericyte precursors and play a mural cell-like role. Additionally, CAFs appear to regulate the basement membrane via secretion of ECM proteins such as collagen IV and laminin to stabilize nascent tubules. Overall, this work provides a better understanding of how the complex crosstalk established between ECs, CAFs and their surrounding ECM affects vessel formation. Controlling this complex crosstalk can provide means for developing new therapies to target vessels that potentially enhance tumor survival and growth.

# 3. Influence of ECM-derived cues in modulating vessel assembly and endothelial cell tubulogenesis

A significant portion of this chapter is from Saniya Ali, Jennifer E. Saik, Dan J. Gould, Mary E. Dickinson, and Jennifer L. West. Immobilization of cell-adhesive laminin peptides in degradable PEGDA hydrogels influences endothelial cell tubulogenesis. *BioResearch Open Access*. 2013, 2(4).

## *3.1 Introduction*

In the previous section, we observed the accumulation of laminin surrounding vessel networks composed of endothelial cells and CAFs. A mechanism by which CAFs can enhance vessel formation may be related to the production of ECM proteins, such as laminin, as vessel development is mediated by interactions between cells and the ECM[25,138]. These matrix interactions regulate several cellular functions, including adhesion, proliferation, migration, and differentiation.[139,140]

Laminins, present at high density in the microvascular basal lamina, are family of heterotrimeric glycoproteins, with each protein containing one $\alpha$, $\beta$, and $\gamma$ chain[141,142]. The $\alpha$, $\beta$, and $\gamma$ subunits characterize the functions and properties of the laminin proteins. For example, the $\alpha$ chain is central in determining integrin ligand specificity, whereas the $\beta$ subunit connects to the cytoskeleton and affects multiple signaling pathways[143].

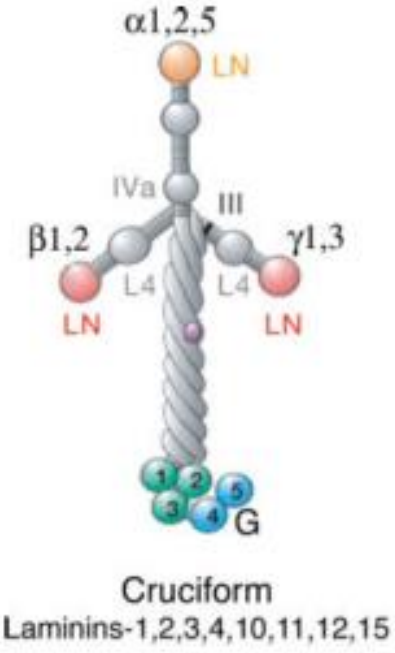


**Figure 24: The $\alpha$, $\beta$, and $\gamma$ subunits characterize the functions and properties of the laminin proteins. From Miner *et al*[141].**

Laminin can interact with cells through integrins. This integrin binding occurs at specific motifs. Several cell binding motifs based on laminin-derived peptides have been investigated to modulate cell adhesion and spreading including those based on the RGD, IKVAV, and YIGSR amino acid sequences[144,145].

The extensively studied RGD sequence is found in many ECM proteins and serves as binding motif for multiple cell surface integrin receptors. For example, HUVECs seeded upon RGDS-modified poly(ethylene glycol) diacrylate (PEGDA) hydrogels showed increased spreading and adhesion 24 h post-seeding when compared to the same cells on the unmodified polymer or polymer modified with RGES[146]. In other

work with this peptide, PEG hydrogels functionalized with protease-cleavable peptide sequences and RGDS showed that immobilized RGDS facilitated initial cell adhesion while degradation of the polymer from cell secreted matrix metalloproteinases facilitated cells to spread, migrate, and organize into capillary-like networks in co-cultures consisting of endothelial and mesenchymal stem cell progenitor cells[91]. Furthermore, adhesion and proliferation studies using HUVECs indicated that cells spread better on the RGDS-modified surface[147,148].

IKVAV, a peptide derived from the $\alpha$-chain of laminin, has been previously shown to induce endothelial cell adhesion and subsequent tubule formation[149]. In a study conducted by Grant *et al*., the IKVAV peptide demonstrated increased endothelial cell mobilization, capillary branching, and vessel formation in both a murine angiogenesis assay and experiments with the chick yolk sac/chorioallantoic membrane[150]. Immobilized IKVAV on collagen type I hydrogels, stimulated vascular endothelial cells to migrate, adhere, and form capillary networks[151]. This immobilized peptide has also been shown to mediate revascularization of ischemic tissue[152], making it of great interest to those seeking to induce microvascular networks *de novo*.

The integrin receptor ligand YIGSR, found in a cysteine-rich site of the laminin $\beta$ chain[153], has been extensively investigated as a mediator of cell adhesion[153,154]. Various studies have demonstrated that YIGSR plays a key role in endothelial cell-to-cell interactions and tubule formation[148,155,156]. In one study, incorporation of YIGSR in a polyurethane urea scaffold resulted in improvement in endothelial cell adhesion,

proliferation, migration, and ECM production[155–158]. In another study, surface presentation of both RGD and YIGSR peptides was shown to increase endothelial cell tubule formation as opposed to unmodified materials[155]. When RGD and YIGSR were tested separately, YIGSR-modified MG induced endothelial cells to organize in tubules, while RGD-modified MG only supported cell attachment, providing key evidence that these peptides have separate effects on endothelial cells[155].

In the present study, we demonstrate that the degree of endothelial cell tubule formation varies with the peptide sequences presented in the material. Laminin-derived peptides were conjugated to heterobifunctional poly(ethylene glycol) (PEG) chains and covalently incorporated in PEGDA hydrogels. In response to these immobilized peptides, encapsulated HUVECs organized into extensive networks of capillary-like structures in 3D. Pericyte precursor cells (10T1/2s) stabilized the resulting structures. Additionally, hydrogels incorporated with laminin-derived peptides and implanted in the mouse cornea stimulated the formation of functional blood vessels. This work shows that YIGSR, IKVAV, and RGD peptides have different abilities to modulate vessel assembly and long-term tubule stability both *in vitro* and *in vivo*. Based on these results, we believe that laminin derived peptides play an integral role in regulating the formation of microvasculature in tumors.

## *3.2 Materials and Methods*

### 3.2.1 Cell Maintenance

Human umbilical vein endothelial cells (HUVECs; Lonza, Walkersville, MD; passages 2-5) were grown in endothelial growth medium (EGM-2) supplemented with ascorbic acid, epidermal growth factor, fibroblast growth factor, heparin, hydrocortisone, insulin-like growth factor, GA-1000 (gentamicin, amphotericin-B), and 2% fetal bovine serum (Lonza). 10T1/2 pericyte precursor cells (American Type Culture Collection, Manassas, VA; passages 15-18) were cultured in Dulbecco's Modified Eagle's Medium (DMEM) (Gibco, North Andover, MA) supplemented with 10% fetal bovine serum and 2 mM L-glutamine, 1000U/mL penicillin, and 100 mg/L streptomycin (Sigma, St. Louis, MO). All cells were incubated at 37°C and at 5% $CO_2$.

### 3.2.2 Peptide Synthesis

The laminin-derived sequences YIGSR and IKVAV were synthesized on an APEX 396 solid phase peptide synthesizer (Aapptec, Louisville, KY) using standard Fmoc chemistry. After purification, the peptides were characterized via MALDI-ToF (Bruker Daltonics, Billerica, MA). The same methods were used to generate the protease-sensitive peptide sequence, GGGPQGIWGQGK (PQ).

### 3.2.3 Polymer Conjugation

The cell-adhesive peptide RGDS (American Peptide, Sunnyvale, CA) was conjugated to acryloyl-PEG-succinimidyl carboxymethyl (PEG-SCM, 3400 Da, Laysan

Bio Inc., Arab, AL) to form PEG-RGDS following the same synthesis and purification methods outlined in chapter 2, section 2.2.4. The PQ peptide conjugation was achieved in process similar to that for PEG-RGDS but with a PEG-SCM:PQ peptide molar ratio of 2:1 generating an MMP-degradable segment that is flanked on both sides by PEG (PEG-PQ-PEG). The same reaction and purification protocols were followed for the laminin peptides, YIGSR and IKVAV, to yield PEG-IKVAV and PEG-YIGSR. Successful conjugation of the peptide to PEG was confirmed via a gel permeation chromatography system equipped with UV-VIS and evaporative light scattering detectors (GPC, Polymer Laboratories, Amherst, MA).

### 3.2.4 Encapsulation of Endothelial Cells and 10T1/2 Pericyte Precursors in Degradable Hydrogels

HUVECs and 10T1/2 cells were encapsulated in degradable hydrogels in order to observe the effects of covalently immobilized IKVAV and YIGSR on tubule formation. HUVEC and 10T1/2 cells were encapsulated at ratio of 4:1. Hydrogels were formed from prepolymer solutions composed of 10% (w/v) PEG-PQ-PEG in sterile HEPES buffered saline (HBS) containing 1.5% (v/v) triethanolamine, 1 mM eosin Y, and 3.95 μL/mL N-vinyl-2-pyrrolidone (NVP). PEG-peptides were added to the prepolymer solution to create four treatment groups: (1) 3.5 mM PEG-IKVAV, (2) 3.5 mM PEG-YIGSR, (3) 3.5 mM PEG-IKVAV with 1.0 mM PEG-RGDS, and (4) 3.5 mM PEG-YIGSR with 1.0 mM PEG-RGDS. A prepolymer solution containing 3.5 mM PEG-RGDS alone was used as a control group. HUVECs and 10T1/2 were harvested using trypsin-EDTA and pelleted by

centrifuging at 700 x g for 4 min. The cell pellets were then resuspended in the prepolymer solutions to concentrations of 10,000 cells/μL. 5 μL droplets of cell-laden polymer were sandwiched between a Sigmacote® functionalized (prepared as described below, Sigma, St. Louis, MO) glass slide and a methacrylate-modified cover glass (prepared as described below) separated by a 380 μm polydimethylsiloxane (PDMS) spacer. For the process and protocols on preparation of Sigmacote® functionalized glass slide and Methacrylate-modified coverslips, please refer to Chapter 2, Section 2.2.5. The solutions were cross-linked under white light at a power of 200 mW/cm$^2$ for 35 s to form hydrogels that were then immersed in EGM-2 media and incubated at 37°C in a 5% $CO_2$ environment for up to 28 d. Media on the hydrogels was replenished every other day.

### 3.2.5 Assessing Tubule Morphology and Extracellular Matrix Protein Production

Endothelial cell tubule formation was evaluated by measuring total tubule length per volume and average tubule diameter in hydrogels that were stained to visualize actin filaments and cell nuclei. Hydrogels were first fixed in 4% paraformaldehyde for 20 min and then washed with phosphate buffered saline (PBS, pH 7.4). Next, a 0.5% Triton-X solution was added for 30 min to permeabilize encapsulated cells. Following another PBS wash, nonspecific binding was blocked by incubation with 1% bovine serum albumin (BSA) overnight. Gels were finally exposed to a 1:100 dilution of rhodamine phalloidin (Invitrogen, Carlsbad, CA) containing 2 μM of 4',6-diamidino-2-phenylindole (DAPI) in HBS with 0.1% BSA for 2 h to stain actin and cell nuclei, respectively. The

hydrogels were visualized using a confocal microscope (Zeiss 5-LIVE, Plan-Apochromat 20x objective with 0.8 NA) with a z-stack depth of 20 μm. Imaris analysis software (Bitplane Inc., South Windsor, CT) was used to trace and measure tubule length and tubule diameter in three fields of view for each hydrogel (n = 3 hydrogels per experimental group, FOV =318 μm x 318 μm)[73,159].

To visualize collagen IV and laminin, hydrogels were first blocked with 1% BSA overnight and then incubated with primary antibodies on a rocker table at 4 ˚C for an additional overnight period to insure antibody infiltration into the samples. For these studies, primary antibodies included rabbit anti-collagen IV (1:100 in PBS with 0.1% BSA, Abcam, Cambridge, MA) and chicken anti-laminin (1:200 in PBS with 0.1% BSA, Sigma, St. Louis, MO). Hydrogels were rinsed in PBS five times at one-hour intervals and then incubated with a 1:400 dilution of Alexa Fluor 488 donkey anti-rabbit IgG (Invitrogen) or Alexa Fluor 488 goat anti-chicken IgG (Invitrogen) overnight at 4 ˚C to visualize the primary antibodies. Subsequently, samples were rinsed with PBS and then imaged using a confocal microscope under a 20x objective. Image slices of 1 μm thickness from a z-stack of 20 μm deep in the gel were taken for three fields of view from each of three hydrogels. Relative amounts of laminin and collagen IV were determined by measuring Alexa Fluor 488 pixel intensity in ImageJ (National Institutes of Health, Bethesda, MD), and normalizing against DAPI pixel intensity.

### 3.2.6 In vivo Angiogenesis Assay: Hydrogel Implantation into the Mouse Cornea

All animal procedures in this study were approved by the Institutional Animal Care and Use Committee (IACUC) at Baylor College of Medicine. In order to assess the effects of laminin peptides on tubule formation *in vivo*, degradable PEGDA hydrogels were implanted into the corneas of *Flk1-myr::mCherry* transgenic mice according to previously published procedures[160]. These transgenic mice express an endothelial cell specific fluorescent protein that allows formed tubules to be visualized via fluorescence microscopy[161]. Briefly, a Von Graefe knife was used to generate micropockets by partial thickness incisions into the cornea of anesthetized mice. Hydrogels were formed from prepolymer solutions composed of 10% (w/v) PEG-PQ-PEG in sterile HBS containing 10 μL/mL of 300 mg/mL 2,2-dimethoxy-2-phenylacetophenone (DMAP) in NVP and 320 ng soluble PDGF-BB & 80 ng FGF-2 per gel. PDGF-BB and FGF-2 were added to the gels to initiate the angiogenic response of vessels from the limbus of the eye. PEG-peptides were added to the prepolymer solution to create four treatment groups: (1) 3.5 mM PEG-IKVAV, (2) 3.5 mM PEG-YIGSR, (3) 3.5 mM PEG-IKVAV with 1.0 mM PEG-RGDS, and (4) 3.5 mM PEG-YIGSR with 1.0 mM PEG-RGDS. A prepolymer solution containing 3.5 mM PEG-RGDS alone was used as a control. Once hydrogel solutions were formulated, 0.12 μL of polymer solution was injected into a mold made of two glass slides separated by a 125-μm PDMS spacer. Following 2 min of exposure to ions wavelength UV light (365 nm, 10 mW/cm$^2$), the polymerized gels were immediately implanted in the cornea

micropockets. For analysis of blood vessel structure and angiogenesis, mice corneas were harvested 7 d post-implantation and fixed in 4% formaldehyde. A 543 nm laser on the Zeiss LSM 510 META confocal microscope (Plan Apochromat 20X/0.75 NA objective) was used to excite the *mCherry* fluorophore in order to visualize and acquire z-stack images of endothelial cells that had migrated and invaded into the modified hydrogels. FARSIGHT software (http://farsight-toolkit.org/wiki/Main_Page) was used to measure vessel diameter and count vessel branch points in the acquired images (n =5-7).

### 3.2.7 Statistics

Single factor ANOVA and subsequent Bonferroni post hoc tests were used to analyze vessel formation and extracellular matrix production. For each analysis, $p < 0.05$ was considered to be significant.

## *3.3 Results*

### 3.3.1 Encapsulated Endothelial Cells Exposed to Laminin-derived Peptides Form Tubule Networks

HUVECs and pericyte-precursor cells encapsulated in degradable PEGDA hydrogels underwent tubulogenesis with the extent of this response dependent upon the combination of laminin-derived peptides included in the polymer matrix. The tubule networks were visualized as early as 7 d after encapsulation by staining for cell nuclei via DAPI and actin filaments via phalloidin (Figure 25). Tubules persisted up to 28 d, with the highest tubule formation response observed in hydrogels with both PEG-YIGSR and PEG-RGDS. The tubule formation response to immobilized peptides was

quantified for average tubule diameter and total tubule length. All groups, when compared individually, showed an increase in tubule diameter and total tubule length per volume over time (Figure 25). Additionally, cells that were exposed to a combination of PEG-YIGSR and PEG-RGDS had a significantly higher tubule length and tubule diameter when compared with all other treatment groups (*p<0.05).

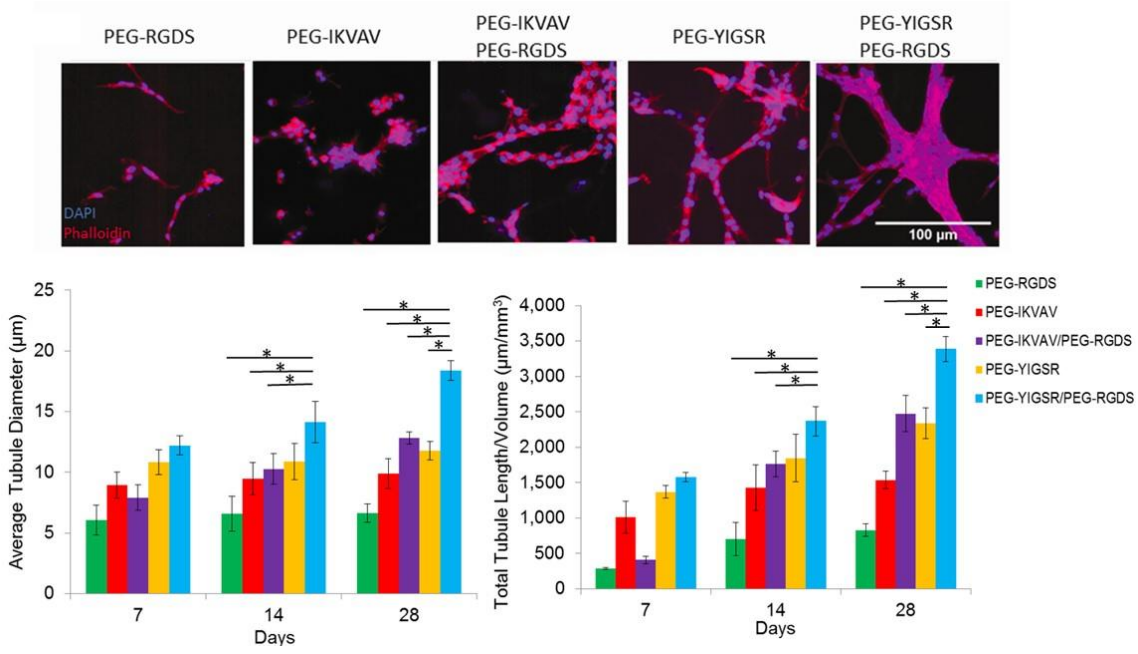


**Figure 25: Images of cells labeled with DAPI for nuclei (blue) and phalloidin for actin filaments (red) in modified hydrogels were taken after 7 d in culture. To quantify the resulting tubule formation *in vitro*, the average tubule diameter and total tubule length per volume were calculated (*p<0.05).**

### 3.3.2 Collagen IV and Laminin Expression in Tubule Networks

Extracellular matrix proteins are generated by vessel cells in the process of tubule formation and establishment of long-term stability. In light of this,

immunohistochemistry was performed to measure production of collagen IV and laminin in the experimental hydrogels.

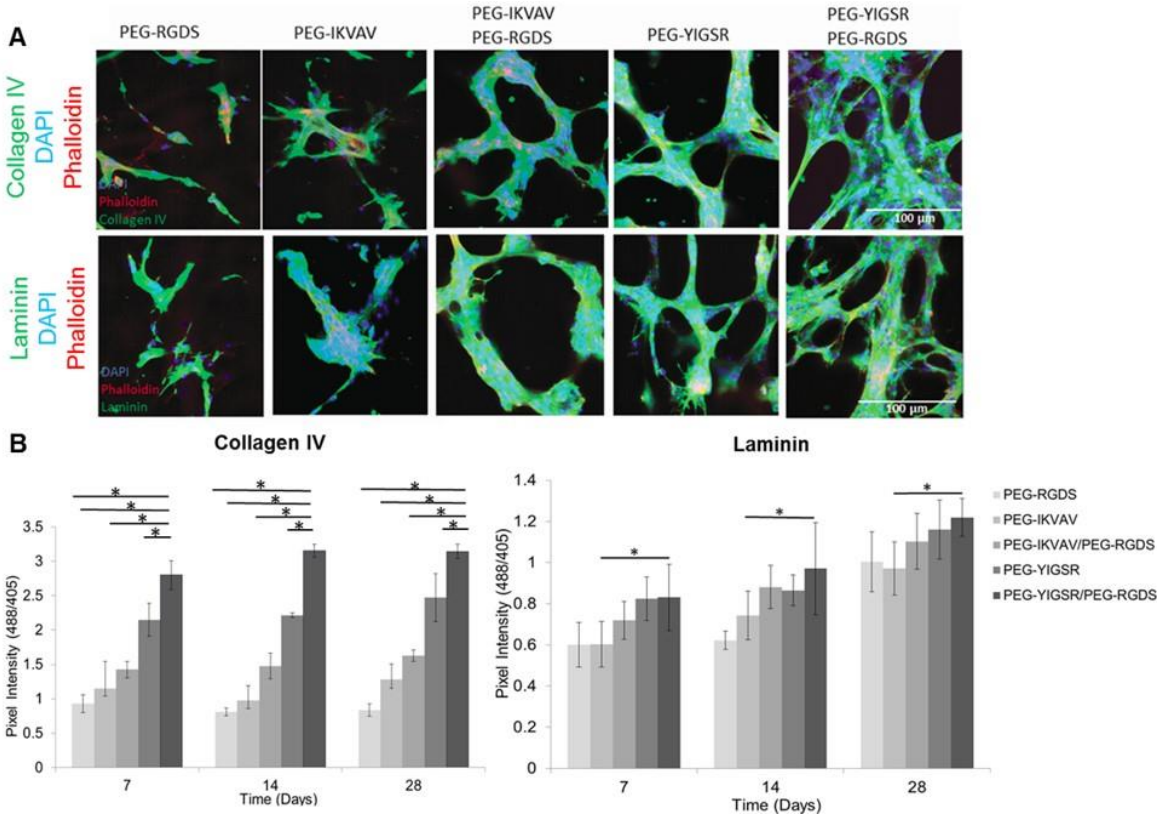


**Figure 26: The amount of ECM proteins produced by tubules is dependent on the type of peptide presented to encapsulated cells. Images of cells in modified hydrogels (A) were taken after 14 d in culture (B) Collagen IV and laminin deposition was quantified and found to correspond to areas of high tubule formation. (*p<0.05)**

Regions of defined tubule formation in hydrogels were found to correspond to areas with high amounts of collagen IV deposition (as measured by pixel intensity). Specifically, cells exposed to a combination of PEG-YIGSR and PEG-RGDS showed the highest expression of this important ECM protein (Figure 26), which was further found

to increase over time and to be dependent on the type peptide sequences presented. In treatment groups with PEG-YIGSR alone and combinations of PEG-IKVAV or PEG-YIGSR with PEG-RGDS, the amount of collagen IV increased significantly from 7 d to 28 d ($p<0.05$) as tubules were stabilized and maturing. For all time points, collagen IV production by cells was significantly higher ($p<0.01$) in gels with PEG-YIGSR as compared to those with PEG-IKVAV. Furthermore, the addition of PEG-RGDS to PEG-IKVAV or PEG-YIGSR induced more collagen production than when PEG-IKVAV or PEG-YIGSR was presented alone. For example at 14 d, the amount of collagen production in hydrogels with PEG-YIGSR co-immobilized with PEG-RGDS was 35% greater than with PEG-YIGSR alone.

Laminin deposition was also highly dependent on the peptide sequences presented as evidenced by significantly higher ($p<0.05$) protein accumulation in all treatment groups containing PEG-YIGSR as compared to those with PEG-IKVAV alone (Figure 26). Specifically, at 7 d hydrogels with PEG-YIGSR contained 25% more laminin than those with PEG-IKVAV.

### 3.3.3 PEG-laminin Peptides Enhance the *In Vivo* Vascular Response

To investigate the impact of laminin derived peptides *in vivo*, hydrogels were implanted into corneal micropockets created in *Flk1-myr::mCherry* transgenic mice. Using this established angiogenesis assay[91,160], we demonstrate that the addition of IKVAV and YIGSR peptides to PEGDA hydrogels enhances cell organization into vessel

networks as visualized by the mCherry fluorescence of mouse endothelial cells (Figure 27). Soluble PDGF-BB and FGF-2 were added to the hydrogels with immobilized peptides to induce angiogenesis from the limbal vessels of the eye. Covalent immobilization of either PEG-IKVAV or PEG-YIGSR with PEG-RGDS produced tubules with a significantly greater vessel density and tubule branching than did treatment groups with either peptide alone ($p<0.01$). Conversely, presentation of PEG-IKVAV in combination with PEG-RGDS induced vessels of smaller diameter, suggesting that the type of peptide presented to cells for attachment plays a critical role in determining vessel morphology.

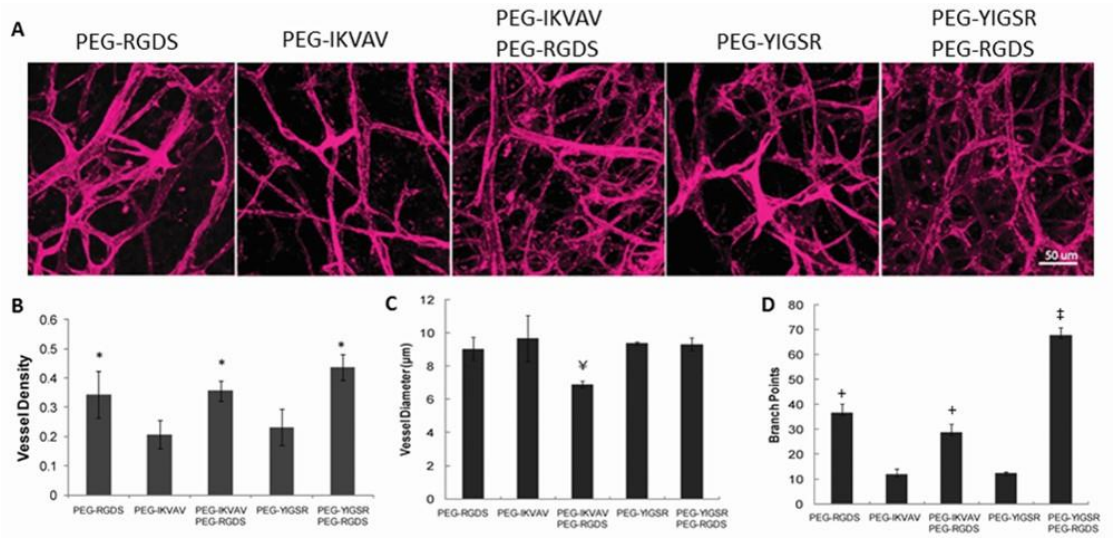


**Figure 27: Images of the angiogenesis response to modified hydrogels implanted in the cornea (A) were taken after 7 d post-implantation. For analysis of angiogenesis and blood vessel structure, (B) vessel density, (C) vessel diameter, and (D) branch points were calculated. * significantly different from PEG-YIGSR and PEG-IKVAV ($p < 0.01$). ¥ significantly different from all other groups ($p < 0.05$). ‡**

**significantly different from all other groups ($p<0.01$). + significantly different from PEG-YIGSR and PEG-IKVAV ($p<0.05$)**

## *3.4 Discussion*

A mechanism by which tumor angiogenesis is regulated involves cell adhesion and interaction with ECM. Cell surface integrins recognize and bind to short peptide sequences on ECM proteins which can then initiate signaling events that exert cellular effects. Previous studies have shown laminin, the predominant glycoprotein in the basement membrane, to simulate tumor cell adhesion[162], migration[163], and metastasis[162,164]. We postulate that laminin may also contribute to tumor growth and metastasis by promoting tumor angiogenesis.

To investigate this theory, in our current work we explored the effects of cell binding motifs based on laminin-derived peptides on tubule formation and angiogenesis. Specifically, immobilized RGDS, YIGSR, and IKVAV, which are known to influence cell migration and invasion, were investigated. In 3D degradable scaffolds, PEG-YIGSR and PEG-IKVAV alone and in combination with PEG-RGDS induced HUVEC tubule formation as early as 7 d and tubules maintained up to length of the study (4 weeks). Immobilized laminin-derived peptides enhanced cell-cell interactions and promoted the formation of long-lasting tubule structures. In comparison with all other treatment groups, cells exposed to PEG-YIGSR in combination with PEG-RGDS arranged in stable tubule networks with a significant increase in total tubule

length/volume and average diameter over a 4-week period. This rapid increase in vascularization is a desirable effect for sustained tumor cell survival and proliferation over a long period of time. At 28 d, tubules in hydrogels with PEG-YIGSR & PEG-RGDS were 86% greater in tubule length/volume than those with only PEG-RGDS. The biological effects of YIGSR are mediated by its binding to 67 kDa laminin receptor[157,165]. The 67 kDa laminin receptor mediates cell attachment and spreading. Increased expression of the receptor correlates with cell proliferation and migration[165]. Endothelial cells have been reported to express high levels of 67 kDa laminin receptor that is localized with actin filaments[166]. The carboxyl terminal of 67kDa laminin receptor binds to the peptide YIGSR which induces down regulation of mitogen-activated protein kinase phosphatase-1 (MKP-1) expression and dephosphorylation of mitogen-activated protein kinase (MAPK)[165]. Higher MAPK activity induced by the 67 kDa laminin receptor has been previously correlated with expression of matrix metalloproteinases and enhanced vessel invasion, growth and angiogenesis[167].

The trend of increased vessel growth in the presence of YIGSR correlates well with previous *in vivo* and *in vitro* studies that have shown that YIGSR promotes attachment, proliferation, migration, and spreading of endothelial cells[154,155,157,158]. In a recent study, endothelial cells seeded in polyurethane urea-modified PEG scaffolds containing YIGSR showed higher levels of cell migration and collagen production[158]. Other studies have shown that when RGDS and YIGSR sequences were covalently attached to amine-modified glass, endothelial cell attachment and spreading were

enhanced significantly[168]. Although RGDS has been shown to promote cell binding, YIGSR enhances cell-to-cell interactions[155,157]. Results from our current study suggest that if RGDS and YIGSR are presented simultaneously from the commencement of complex cell interactions, their additive signaling promotes formation of mature, stable vessels. In fact, vessel density was significantly higher in hydrogels with both YIGSR and RGDS then hydrogels with YIGSR alone. The possibility of an additive effect is further supported by the fact that collagen IV production for the PEG-RGDS/PEG-YIGSR combination was significantly greater for the duration of the 4 weeks as compared to any of the other experimental groups. The *in vivo* results corroborate this finding with a significantly greater vessel density and more extensive branching for the PEG-YIGSR/PEG-RGDS treatment as compared to PEG-YIGSR alone. After only 7 d *in vivo*, the average blood vessel density under combined PEG-YIGSR and PEG-RGDS conditions was approximately twice that of hydrogels with only PEG-RGDS or only PEG-YIGSR. This suggests that the presence of the RGDS peptide further enables YIGSR to initiate formation of complex, defined vasculature. Previous studies have demonstrated the combination of these two peptides[25,168]. In a study of bovine artery cell adhesion, cells exposed to YIGSR and RGDS sequences in combination adhered more readily to amine-modified[168]. The additive effect was also observed in modified fluorinated ethylene propylene films, which displayed greater neural cell aggregation and anchorage in the presence of the two peptides[25]. These combination effects on cell

adhesion, aggregation, and motility increase the likelihood that such a relationship may hold true for tubule formation in tumor angiogenesis as well.

Hydrogels modified with laminin-derived peptides and implanted in the mouse cornea induced vessel formation, with a particularly heightened response when the materials contained a combination of YIGSR and RGDS. Tubules formed in gels with YIGSR or IKVAV co-immobilized with RGDS displayed higher vessel density *in vivo* than gels with YIGSR or IKVAV alone. Similar findings were illustrated when combinations of cell adhesion peptides derived from laminin (YIGSR and PDSGR) and fibronectin (PHSRN and RGDS) were covalently attached to a poly(dimenthylsiloxane) substrate to facilitate the adhesion of corneal epithelial cells[169]. Multiple peptides on the substrate resulted in greater adhesion than modification with the individual peptides. Results *in vivo* also show that the response to a YIGSR-RGDS combination includes vessels of higher branch points than all other groups. These results suggest that specific combination of these laminin-derived motifs results in different vessel morphologies. Higher vessel density and branching are morphological characteristics of vessels observed in tumors[60,170]. Weidner and colleagues evaluated women with invasive breast adenocarcinoma and found an increase in risk of tumor metastasis of 1.17 fold for every 10 fold increase in microvessel density as compared to women without metastatic tumors[171]. In addition to vessel density, vessel branching count has also been found to have a positive correlation with aggressive tumor growth in patients with astrocytic brain tumors[172]. The correlation between vessel morphologies in tumors reported in

previous studies and the vessel response observed in our hydrogels with immobilized laminin-derived peptides suggests that YIGSR and IKVAV may be cell binding domains that are functionally important in tumor angiogenesis and may be responsible in producing the morphological characteristics of tumor vessels.

The mechanism by which laminin-derived peptides stabilize vessel formation may be related to production of basement membrane proteins, including laminin and collagen IV, as the ECM layer is necessary for tissue development and vessel stabilization[138,173]. In the current work, the accumulations of both laminin and collagen IV were shown to depend on the type and combination of peptides presented, and laminin deposition, in particular, varied significantly with time in culture. Previous studies suggest that the varied composition and structural organization of the ECM during vessel development may have important effects on endothelial cell behavior and tubule morphogenesis[25,138]. In this process, the maturation of vessels is accompanied by an increase in laminin[174,175], and collagen IV influences the structural integrity of the basement membrane[176,177]. Endothelial cell binding to laminin and collagen IV is mediated by integrins and influences cell migration and proliferation[174–177]. Cell binding to both proteins is mainly mediated by the $\alpha_v\beta_3$ integrin, which is the same integrin that was shown to induce endothelial cell adhesion in response to immobilized peptide fragments such as IKVAV and YIGSR[178]. Several findings suggest that laminin fragments such as IKVAV and YIGSR can induce greater susceptibility to cell-triggered proteolysis, which permits tumor cell invasion and subsequent ECM matrix remodeling, both of

which are necessary for vessel formation and tumor angiogenesis[179,180]. In addition to endothelial cells, $\alpha_v\beta_3$ integrin is also expressed on a variety of tumor cells and has been shown to stimulate MMP activity[181,182] and release of growth factors such as TGF[182,183] that can promote tumor progression. As such, inhibition of $\alpha_v\beta_3$ integrins to prevent ligand binding and thereby disrupt cell interactions with the ECM could potentially serve as a treatment option for reducing tumor angiogenesis and growth.

## 3.5 Conclusion

In this study, we have shown that ECM-derived motifs, which are known to regulate the adhesion, migration, and proliferation of endothelial cells, instigated the formation of stable vessel-like networks both *in vitro* and *in vivo* [149,156].The covalently immobilized cell adhesion ligands PEG-RGDS, PEG-IKVAV, and PEG-YIGSR have differing effects on tubule formation when presented to endothelial and pericyte precursor cells individually or in combinations. Presentation of PEG-RGDS and PEG-YIGSR together induced greater tubule length and diameter *in vitro*, while resulting in greater vessel density and branching *in vivo*. The results of this study indicate that laminin derived peptides localized in a matrix can enhance the formation of blood vessels. These findings can be exploited as a strategy to inhibit cell survival and angiogenesis in growing tumors by targeting integrin binding motifs. Inhibiting integrin binding may be an attractive strategy for cancer therapy.

# 4. 3D *In Vitro* Lung Adenocarcinoma Model as a Drug Testing Platform of Anti-Angiogenesis Drugs

## *4.1 Introduction*

The rise in the development of new anticancer agents presents a great challenge to the cancer research community to evaluate, identify, and incorporate promising drug candidates into clinical practice. Evaluation of anticancer agents depends on the interaction of *in vitro*, preclinical, and clinical research where ideally results from *in vitro* studies and preclinical animal models converge towards clinical trials and eventually to standard of patient care[184]. However, in current practice the translational process is not so straightforward. In many cases, drugs candidates that are shown to be effective on tumor cells in *in vitro* studies show nominal effect on tumors in animals or humans[184–186]. Many drugs that are tested through the use of standard *in vitro* methods for high efficacy and low toxicity and that are selected as promising drug candidates tend to fail in clinical trials[184–187]. In fact, more than 95% of anti-cancer drug candidates fail in clinical studies[188]. One reason for this is that the experimental models utilized commonly in cancer therapy research and drug discovery do not represent the disease state sufficiently.

The validity of an experimental model depends on how closely it mimics *in vivo* conditions. For decades, cancer studies have used 2D monolayer cultures to evaluate the safety and efficacy of anti-cancer agents. Two-dimensional studies involve functional assays where monolayer of cells are exposed to different drug concentrations and

response is monitored via metabolic or proliferation assays[63]. In general, *in vitro* studies are essential to the development and testing of anti-cancer therapies. They have the potential to facilitate the selection of promising drug candidates and the effective dosage for translation to preclinical and clinical studies. Additionally, to move forward to preclinical studies with animals and receive approval by the Institutional Animal Care and Use Committee (IACUC), data and results are required from *in vitro* studies to develop protocols for studies in animals. Compared to animal tumor models, *in vitro* methods are less expensive and less time consuming, thereby allowing higher throughput evaluation of multiple anticancer agents. Despite their importance for anti-cancer drug testing, 2D *in vitro* methods fail to mimic the natural phenotype and behavior of cells exhibited in the target tissue microenvironment[189].

For preclinical studies, animal *in vivo* xenograft models are most commonly used[190,191]. In these models, human tumor explants and cells are transplanted usually subcutaneously into immunocompromised mice so that they do not reject the transplantation of human cells. Although there are several advantages to using human tumor xenografts, these models do not permit the manipulation of or independent control over parameters that affect tumor progression and vascularization such as mechanical forces, nutrient gradients, cell-cell interactions, or oxygen tension[190]. Furthermore, tumors in animal xenograft models do not behave like the tumors found in humans due to physiological differences[190–192]. For example, tumors in animals usually grow at a faster rate than human tumors, which results in immature vessels that cannot

compare to the tumor-feeding vessels found in humans which have usually developed and stabilized over a long period of time[192]. Also, with immunodeficiency, the mice lose the lymphocyte-mediated response to tumor cells that is observed in humans[190]. The lack of T- and B- cell responses in immunocompromised mice weakens their value to predict drug activity and efficacy of cancer in humans in whom an active immune system is present.

Due to these inherent pitfalls, striking differences in anti-cancer drug effects on cells have been observed in 2D conventional testing methods and preclinical models. For example, a study aimed at evaluating the therapeutic effects of Gefitinib®, a potent epidermal growth factor receptor (EGFR) inhibitor, with A431 human squamous carcinoma cells showed that the drug tested in 2D monolayer culture studies inhibited both EGFR and MET receptor tyrosine kinase signaling resulting in a significant decrease in cancer cell proliferation & viability[193]. However, a different response was observed in *in vivo* studies with Gefitinib® treated mice bearing A431 tumor cell xenografts[194]. Studies *in vivo* showed that treatment with the EGFR inhibitor alone had no pronounced effect on cell apoptosis and tumors developed resistance to treatment[194]. Only combined treatment with a MET inhibitor, in addition to Gefitinib®, reduced tumor volume significantly[194].

The challenge of evaluating new drugs and eventually integrating them into the clinical routine can be accomplished by using experimental models that more closely represent the pathological properties of the target tissue or disease. To improve drug

development and testing in the early phase, the use of 3D *in vitro* culture systems has been suggested as a potential link to bridge the gap between 2D conventional cultures and animal model studies[195,196]. The support for using 3D *in vitro* systems stems from many reported studies that have suggested and verified that cells grown in 3D are more representative of their natural state *in vivo*[77,89,197–200]. The most common approach implemented for 3D culture of cancer cells is tumor cells spheroids[67,201]. Micro-scale tumor cell spheroids are most commonly formed by the hanging drop method in which cells self-aggregate into a dense cluster by hanging cell suspension droplets on the underside of a lid of a TC plate (Figure 28)[67].

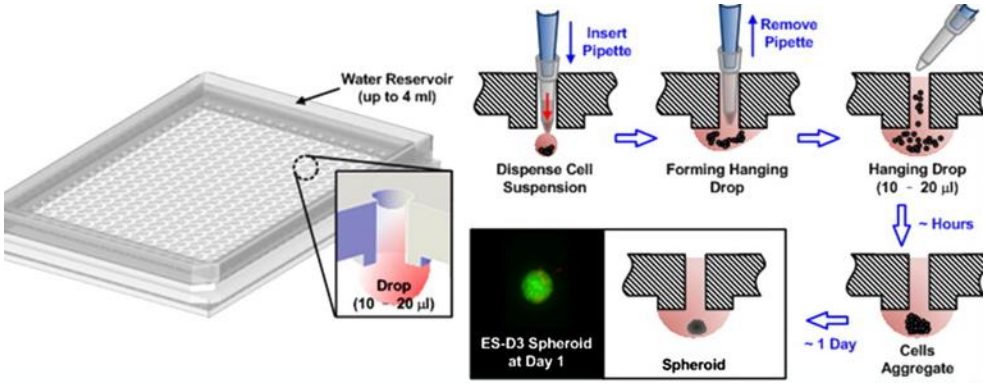


**Figure 28: Schematic of the hanging drop method where hanging cell suspension droplets on the underside of a lid of a TC plate leads to cells aggregating via gravity into a dense cell cluster at the bottom of the droplet by Tung et al[67].**

Although tumor cell spheroids have been demonstrated as 3D models for cancer drug testing, there are several drawbacks to this method that limit their reproducibility and utility. The formation of tumor spheroids provide little to no control over

uniformity in architecture and cell-cell interactions[196]. Cells spontaneously aggregate into clusters due to gravitational forces and form their own 3D geometry which may or may not be representative of tumors in the *in vivo* environment. Also, certain physiological structures and processes of the tumor microenvironment such as vascularized tumors are challenging to recapitulate in 3D tumor cell spheroid models.

To overcome these limitations, 3D tissue engineering scaffolds have been proposed as an alternative strategy to engineer the tumor microenvironment. The tumor microenvironment consists of tumor cells within a 3D matrix, surrounded by stromal cells such as endothelial cells and fibroblasts that interact with each other and the extracellular matrix. Through these interactions, tumor cell behavior and growth is modulated. Tumor growth in the microenvironment is also facilitated and dependent on the formation of blood vessels (Figure 29).

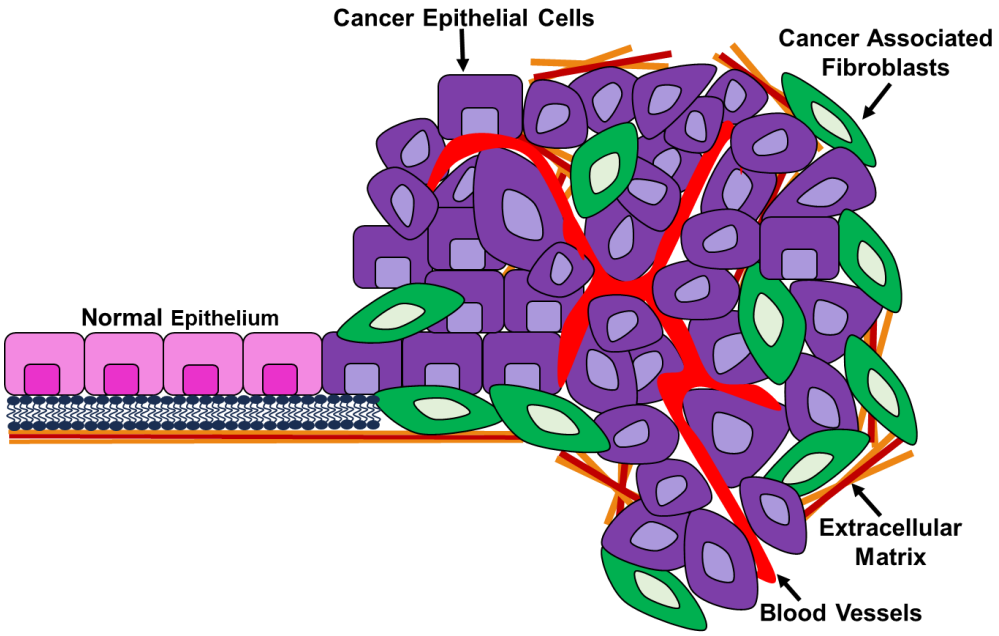


**Figure 29: Representation of the tumor microenvironment which consists of cancer epithelial cells within a 3D extracellular matrix interacting with non-malignant cells such as endothelial cells and cancer-associated fibroblasts. The need for the tumor to continuously grow and spread triggers angiogenesis and vessel formation.**

We demonstrate the feasibility of a tumor mimicking 3D platform in facilitating a better understanding of the biochemical and stromal cellular factors that promote tumor growth and elicit *in vivo*-like drug sensitivity. Focusing specifically on lung tumors, a 3D multicellular metastatic lung adenocarcinoma *in vitro* model encompassing metastatic-prone lung-derived CAFs, HUVECs, and human lung adenocarcinoma derived A549 tumor cells was established within degradable PEG hydrogels. Due to the extensive research on the behavior, function, and drug response of A549 cells shown in previous studies[202–205], we chose to incorporate human A549 lung carcinoma cells in our 3D tumor

model as the malignant cell type. Similar to the complex tumor microenvironment consisting of interacting malignant and non-malignant cells, the 3D lung adenocarcinoma PEG-based model consists of both tumor and stromal cells that support vessel formation and tumor cell growth. Within the 3D PEG scaffold, *ex vivo* lung tumor traits were observed to be very similar to those *in vivo* with respect to tumor cell morphology and growth kinetics.

Drug sensitivity of cancer cells to standard anti-cancer drugs with the potential of disrupting cell-cell interactions and vessel development were evaluated using the 3D lung tumor model. Due their strong clinical relevance to lung adenocarcinoma[202,203,206–208], small-molecule inhibitors such as doxorubicin, cilengitide, and semaxanib were selected for our studies to evaluate their effect on tumor and stromal cells found in the cancer microenvironment. Cilengitide is a cyclic pentapeptide that blocks $\alpha v\beta 3$ and $\alpha 5\beta 1$ integrins and has shown to disrupt cell-cell and cell-ECM interactions[209]. Doxorubicin acts via intercalating with DNA and by this means inhibiting DNA replication[203,206]. Semaxanib is a receptor tyrosine kinase inhibitor and indicated in inhibiting angiogenesis and endothelial cell proliferation[207]. The effect of drugs on tubule formation, tumor spheroid growth, and cell proliferation and viability was assessed using the 3D *in vitro* lung tumor model and compared with conventional 2D monolayer cell culture.

## *4.2 Materials and Methods*

### 4.2.1 Cell Culture and Maintenance

A549 lung carcinoma epithelial cells (ATCC, Manassas, VA) were cultured in F-12K Medium (ATCC) and supplemented with 10% FBS and 1000 U/mL penicillin, and 100 mg/L streptomycin (Sigma, St. Louis, MO). HUVECs (Lonza) were grown in endothelial basal medium (EBM), supplemented with EGM-2 bullet kit containing ascorbic acid, epidermal growth factor, fibroblast growth factor, heparin, hydrocortisone, insulin-like growth factor, GA-1000 (gentamicin, amphotericin-B), and 2% FBS (Lonza). CAFp53kras cells were cultured in Minimum Essential Medium Eagle Alpha Modification (Gibco, North Andover, MA) with 20% FBS (Lonza, Walkersville, MD). Human brain vascular pericytes (HBVP) (ScienCell, Carlsbad, CA) were grown in proprietary pericyte medium consisting of basal medium with 10% FBS (ScienCell), 5% v/v of pericyte growth supplement (PGS; ScienCell), and 5% v/v penicillin/streptomycin solution (P/S; ScienCell). To promote cell adhesion and optimal cell survival, HBVP cells were cultured in T-75 flasks coated with poly-l-lysine. Poly-l-lysine (PLL; SceinCell) was dissolved in sterile tissue culture grade water at a concentration of 150 μg/mL. For even coating of PLL on the plastic surface, the T-75 flask was incubated with PLL solution and placed on a rocker at room temperature for 4 hr prior to cell seeding. Experiments were conducted with CAFp53kras (see section 2.2.1 on isolation of CAFs from mice) from passages to 2 to 9. HUVEC cells were used from passages 2 to 8, and HBVP were used

from passages 2 to 8. All cells were incubated at 37°C and 5% $CO_2$, and medium was changed every other day.

### 4.2.2 Synthesis of PEG-RGDS and PEG-PQ-PEG

For conjugation of the cell-adhesive peptide RGDS and protease sensitive peptide sequence GGGPQGIWGQGK (PQ) to PEG-SVA, refer back to chapter 2, and section 2.2.4.

### 4.2.3 Labeling Cells with CellTracker™

Prior to encapsulations, cells were labeled with CellTracker™ dyes (Thermo Fisher Scientific, Waltham, MA) to differentiate cells and their interactions in triculture in a single hydrogel. Specifically, HUVECs, CAFp53kras cells, and A549 cells were labeled with CellTracker™ green CMFDA (Ex. 492/Em. 517), red CMTPX (Ex. 577/ Em. 602), and blue $CMF_2HC$ (Ex. 371/Em. 464), respectively. To prepare the cell CellTracker™ dyes, 4 μL of sterile DMSO was added to a 50 μg CellTracker™ dye vial and mixed to dissolve the dye. Following this, 500 μL of cell media was added to the dye vial and mixed thoroughly. All of the CellTracker™ dye was added to 4.5 mL of cell media. Following preparation of CellTracker™ media solution, cell media from T-75 flasks was aspirated and cells were rinsed with PBS once before adding the 5 mL of media with CellTracker™ dye. Cells were incubated with the dye solution at 37°C and 5% $CO_2$ for 1.5 hr. Media with CellTracker™ dye was aspirated and 15 mL of fresh cell

culture media was added to the flasks. Cells were incubated overnight and then washed with sterile PBS twice before detaching cells with trypsin-EDTA.

### 4.2.4 A549 Tumor Cells Growth Relative to Time in Culture and Cell Concentration in 3D PEG Hydrogels

To evaluate growth profile and formation of A549 tumor spheroids in culture in 3D over time, A549 lung epithelial cells were encapsulated at a concentration of 500,000 cells/mL in 5% w/v PEG-PQ hydrogels with 3.5 mM RGDS and cultured for up to 5 d. To determine the effect of cell concentration on the formation of tumor spheroids, A549 lung epithelial cells were incorporated in 5% w/v PEG hydrogels with 3.5 mM RGDS at different cell concentrations ranging from 250 cells/μL to 22,500 cells/μL. Cells in gels were fixed at 6, 24, 72, or 120 hr post encapsulation. Cells were fixed in 4% paraformaldehyde for 20 min and then washed with PBS. Encapsulated cells were permeabilized with 0.5% Triton-X for 30 min and then washed with PBS. Afterwards, nonspecific binding was blocked by incubation with 1% BSA overnight. Hydrogels were rinsed in PBS five times and exposed to a 1:100 dilution of rhodamine phalloidin (Invitrogen) containing 2 μM 4',6-diamidino-2-phenylindole (DAPI) in HBS with 0.1% BSA for 2 hr to stain actin and cell nuclei. The hydrogels were visualized using a confocal microscope (Zeiss 510, Plan-Apochromat 20x objective with 0.8 NA) with a z-stack depth of 50 μm with 2 μm thick slices (at excitation/emission wavelengths: 405nm/421nm for DAPI, and 633nm/665nm for phalloidin). Imaris software was used to measure the diameter of tumor cell spheroids in 3D.

### 4.2.5 Triculture Encapsulation of Cells in Degradable PEG Hydrogels

HUVEC cells at a concentration of 20 million cells/mL were encapsulated in 5 μL degradable hydrogels with CAFp53kras or HBVP at a concentration of 2 million cells/mL, and A549 cells at a concentration of 500,000 cells/mL. The total cell density in a hydrogel was 22.5 million cells/mL. Hydrogels were formed from a pre-polymer solution composed of 5% (w/v) PEG-PQ-PEG and 3.5 mM PEG-RGDS in sterile HEPES buffered saline (HBS) containing 1.5% (v/v) triethanolamine, 1 mM eosin Y, and 3.5 μL/mL N-vinyl-2-pyrrolidone (NVP). All cells were detached using 0.05% trypsin-EDTA and pelleted by centrifuging at 700 x g for 4 min. The cell pellets were then re-suspended in the pre-polymer solution to concentrations of 22.5 million cells/mL. 5 μL droplets of cell-laden polymer were sandwiched between a Sigmacote® functionalized (prepared as described in chapter 2 section 2.2.5, Sigma, St. Louis, MO) glass slide and a methacrylate-modified cover glass (prepared as described in chapter 2 section 2.2.5) separated by a 380 μm polydimethylsiloxane (PDMS) spacer. The pre-polymer solutions were cross-linked under white light for 40 s to form hydrogels. All gels containing HUVECs were immersed in EGM-2 media (Lonza) and incubated at 37°C in a 5% $CO_2$ environment for up to 5 d. Media was replenished every other day. For comparison studies between tri-culture with HUVEC monoculture or A549 monoculture in 3D, cell seeding density for the cell type was kept constant in between tri-culture and monoculture. For example, HUVEC cells at concentration of 20 million cells/mL were

encapsulated for hydrogels with monoculture of HUVECs and hydrogels with triculture.

### 4.2.6 Drug Treatment in 2D and 3D cultures

Cell-laden hydrogel constructs were maintained for 5 d before treatment with drugs. The dose response for doxorubicin (Sigma-Aldrich, St. Louis, MO), cilengitide (Medkoo Biosciences, Chapel Hill, NC), and semaxanib (Medkoo Biosciences) were evaluated both in 2D and 3D culture at concentrations 0, 1, 5, and 10 μM in cell medium. Cells were exposed to drugs for 24 hr after which drug containing media was removed and fresh media was added to the cells before proceeding to fixation and analysis. The average weight of our triculture hydrogel was approximately 15.2 ± 3.5 mg (n = 8 gels). Hydrogels were treated by adding the drug directly in 1 mL of media. Based on this information, we were able to calculate 1015.25 mg as the average weight for each experimental well. To compare with drug concentrations reported as mg/kg in preclinical and clinical studies, we administered (at the highest concentration of 10 μM in our studies) approximately 5 mg/kg for doxorubicin, 2 mg/kg for semaxanib, and 5.5 mg/kg for cilengitide. These concentrations fall within the range that have been tested and reported in A549 tumor cell xenograft studies or clinical studies[202,205,207,208,210,211].

For evaluating doxorubicin uptake in tumor cells cultured in 2D, A549 cells were seeded in a 2-well glass chamber slide at a density of 500,000 cells/cm$^2$ and cultured for 5 d at 37°C and 5% $CO_2$ before treatment with 10 μM doxorubicin. After 4 hr and 12 hr

post incubation, cells and hydrogels were rinsed with PBS twice to remove unbound free doxorubicin. Following rinses, Hoechst 33342 dye (0.3 μg/ml final concentration, Invitrogen-Molecular Probes, CA) in PBS was also added to cells in culture and incubated for at least 30 min at 37°C to stain for the cell nucleus. Cellular uptake of doxorubicin was assessed by fluorescent microscopy at excitation and emission wavelength of 488 nm and 585 nm using a confocal microscope (Zeiss 510, Plan-Apochromat 20x objective with 0.8 NA). For evaluating drug uptake in tumor cells encapsulated in hydrogels and cultured in 3D, A549 cells were encapsulated in 5 μL degradable hydrogels (as described in section 4.2.4) at a concentration of 500 cells/uL and cultured for 3 d at 37°C and 5% $CO_2$ before treatment with 10 μM doxorubicin. Just as with 2D culture, cellular uptake of doxorubicin in cells in 3D was assessed by fluorescent microscopy using confocal microscope (Zeiss 510, Plan-Apochromat 20x objective with 0.8 NA) also after 4 hr and 12 hr post treatment. The colocalization function in the Imaris analysis software was utilized to assess percent of cells with doxorubicin in the nucleus. Relative amount of doxorubicin accumulation in the nucleus of cells in 2D and 3D was determined by measuring pixel intensity of doxorubicin (488 nm) in the nucleus (defined by Hoechst dye) in Image J.

### 4.2.7 Immunostaining

Cell proliferation and apoptosis was assessed via immunohistochemistry for ki67 to indicate proliferative cells (s-phase) and caspase-3 for apoptotic cells. For examining

cells in 2D, cells were seeded on polystyrene plates were fixed with 4% paraformaldehyde for 20 min at room temperature and then rinsed with PBS three times at room temperature. After fixation, cells were then permeabilized with 0.125% Triton-X in PBS for 10 min, rinsed three times with PBS, and then incubated with 5% BSA for 30 min. After blocking, cells were incubated with either primary antibody against Ki67 or caspase-3 at room temperature for 1 hour. The primary antibodies were rabbit anti-ki67 (1:250 in PBS with 0.1% BSA, Abcam) and rabbit anti-caspase-3 (1:250 in PBS with 0.1% BSA, Cell Signaling Technologies, Danvers, MA). Cells were rinsed in PBS three times and then incubated with Alexa Fluor 488 donkey anti-rabbit IgG (1:400 in in PBS with 0.1% BSA, Invitrogen) for caspase-3 or ki67 expression for 1 hour at room temperature to visualize the binding of the primary antibodies. Following another PBS wash, cells were finally exposed to 2 μM 4',6-diamidino-2-phenylindole (DAPI) in HBS with 0.1% BSA for 30 min to cell nuclei and imaged using a Zeiss Axio Observer widefield fluorescence microscope with a 20x objective (Carl Zeiss Microscopy, Jena, Germany).

For examining cells encapsulated in PEG hydrogels in 3D, hydrogels were fixed in 4% paraformaldehyde for 20 min and then washed with PBS. Encapsulated cells were permeabilized with 0.5% Triton-X for 30 min and then washed with PBS. Afterwards, nonspecific binding was blocked by incubation with 1% BSA overnight. Half of the hydrogels from testing group were incubated with a 1:250 dilution of rabbit anti-caspase-3, while the other half of hydrogels were incubated with 1:250 dilution of rabbit anti-ki67 in HBS with 0.1% BSA overnight on a rocker table at 4°C to stain apoptotic cells

and proliferative cells, respectively. Hydrogels were rinsed in PBS five times at one-hour intervals and then incubated with a 1:400 dilution of Alexa Fluor 488 donkey anti-rabbit IgG (Invitrogen) overnight at 4°C to visualize the primary antibodies. Samples were then rinsed with PBS and exposed to a 1:100 dilution of rhodamine phalloidin (Invitrogen) containing 2 μM 4',6-diamidino-2-phenylindole (DAPI) in HBS with 0.1% BSA for 2 hr to stain actin and cell nuclei. The hydrogels were visualized using a confocal microscope (Zeiss 510, Plan-Apochromat 20x objective with 0.8 NA) with a z-stack depth of 50 μm with 2 μm thick slices (at excitation/emission wavelengths: 488 nm/519 nm for ki67 or caspase-3, 405nm/421nm for DAPI, and 633nm/665nm for phalloidin). Image J software was used to count cells positive for ki67 or cleaved caspase-3 in each hydrogel (n = 4 hydrogels per experimental group).

### 4.2.8 Assessing Cell Viability

Cell viability was assessed using the LIVE/DEAD® viability/cytotoxicity kit as per manufacturer's instructions. Briefly, control (untreated) and drug treated cell encapsulated hydrogels 24 hr post drug treatment were incubated in 2 μM calcein-AM and 4 μM ethidium homodimer-1 (Ethd-1) in PBS for 30 min at 37°C. Hoechst 33342 dye (0.3 μg/ml final concentration, Invitrogen-Molecular Probes, CA) in PBS was also added to cells in culture and incubated for at least 30 min at 37°C to stain for the cell nucleus. Cells were imaged on the confocal microscope (Zeiss 510, Plan-Apochromat 20x objective with 0.8 NA) with a z-stack depth of 50 μm with 2 μm thick slices (at

excitation/emission wavelengths: 488 nm/519 nm for calcein-AM, 555nm/600nm for Ethd-1, and 405nm/421nm for Hoechst 33342 dye). Percentage of viable cells was calculated by counting number of live cells over total cell population (determined from cell nuclei staining) in a field of view for each image per hydrogel (n=4 hydrogels).

### 4.2.9 Assessment of Vessel Formation and Tumor Spheroid Growth

Imaris software (Bitplane Inc., South Windsor, CT) was used to trace and measure tubule length per volume and tubule diameter in 3D images with CellTracker™ green stained endothelial cells. Imaris software was also used to measure the diameter of a tumor cell spheroid in 3D images with A549 cells by tracing at multiple planes through the center of the spherical structure. Diameter values for all spheroids within a field of view were averaged to get a mean spheroid diameter value.

### 4.2.10 Statistical Analysis

Single factor ANOVA and subsequent post hoc Tukey test were used to analyze vessel formation and tumor spheroid growth over time in culture. Two factor ANOVA and subsequent post hoc Tukey test were used to analyze drug efficacy at different concentrations on vessel formation and tumor spheroid growth. For each analysis, $p<0.05$ was considered to be significant. All data is presented as mean ± standard deviation.

## *4.3 Results*

### 4.3.1 A549 lung carcinoma cell in 3D PEG hydrogel system

A549 lung epithelial carcinoma cells encapsulated in 3D PEG hydrogels display different cell interactions and morphology than cells cultured in 2D. A549 lung tumor cells cultured in 3D organized into multicellular agglomerates in 3D culture whereas cells seeded in 2D TC plastic remained in cobblestone-like, flat morphology (Figure 30). To evaluate growth profile and behavior of tumor cells in culture in 3D over time, A549 lung epithelial cells were encapsulated at a concentration of 500,000 cells/mL in degradable PEG hydrogels and cultured for up to 5 d. Cells in gels were fixed at 6, 24, 72, or 120 hr post encapsulation and stained with phalloidin for actin filaments and DAPI for cell nuclei. Spheroid formation was assessed by measuring the diameter of tumor cell spheroids. Our results show that tumor cells form spheroids that appear to grow larger with prolonged time in culture (Figure 31). Average size of tumor spheroids formed after 5 d in culture was 42.1 ± 4.3 μm and consisted of multiple cells coalescing into a single spheroid. The diameter of tumor spheroids increased by more than 2-fold from 24 hr in culture to 120 hr in culture. Figure 32 shows the effect of A549 cell seeding density on spheroid size. Interestingly, the spheroid size increased with cell density up to 1000 cells/μL. Beyond this cell concentration, spheroid growth was stunted, which was evident by the decrease in mean spheroid diameter with increasing cell concentration. Strikingly, lung carcinoma cells encapsulated at a concentration of 1000 cells/μL produced spheroids similar in size to cells encapsulated at 500 cells/μL

after 5 d in culture. Average spheroid size at the end of 5 d was found to be 39.5 ± 2.0 μm for cell concentration of 500 cells/μL and 43.5 ± 4.7 μm for cell concentration of 1000 cells/μL. With consideration of optimal spheroid growth characteristics and size distribution, cell concentration of 500 cells/μL for a 5 μL cell-laden degradable PEG hydrogel was chosen for establishing a vascularized 3D tumor model.

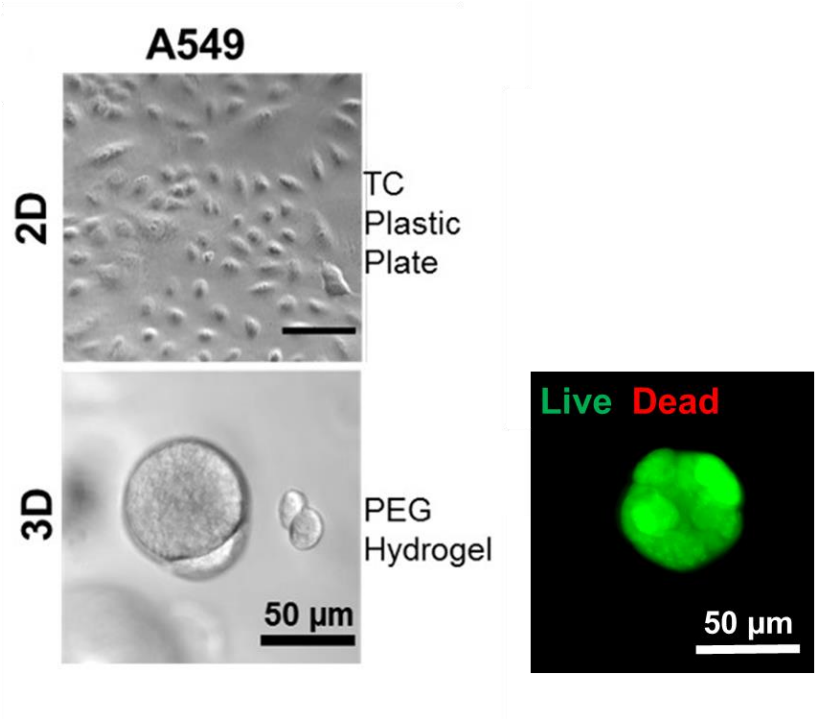


**Figure 30: A549 cells seeded on tissue culture polystyrene plates (2D) adopt a flattened, cobblestone morphology whereas A549 cells encapsulated and cultured in PEG hydrogels (3D) form multicellular tumor spheroids. Majority of the cells in the tumor spheroids appear to be viable post 5 days in culture.**

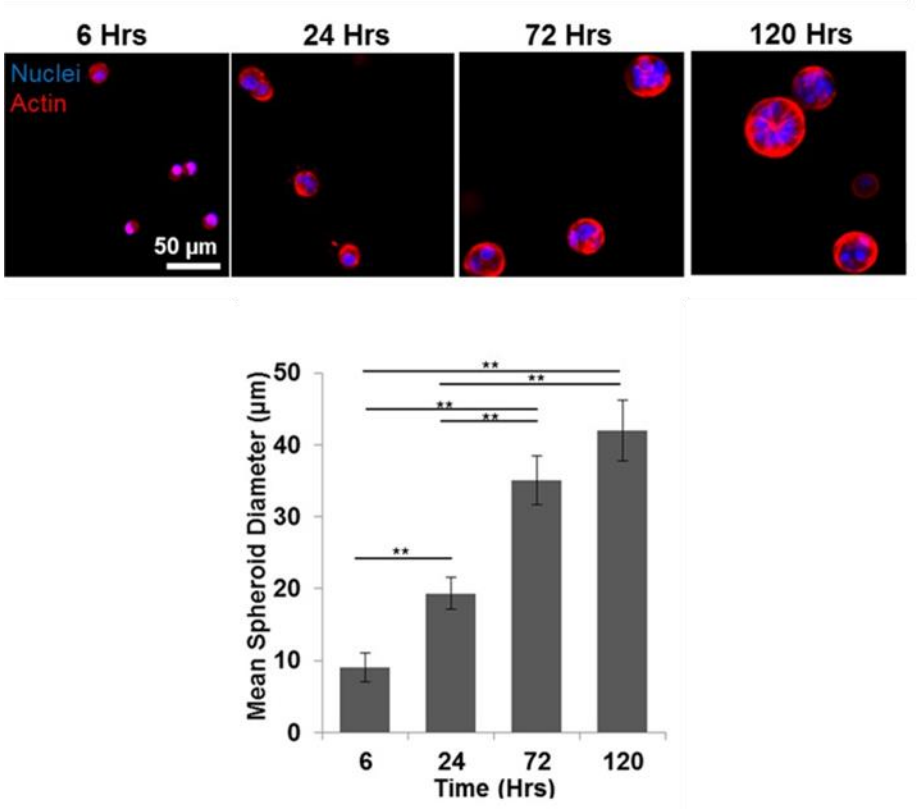


**Figure 31: Multicellular A549 tumor cell spheroids form as early as 3 d and appear to grow larger over time. Scale Bar = 50 µm (p**<0.01).**

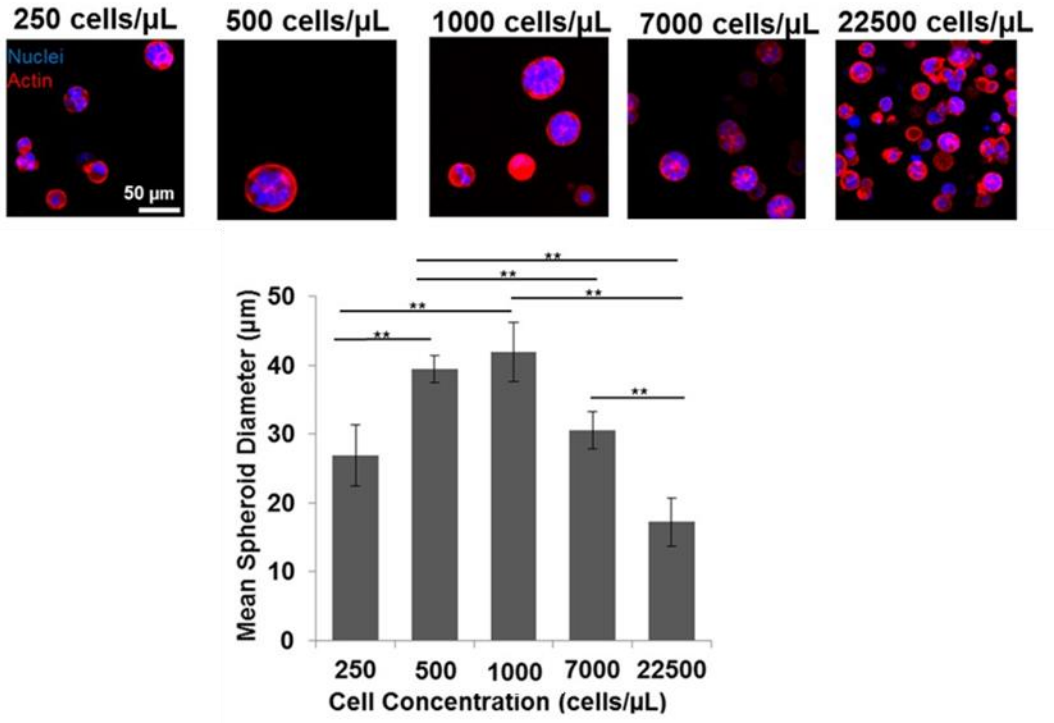


**Figure 32: Cell seeding concentration in PEG hydrogels affects tumor spheroid growth and size. A549 cells encapsulated at a concentration of 500 cells/µL produced significantly larger spheroids than all other concentrations tested (p**<0.01).**

### 4.3.2 Doxorubicin uptake in A549 lung carcinoma cells in 2D and 3D culture systems

Tumor cell spheroids in 3D and cells seeded in 2D were incubated with 10µM doxorubicin for 4 hr or 12 hr. At these time points, the fluorescent intensity was measured from cells with drug uptake in the nucleus. Colocalization analysis of Hoechst 33342 fluorescent signal for the cell nuclei with fluorescent signal from doxorubicin was conducted to determine percent of cells with localization of the drug in the nucleus (Figure 33). Between 4 hr and 12 hr post treatment, the percent of cells with drug

localized in the nucleus increased by 8-fold. No significant difference for doxorubicin uptake, based on nuclear fluorescence of doxorubicin, between cells in 2D and 3D at 12 hr post drug incubation was observed ($p<0.01$).

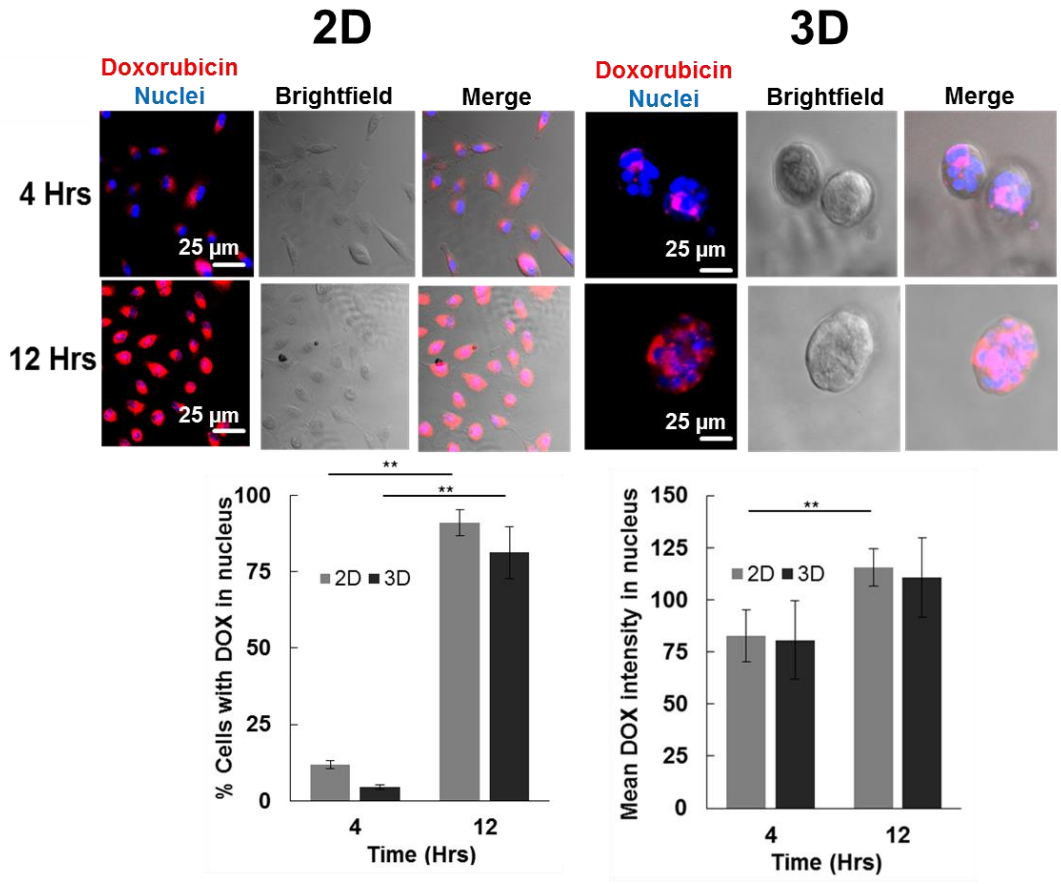


**Figure 33: Doxorubicin (DOX) drug uptake by cells in 2D and 3D was evaluated at 4 hr and 12 hr time point. Quantitative analysis of percentage of cells with dox localization in the nucleus does not show any significant difference in drug uptake between cells in 2D and 3D. Scale Bar = 25 µm and p**<0.01.**

### 4.3.3 Response of A549 lung carcinoma cells in 2D and 3D culture systems to cytotoxic drugs

Immunostaining for ki67 and cleaved caspase-3 was performed to compare the drug response of A549 lung carcinoma cells cultured in 2D and 3D and to study anti-cancer drug induced effects on proliferation and apoptosis, respectively. For a direct comparison of cells in 2D and 3D, cells were seeded at a concentration of 500 cells/μL in a 5 μL cell laden hydrogel for 3D studies and 1250 cells/cm$^2$ for 2D studies in a single well of a 24 -well plate and cultured for 5 d before treated with drugs in media for 24 hr.

To understand the effect of anti-cancer drug on each cell type independent of interactions with other cells, cell proliferation and apoptosis post drug treatment were first compared between 2D and 3D monoculture of HUVECs, A549 cells, and CAFp53kras cells. Significant differences in cell apoptosis and proliferation between cells in 2D and 3D were observed. For HUVEC, A549, and CAFp53kras cells, the percentage of cells positive for cleaved caspase-3 were found to be significantly higher in 2D culture as compared to 3D culture. Percentage of apoptotic cells was 1.6- and 2.1-folds less in 3D cultures as compared to 2D monolayer culture of A549 cells with 10 μM cilengitide or semaxanib treatment, respectively. This decrease in drug sensitivity detected in cells cultured in 3D systems as compared to cells cultured in 2D resembles drug sensitivity of tumors *in vivo*[197,212,213].

Similar to the analysis of apoptotic cells, immunostaining of ki67 (proliferative marker) of cells in 2D and 3D showed significant differences in the percentage of

proliferative cells between 2D and 3D culture systems post drug treatment. Compared to conventional 2D culture conditions, the percentage of proliferative cells post treatment with cilengitide, semaxanib, or doxorubicin was found to be significantly higher in cells cultured in 3D ($p<0.01$).

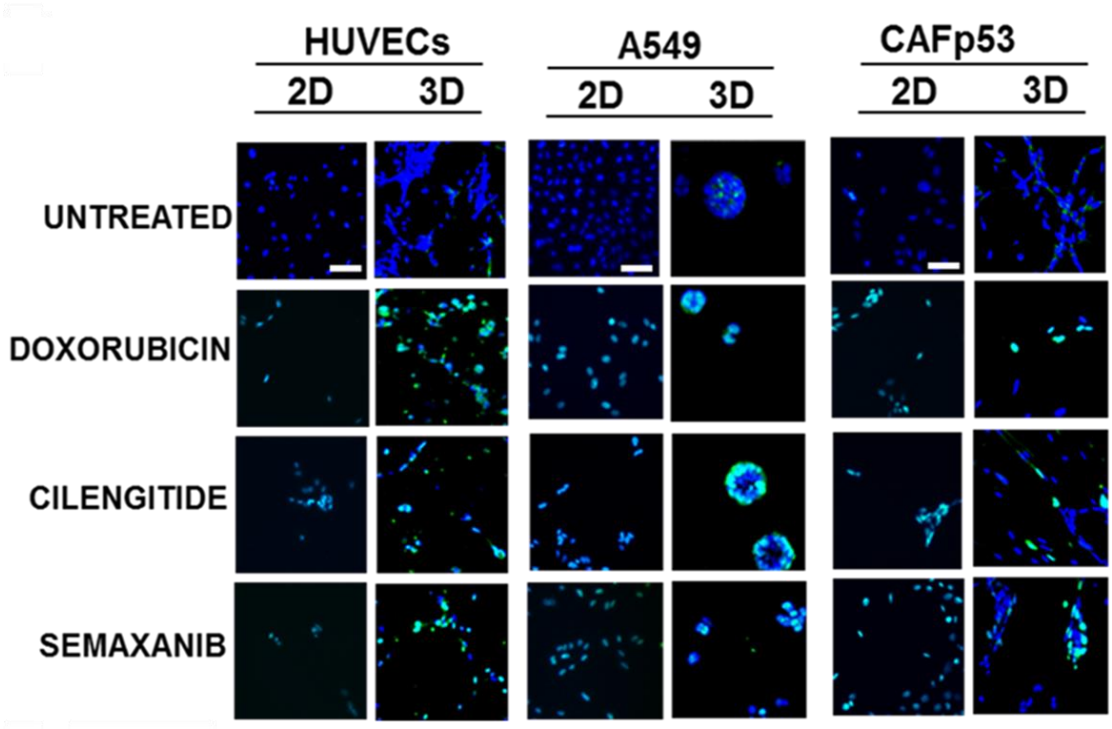


**Figure 34: Immunostaining of cleaved caspase-3 in HUVECs, A549 cells, and CAFp53kras cells cultured in 2D TC Plate or encapsulated in 3D PEG hydrogels and treated with anti-cancer drugs. Scale Bar = 50 μm.**

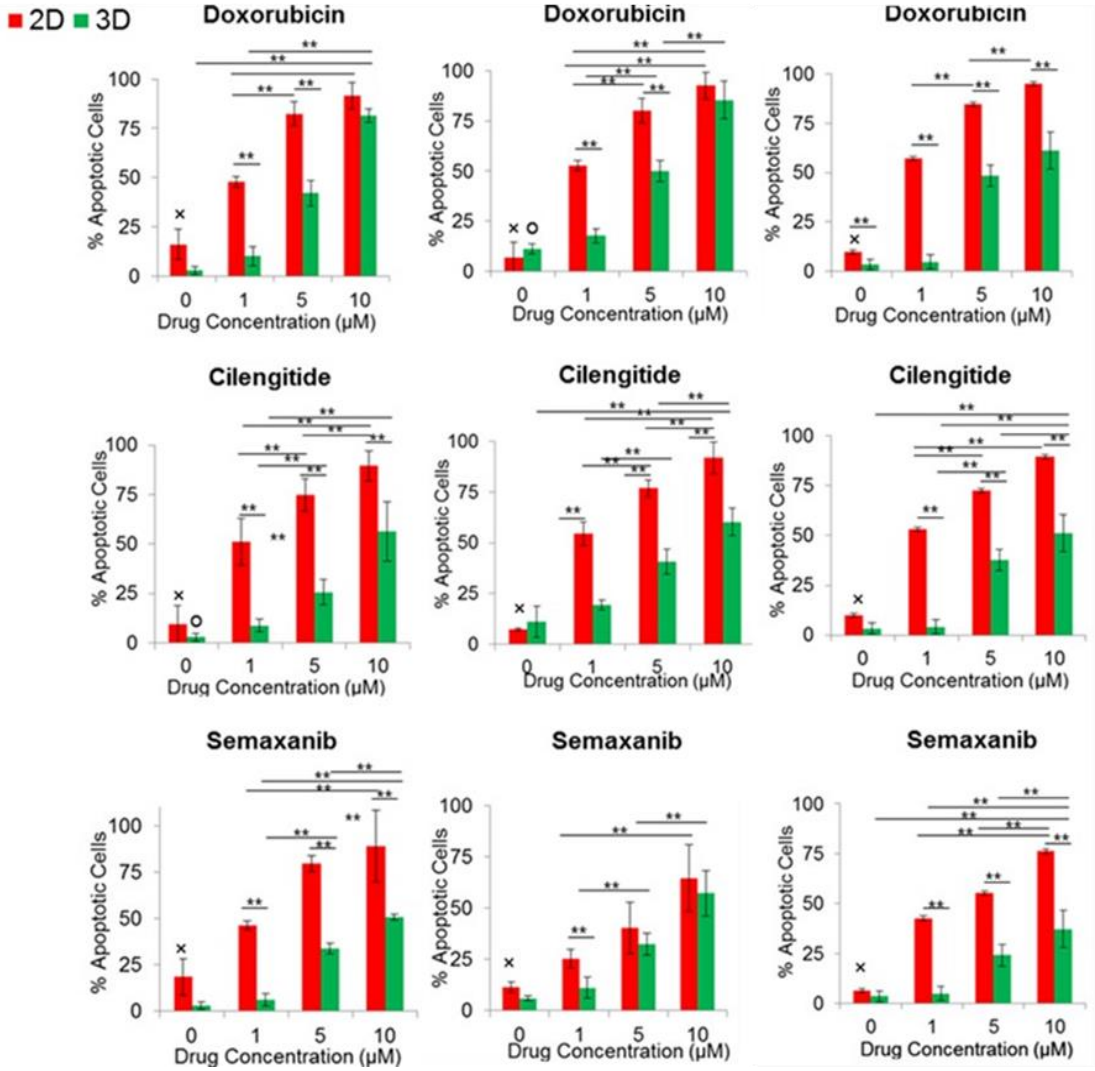


**Figure 35: Quantitative analysis of the percentage of apoptotic cells post 24 hr drug treatment with doxorubicin, cilengitide, and semaxanib in cells cultured in 2D (red bar) versus in 3D (green bar). (n=4; *p<0.05 and **p<0.01; x is significantly different (p<0.01) than all other concentration groups tested in 2D; o is significantly different (p<0.01) than all other concentration groups tested in 3D).**

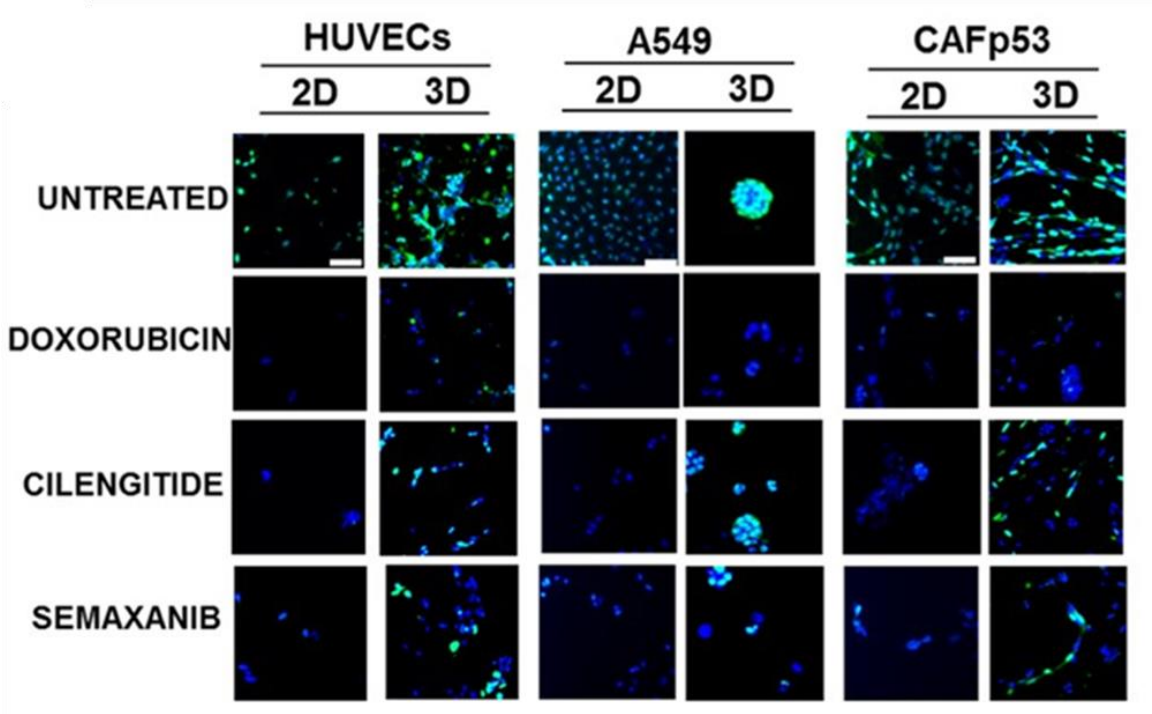


**Figure 36: Immunostaining of ki67 in HUVECs, A549 cells, and CAFp53kras cells cultured in 2D TC Plate or encapsulated in 3D PEG hydrogels and treated with anti-cancer drugs. Scale Bar = 50 μm.**

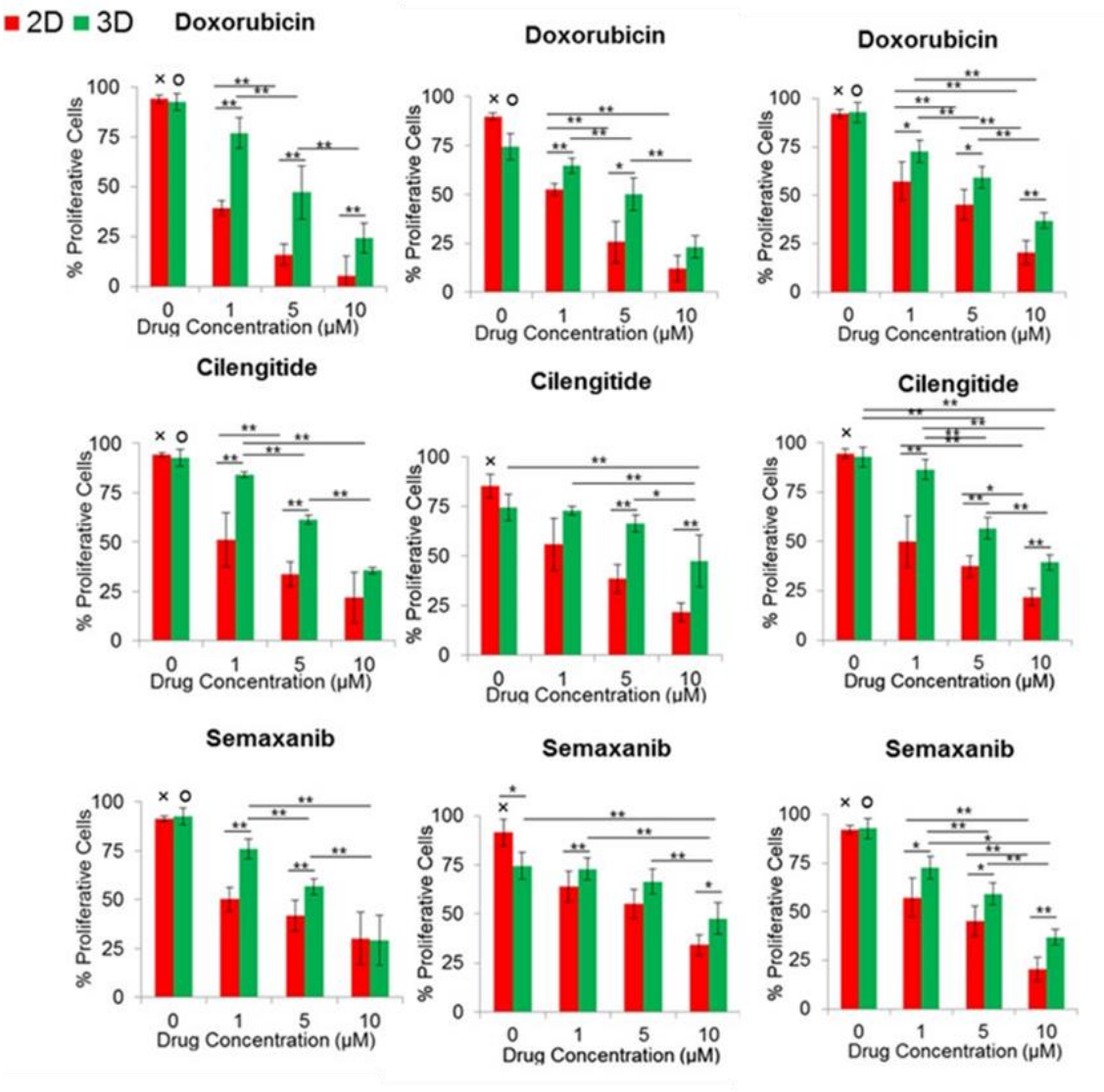


**Figure 37: Quantitative analysis of percentage of proliferative cells post 24 hr drug treatment with doxorubicin, cilengitide, and semaxanib in cells cultured in 2D (red bar) versus in 3D (green bar). (n=4; *p<0.05 and **p<0.01; x is significantly different (p<0.01) than all other concentration groups tested in 2D; o is significantly different (p<0.01) than all other concentration groups tested in 3D).**

### 4.3.4 Vascularized 3D tumor model in Biomimetic PEG Hydrogels

The vascularized 3D tumor model was developed by encapsulating HUVEC cells with CAFp53kras and A549 cells in 5% (w/v) degradable PEG-PQ hydrogels with 3.5 mM PEG-RGDS. To differentiate the behavior and locations of these cells in the hydrogel, HUVECs, CAFp53kras cells, and A549 lung cancer cells were labeled with green, red, and blue CellTracker™, respectively before encapsulation. HUVEC cells organized into interconnected and lumenized vessel-like networks visible as early as 3 d with CAFp53kras cells closely associating with vessel-like structures. To quantify vessel formation over time in culture, total tubule length per volume and average tubule diameter were evaluated. At 72 hr or 120 hr in culture, vessels had an average tubule diameter of 26.0 ± 2.2 μm and 29.9 ± 1.6 μm, respectively. Total tubule length per volume of vessels increased over time with significantly higher total tubule length/volume at 120 hr in culture ($p<0.01$) with a value of 1153.4 ± 143.8 $\mu m/mm^3$ as compared to 24 hr in culture where total tubule length/volume was 559.8 ± 93.3 $\mu m/mm^3$. Connections between tumors and vessels predominately consisting of HUVECs and CAFp53kras were observed at the periphery of vessels and became more visibly apparent with prolonged time in culture. Interaction of tumor cells with HUVECs or CAFp53kras does not seem to hinder tumor cell proliferation or spheroid formation as evident by the increase in tumor spheroid diameter over time. Extended focus images also indicate vascular lumen formation and tumor spheroids consisting of multiple interacting tumor cells (Figure 38B).

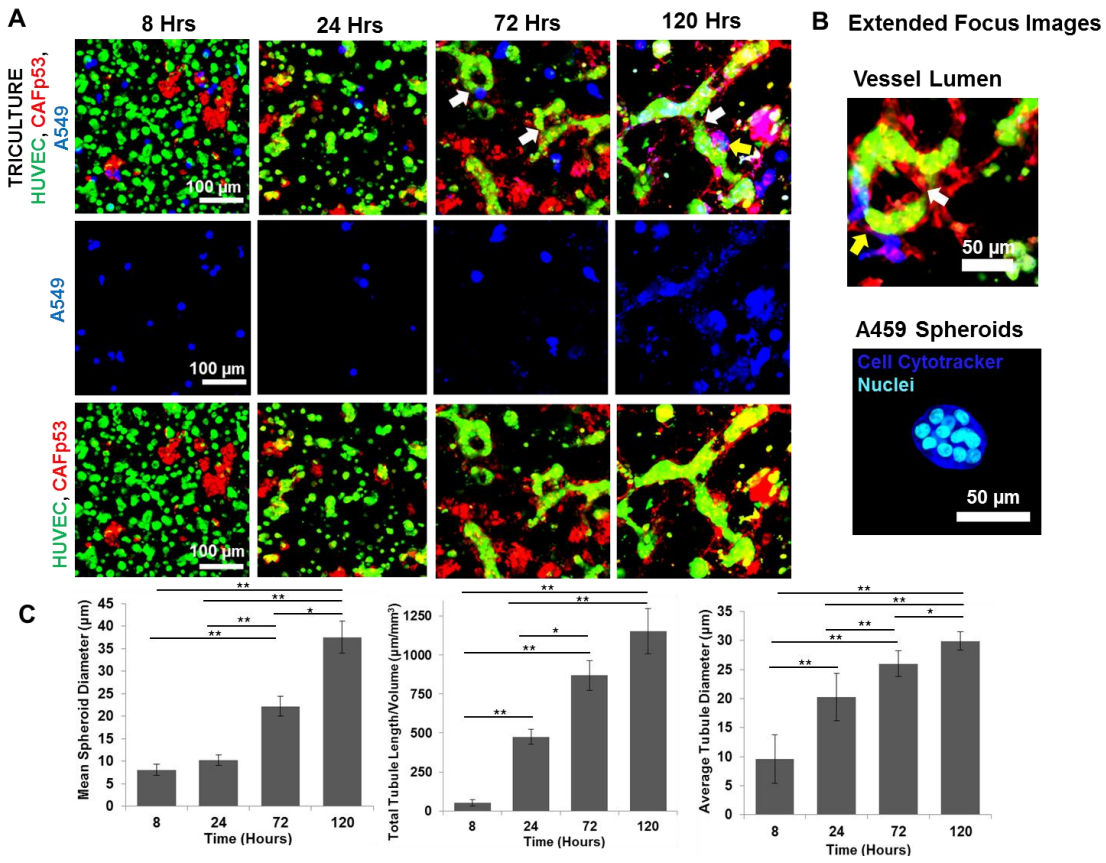


**Figure 38: A) Tri-culture of A549 cells with HUVECs and CAFs in degradable PEG hydrogels shows the formation of tumor spheroids, complex vessel networks, and vessel lumens. B) Extended focus images show that tumor spheroids are multicellular and that vascular lumen is present in vessel networks. C) Analysis of vessel formation and tumor spheroid growth shows that mean spheroid diameter (µm), total tubule length/volume (µm/mm³), and average tubule diameter (µm) increase with longer time in culture. (n=6; *p<0.05 and **p<0.01)**

### 4.3.5 Responsiveness of Vascularized 3D Tumor Model to Anti-cancer Drugs

The response of A549 tumor cell only and vascularized tumor 3D culture models to anti-cancer drugs was evaluated. In previous work (chapter 2), we have demonstrated that CAFp53kras cells derived from metastasis-associated lung tumors can influence ECs and enhance vessel formation via secretion of angiogenic growth factors such VEGF-A and FGF-2. Additionally, their ability to closely interact with EC vascular networks suggests that CAFp53kras cells can potentially act as pericytes by supporting and stabilizing vessel formation. To determine if malignant tumor stromal cells like CAFs and their interaction with tumor cells contributes to drug resistance and enhanced tumor cell survival, we compared drug response in between two types of tumor angiogenesis 3D models with one containing human brain vascular pericytes (HBVP) as mural cells and the other containing CAFp53kras cells along with a A549 tumor only 3D model. These 3D culture models were treated with 5 μM doxorubicin or semaxanib. The anti-cancer drugs were added to the hydrogel culture in 1 mL of media. Cell viability of untreated and drug treated cells was evaluated and quantified (Figure 39).

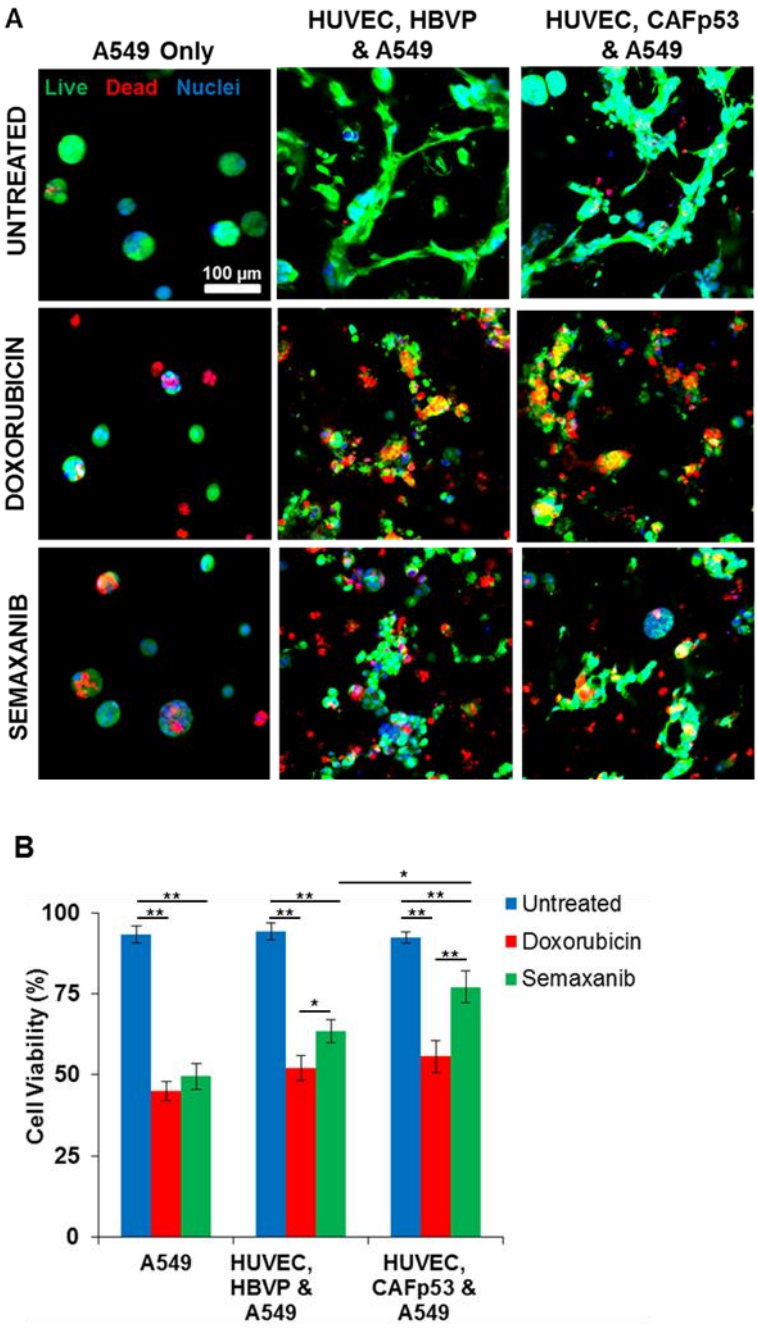


**Figure 39: A) Live and dead staining of untreated and doxorubicin (at 5 µM) or semaxanib (at 5 µM) treated 3D PEG hydrogels with either A549 cells only, triculture with HBVPs, or triculture with CAFp53kras cells. B) Quantitative analysis of percent cell viability. Scale Bar = 100 µm. (n=4; *p<0.05 and **p<0.01).**

Similar cell viability was observed in 3D triculture with HBVPs versus CAFs post treatment with doxorubicin. It seems that substitution of HBVPs with CAFs in 3D triculture did not significantly enhance overall cell survival upon treatment with doxorubicin. In contrast to doxorubicin, cells treated with semaxanib displayed differences in cell viability between the tumor only model and 3D triculture models containing HBVPs or CAFs. The 3D triculture model containing CAFs exhibited 1.5-fold higher percent cell viability than the 3D triculture with HBVPs. As opposed to the 3D triculture model with HBVPs, vessel-like structures and tumor cell spheroids were still visible in the triculture group containing CAFs after treatment with semaxanib. This observation indicates that CAFs may enhance survival of ECs and contribute to greater drug resistance than vascular pericytes.

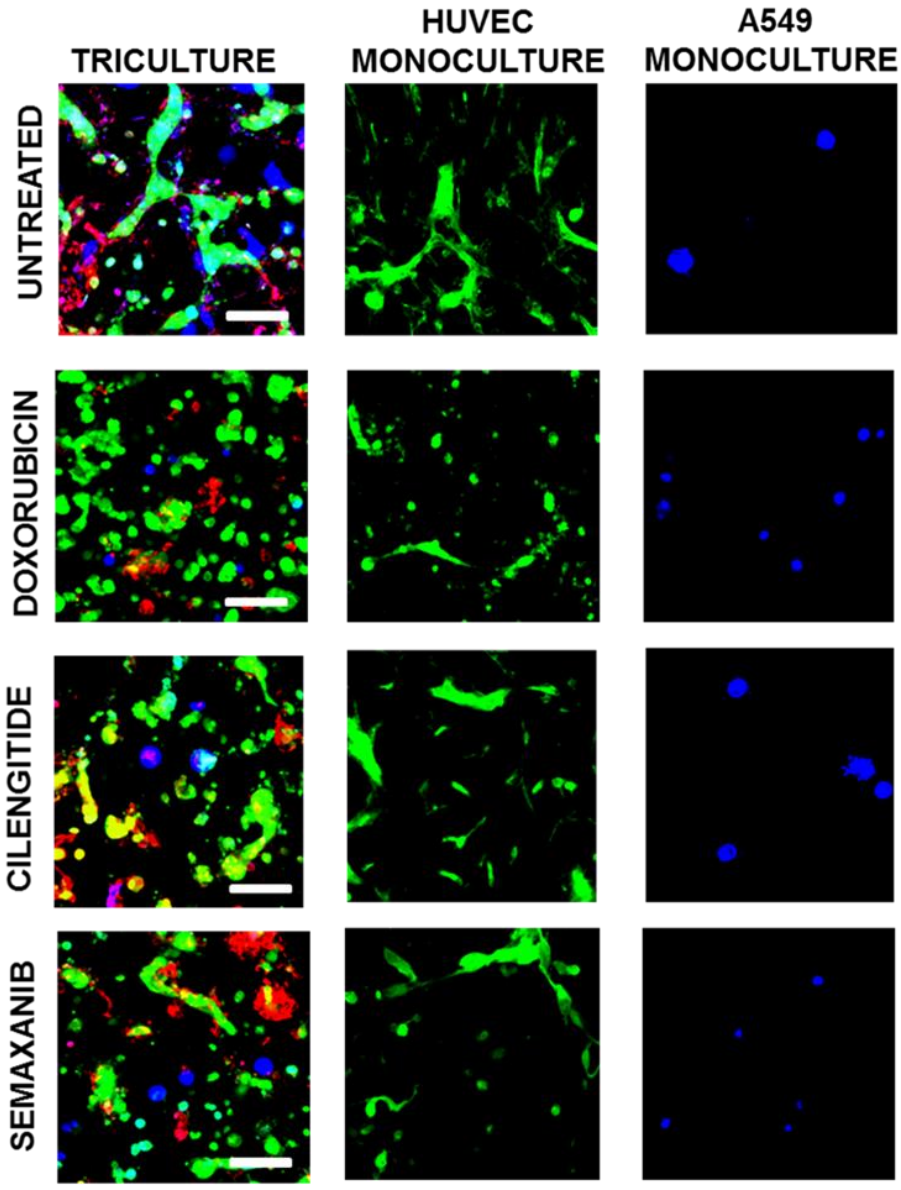


**Figure 40: Images of CellTracker™ labeled cells with HUVECs shown in green, CAFp53kras cells in red, and A549 cells in blue in 3D triculture and monoculture models with or without drug exposure. Scale Bar = 100 μm.**

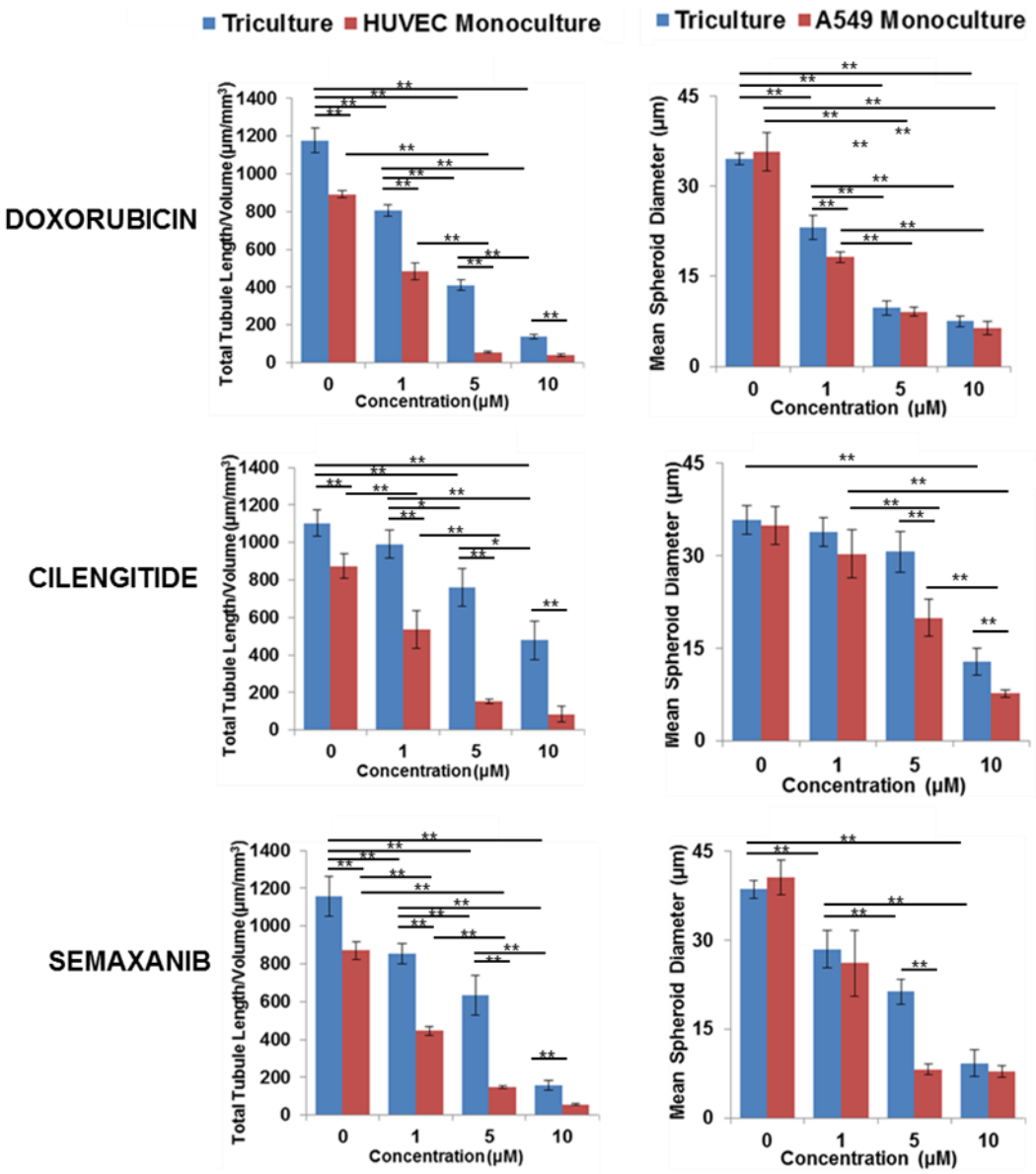


**Figure 41: Tubule formation (based on HUVEC cells organizing into tubules shown in Figure 40) was compared between triculture of A549 cells with HUVECs and CAFs with monoculture of HUVECs in 3D degradable PEG hydrogels with and without exposure to anti-cancer agents. Tumor spheroid diameter was quantified and compared between triculture and monoculture of A549 cells only. (n=4; *p<0.05 and **p<0.01)**

In addition to assessing cell viability, drug response to doxorubicin, semaxanib, and cilengitide was assessed at concentrations ranging from 0 to 10 μM for effects on endothelial tubule network formation in between HUVEC monoculture in 3D hydrogels and vascularized 3D tumor model. The vessel networks formed predominately by HUVECs and CAFp53kras cells in the vascularized 3D tumor model were significantly reduced under semaxanib and doxorubicin treatment relative to the untreated control, whereas vessel-like networks sustained and were visually apparent in the cilengitide treated hydrogels. Comparing total tubule length per volume in the drug treated groups relative to untreated controls, HUVECs in 3D monoculture were more sensitive to drug treatment than the HUVECs in vascularized 3D tumor model perhaps due to the increased levels of angiogenic growth factor (Chapter 2). For example, when the 3D tumor-angiogenesis model was treated with 1 μM concentration of cilengitide, less than a 10% decrease in total tubule length per volume was observed as compared to hydrogels with HUVECs alone ($p<0.01$). Treatment with cilengitide at the same concentration in 3D hydrogels with HUVEC monoculture caused a significant reduction in total tubule length/volume ($p<0.01$) relative to untreated control. The difference in drug sensitivity between 3D HUVEC monoculture and 3D triculture was more pronounced at higher concentrations of cilengitide. For example, shown in Figure 41 total tubule length/volume decreased by ~30% relative to untreated control in the 3D triculture after treatment with 5 μM cilengitide, whereas tubules in the 3D HUVEC monoculture treated at the same dosage decreased by ~80% relative to the untreated

control. With all the drugs tested, a significant difference was visualized between 3D HUVEC monoculture and the vascularized 3D tumor model.

Drug response to doxorubicin, semaxanib, and cilengitide was assessed at different concentrations ranging from 0 to 10 μM on tumor spheroid size in between A549 3D tumor only models and 3D tumor-angiogenesis model. Tumor spheroid size decreased by more than half in 5 μM doxorubicin treated groups relative to the untreated control in both A549 3D tumor only and 3D tumor angiogenesis triculture. In contrast to doxorubicin treatment, treatment of the 3D tumor angiogenesis culture with semaxanib at 5 μM concentration caused a reduction of tumor spheroid size by only 20%. All drugs at maximum concentration hindered tumor spheroid growth or disintegrated vessel-like networks. Significant decreases in tumor spheroid diameter were detected in A549 only 3D cultures as a result of doxorubicin or semaxanib treatment at 5 and 10 μM concentrations relative to untreated control. A549 cells consistently displayed enhanced survival within the vascularized 3D tumor model than in the 3D A549 monoculture after drug treatment.

## *4.4 Discussion*

To see if our proposed culture system is capable of recapitulating aspects of tumor cell behavior observed *in vivo*, we encapsulated A549 lung adenocarcinoma cells alone in degradable PEG hydrogels and monitored cell morphology and behavior in 3D over the time course in culture for up to 5 d. A549 cells were also seeded and cultured

on tissue-culture treated plastic in 2D. Bright-field microscopy of A549 lung epithelial cancer cells revealed clear differences in cell-cell interactions and morphology between 2D and 3D culture. A549 lung adenocarcinoma cells adopt a flattened morphology when grown on 2D plates and form round or oval cell aggregates with strong cell-cell adhesion when cultured in PEG hydrogels in 3D. Similar findings have been reported in previous studies in which A549 lung epithelial cells have shown differential growth morphologies in 3D MG as compared to cells cultured in 2D[214]. Specifically with A549 cells, Cichona and colleagues showed that lung epithelial cells embedded in 3D MG into spheroid agglomerates whereas cells seeded in 2D tissue culture plastic remained in cobblestone-like morphology[214]. Moreover, gene expression profiles associated with organized cell structures in 3D MG correlated with lung patient outcomes and thus indicating that tumor cells organizing into spheroids in 3D parallels cancer cells in the *in vivo* microenvironment where cell-cell and cell-ECM interactions are realistic[214,215]. In our studies tumor cell spheroids in PEG hydrogels formed as early as 3 d and appeared to grow larger in size with prolonged culture. Average size of tumor spheroids formed after 5 d in culture was about 42.1 ± 4.3 μm and consisted of multiple cells coalescing into a single spheroid.

To examine how 2D and 3D *in vitro* microenvironments affect cell response to drugs, proliferation and apoptosis was evaluated after drug treatment via immunostaining of ki67 and cleaved caspase-3, respectively. 2D and 3D cultures of HUVECs, A549 cells, and CAFp53kras cells were examined separately as monocultures

upon drug treatment with cilengitide, semaxanib, or doxorubicin at varying drug concentrations from 0 to 10 μM. Cilengitide, semaxanib, and doxorubicin are all anti-cancer agents that have been indicated for use in the treatment of lung cancer and act via different mechanisms. Cilengitide acts by inhibiting $\alpha v\beta 3$ and $\alpha 5\beta 1$ integrins[202]. Semaxanib inhibits VEGF-R2 (KDR/Flk-1) and doxorubicin intercalates with DNA and induces double-stranded DNA breaks[216,217]. Analysis of cells positive for ki67 (proliferation marker) in both 2D and 3D culture systems after drug treatment revealed significant differences in the inhibition of cell proliferation in 2D relative to 3D. HUVECs, A549, and CAFp53kras cells cultured in 2D all showed a significant reduction in the percentage of proliferative cells after drug treatment as compared to the untreated control. With 1 μM doxorubicin treatment, the percentage of proliferative cells in the 2D culture with A549 cells after drug exposure dropped to approximately 50% whereas >90% of the untreated cells remained proliferative. In contrast to A549 cells cultured and treated with drugs in 2D, A549 cells encapsulated as a monoculture in 3D PEG hydrogels required a higher concentration of doxorubicin at 5 μM to exhibit a ~50% reduction in the percentage of proliferative cells. These drug screening studies for cell monocultures in 2D and 3D systems suggest that 1 μM drug concentration demonstrated to be effective in 2D was not sufficient to elicit a similar decrease in cell proliferation or increase in cell apoptosis in the 3D culture system. The immunostaining analysis of cleaved caspase-3, a cell apoptotic marker, revealed significantly less apoptotic cells in 3D versus cells in 2D when treated with the same drug at the same

concentration. Our results on the effects of drugs on cell apoptosis and proliferation in between cells in 2D and 3D potentially indicate increased drug resistance of cells in 3D culture systems as opposed to conventional 2D monolayer culture systems. This behavior of cells in our 3D PEG hydrogel system reflects a more clinically relevant situation in which tumor cells *in vivo* display drug resistance causing the drug to be ineffective at the same dosage as cells treated in 2D conventional conditions[212,213].

To understand the differences in cytotoxic responses of the drugs observed in 2D and 3D culture systems, we examined the penetration and uptake of doxorubicin into the spheroids. The poor penetration of cytotoxic drugs into tumor spheroids has been indicated as one of the mechanisms by which decreased cytotoxicity is observed in 3D cultures as opposed 2D cell cultures[197,218]. Results from our uptake studies with doxorubicin suggest that the average percent of A549 cells with doxorubicin localized in the nucleus is not significantly different between cells in 2D and 3D. Although no significant differences in the uptake of doxorubicin were evident between cells in 2D and 3D, our results show that doxorubicin uptake is time dependent. Significantly less cells in both 2D and 3D had drug localized in the nuclei at 4 hr post drug incubation as opposed to 12 hr post drug incubation.

Similar doxorubicin uptake between cells cultured in 2D and 3D suggests that drug transport through the hydrogel is not a key factor driving the differential cell responses. A study conducted by Fischbach *et al.* suggests that cell integrin interaction with ECM molecules in the microenvironment is differentially regulated in 2D relative

to 3D culture and may be one of the underlying factors responsible for the variances in drug sensitivity in cells in 2D versus in 3D. Fischbach and colleagues showed with oral squamous cell carcinoma cells (OSCC-3) cultured in 2D on RGDS functionalized alginate disks, or cultured in 3D within unmodified alginate, or cultured in 3D with RGDS modified alginate showed that 3D culture in RGDS modified alginate resulted in significantly enhanced IL-8 levels relative to 2D culture on RGDS modified alginate disks[199]. The upregulation of IL-8 can potentially enhance tumor cell proliferation and contribute to decrease chemosensitivity[199]. The differential response to drugs observed in our studies in between cells in 2D and 3D culture conditions could be attributed to differences between 2D and 3D cell-matrix interactions.

To simulate the multi-cellular environment and cell-cell interactions of tumors *in vivo* in our 3D biomimetic culture system, the A549 lung cancer epithelial cells were encapsulated with the HUVECs and CAFs derived from lung tumors into a single hydrogel. Our past studies with co-culture of HUVEC and CAFp53kras cells at specific cell concentrations and ratios have shown these stromal cells to closely associate, interact, and organize into highly branched vessel networks. In order to simulate the *in vivo* tumor microenvironment, cell encapsulation with vessel generating cells along with A549 lung cancer cells in our 3D PEG based culture system was optimized so that vessel formation and tumor spheroid growth could occur concurrently as it occurs in tumors *in vivo*. Figure 38 shows the cell-cell interactions over time that lead to the formation of vessels and tumor cell spheroids in our protease degradable 3D cell culture system. In

this environment, encapsulated cells remodel the 3D environment by secreting MMP-2 and MMP-9 that facilitate matrix degradation and thereby enable cells to migrate and organize into vessel structures and tumor spheroids. In conjunction with the formation of vessels networks and multi-cellular tumor spheroid, additional tumor-mimicking properties such as tumor contact with vessels, vascular lumens, tumor cell proliferation and growth were observed as early as 3 d in culture. HUVEC cells (labeled with green CellTracker™) organized into tubule networks that increased in proportion to tumor spheroid growth. Unlike other reported angiogenesis assays[175], the biomimetic 3D *in vitro* culture system supports vessel formation without reliance on exogenous pro-angiogenic growth factors to promote angiogenic vessel formation. Moreover, labeling each cell type with a different CellTracker™ before encapsulation into PEG hydrogels allowed for investigating cellular behavior, cell-cell interactions, and drug efficacy in real time. One of the limitations to our 3D *in vitro* culture system is that majority of the multi-cellular tumor spheroids were approximately 40-45 μm in diameter. Since the maximum diffusion limit of oxygen is 100-200 μm[219,220], the tumor spheroids formed in our 3D *in vitro* system are too small in diameter to see effects of hypoxic or necrotic regions in the center of the spheroid. Nonetheless, we demonstrate the feasibility of our vascularized 3D tumor model as a more accurate drug testing platform. HUVECs, A549, and CAFp53kras cells were encapsulated and cultured in degradable PEG hydrogels for 5 d to allow for the formation of vessel-like structures and tumor spheroids before drug treatment. Semaxanib, cilengitide, and doxorubicin were evaluated in the vascularized

3D tumor model for their effect on tubule formation and tumor spheroid growth. In general, tubule structures in the vascularized 3D tumor model were significantly greater in total tubule length per volume before and after treatment with drugs as compared to gels with HUVECs only. It seems that interaction of HUVECs with lung tumor cells and CAFs enhances tubule network formation. To demonstrate the feasibility of our vascularized 3D tumor model for testing angiogenesis inhibitors, we utilized semaxanib, a potent and selective inhibitor of the Flk-1/KDR VEGF receptor tyrosine kinase, which has demonstrated its anti-angiogenic potential in preclinical and clinical studies[207,217,221]. In our study, when cells in the vascularized 3D tumor model were treated with semaxanib, total tubule length per volume and tumor spheroid diameter were both significantly reduced relative to the untreated control. These results correlate with previously reported results from drug studies conducted *in vivo* using animal models. Studies *in vivo* have shown semaxanib to reduce vessel density in tumors, induce tumor regression, and cause apoptosis of endothelial cells in a colon tumor metastasis model[221]. Semaxanib was shown in tumors implanted in nu/nu mice to reduce the growth of tumors upon treatment at a dose 25 mg/kg. When tumors were resected from drug-treated animals, the tumors in semaxanib treated animals were significantly reduced in tumor volume relative to untreated animals and appeared to be pale white. This unhealthy color of tumors resected from animals treated with semaxanib was attributed to reduced blood supply from inhibition of tumor angiogenesis[221,217]. Another set of studies conducted *in vivo* using a A549 lung tumor xenograft mouse model showed that

with semaxanib treatment tumor growth and blood vessels were significantly reduced relative to the untreated mice[207,208].

Results from preclinical studies with doxorubicin also correlate with drug effects on tumor growth witnessed in our 3D tumor microenvironment drug testing platform. For example, Singh and colleagues mixed human lung carcinoma A549 cells in MG and subcutaneously injected it in nude mice (BALB/c nu/nu)[205]. Mice treated with 4 mg/kg doxorubicin displayed approximately ~61% decrease in tumor weight after 8 d when compared with saline injected mice[205]. In comparison, our 3D lung adenocarcinoma model treated with doxorubicin at the highest concentration (~4 mg/kg) displayed a ~60% decrease in tumor spheroid diameter relative to untreated controls.

Interestingly, treating cells in the 3D tumor microenvironment mimicking model with cilengitide (at 1 μM and 5 μM) concentration did not significantly reduce tumor spheroid size relative to the untreated control. As opposed to the 3D tumor microenvironment model, 5μM cilengitide treatment in the tumor cell only 3D cultures caused a 2-fold reduction in tumor spheroid size relative to the untreated control. Cilengitide demonstrated its anti-angiogenic potential in our 3D tumor microenvironment mimicking model with a significant reduction in total tubule length/volume at drug concentrations of 5 μM and 10 μM relative to the untreated group. Results from previous studies conducted with cilengitide in *in vivo* lung carcinoma models corroborate our observations[222]. Reynolds and colleagues tested the efficacy of cilengitide in reducing tumor growth and angiogenesis in Lewis lung

carcinoma (LLC) tumor xenografts in mice[178,222]. Treatment of 200 mg/kg cilengitide in LLC mice did not suppress tumor growth significantly relative to tumors in saline injected mice[222]. In the same study, analysis of microvessel sprouting in mouse aortic rings with 48 hr treatment with cilengitide at concentrations ranging from 0 to 50 μM showed significant reduction in vessel sprouting relative to the untreated control only at concentrations above 20 μM[222]. Similar findings have also been reported in mouse glioblastoma models in which tumor size in cilengitide treated mice stayed unchanged (~1 to 2 mm in tumor size) during the entire length of the study (63 d). In the same study, angiogenesis evaluated by staining of CD31 for endothelial cells in resected tumors decreased significantly relative to control tumors[223].

## *4.5 Conclusion*

In this work, we demonstrate that our 3D *in vitro* lung adenocarcinoma model in biomimetic PEG hydrogel with interacting lung epithelial and stromal cells more closely mimics the tumor microenvironment *in vivo*. Specific conditions representative of the *in vivo* tumor microenvironment such as tumor cell proliferation, continuous tumor spheroid growth, and vessel formation were also exhibited in our 3D *in vitro* tumor model. Moreover, results from drug studies with doxorubicin, cilengitide, and semaxanib on tumor growth and vessel formation in our 3D *in vitro* culture system corresponded with findings reported *in vivo* preclinical studies[205,221,222]. This correlation in results between the 3D *in vitro* culture model and preclinical studies demonstrates that

our 3D culture system describe in this work could be utilized for the rapid screening of anti-cancer agents. Overall, our biomimetic 3D *in vitro* model can serve as a more reliable bridge to preclinical studies and a better anti-cancer therapy predicting platform than the conventional 2D monolayer cultures.

# 5. Future Directions

## *5.1 Influence of Tumor-Associated Macrophages on Cancer Cells & Tumor Angiogenesis*

We have demonstrated the use of PEG hydrogels modified with cell adhesive and enzymatically degradable peptides to study the influence of stromal cells like cancer-associated fibroblasts on lung epithelial cancer cells and endothelial cells. Our findings have provided greater insight into the role of stromal cells, cell-cell, and cell-ECM interactions in contributing to tumor growth.

Future work in similar *in vitro* culture system could explore the influence of inflammatory cells that habitat the tumor stroma on cancer cell behavior. Tumor associated macrophages (TAM) comprise the major inflammatory cellular component of the stroma of many tumors and are capable of promoting tumor growth and progression by release of growth factors and chemokines. Several reports suggest that TAM produce growth factors and cytokines such TGFβ[224], interleukin-6 (IL-6)[225,226], tumor-necrosis factor (TNF)[227], and VEGF[225,226] that can stimulate tumor cell proliferation, promote invasion and metastasis, and simulate angiogenesis. These growth factors and cytokines can act on tumors by remodeling tissue via activation of MMPs, directing cell migration, and stimulating angiogenic-factor production and vessel formation[225]. Future studies could incorporate TAM in 3D *in vitro* culture system in co-culture with epithelial cancer cells to investigate the role of TAM in cell-cell interactions and signaling that contribute to tumor cell proliferation and migration. In addition to growth factors and cytokines,

research findings also suggest that macrophages found in the tumor stroma produce matrix-metalloproteases, such as MMP-2 and MMP-9. MMPs 2 and 9 can degrade proteins of the extracellular matrix thereby paving the way for tumor cell invasion and migration[42,228]. Macrophages have also been implicated in promoting blood vessel formation[225,229]. Macrophages can potentially exert a dual influence on blood vessel formation. On one hand macrophages produce molecules like VEGF that are proangiogenic and stimulate endothelial cells to migrate and organize into vessel structures. On the other hand, recent work published by Hsu *et al.* suggests that another mechanism by which macrophages can contribute to angiogenesis is by exhibiting pericyte-like behavior to closely associate and align with newly formed vessels and thereby provide long-term vessel support and stability[229]. Hsu *et al.* implanted PDGF-BB and FGF-2 releasing hydrogels in the corneal micro-pocket of Flk1-myr::mCherry transgenic mice[229]. Time-lapse studies showed macrophages migrating to the site of angiogenesis and closely interacting with mCherry labeled endothelial tip cells and surrounding vessels in a fashion similar to pericytes (Figure 42). Future work could incorporate tumor-associated macrophages in combination with vascular cells in a 3D *in vitro* system to further investigate the functional role of TAMs in promoting tumor angiogenesis.

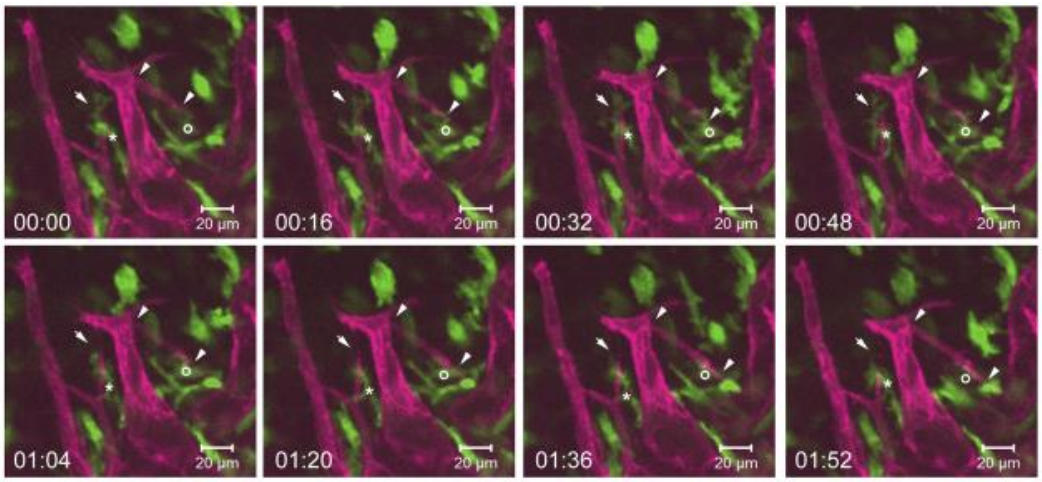


**Figure 42: Time lapse images showing macrophages (labeled in green) interacting and closely associating with mCherry labeled endothelial cells during angiogenesis. From Hsu *et al*[229].**

## *5.2 Engineering perfused 3D tumor models*

The 3D biomimetic PEG-based tumor model described in previous sections is capable of advancing our understanding on the effects of cell-ECM and cell-cell interactions on tumorigenesis and vascularization. We have demonstrated that 3D tumor models that more closely represent the cancer microenvironment can essentially improve the predictive performance of cancer therapies and drugs. Potential future work could seek to improve this system by incorporating other important pathological properties of the cancer microenvironment, such as fluid flow. The increase in permeability of solutes and water within a tumor due the leaky microvessels causes a rise in the interstitial fluid pressure. This localized increase in interstitial fluid pressure causes fluid flow from tumor mass into the surrounding environment. Interstitial fluid

flow is an important feature of the tumor microenvironment and has been shown to influence tumor cell phenotype via flow-derived shear stress[230,231].

Flow-derived shear stress has shown to effect tumor cell proliferation and migration[230,231]. Polacheck and colleagues used a microfluidic cell culture system to culture MDA-MB-231 breast cancer cells in a 3D collagen I matrix and investigate the influence of interstitial flow on the directional bias of cell migration[230]. Net migration vectors for cells in control devices without flow showed cell migration to be random whereas cells under flow at a rate of 3.0 μm/s preferentially migrated in the upstream direction of flow. The fraction of cell population migrating upstream than downstream was dependent on the interstitial flow rate. A flow rate of 3.0 μm/s induced more cells to migrate upstream than an interstitial flow rate of 0.3 μm/s. Polacheck and colleagues also observed that flow induced phosphorylation of focal adhesion kinase (FAK) indicating that flow-induced tension in integrins provided the upstream migratory stimulus[230]. Flow-derived shear stress has also shown to create gradients of chemokines that enhance cancer cell invasion and metastasis[232]. A study conducted by Shield *et al.* showed increase in the metastatic potential of MDA-MB-435S melanoma cells when exposed to flow. The metastatic potential in the MDA-MB-435S cells was activated upon binding of lymphatic endothelial cell-secreted CCL21 ligand to the CCR7 receptor on tumor cells[232]. CCR7 is implicated in lymph node metastasis. At physiologically relevant flow velocity of 0.2 μm/s, fluid flow increased the concentration of CCL21 ligand at the downstream side of the cell causing the distribution of the chemokine factors

downstream thereby creating an autologous gradient that provided a positive chemotactic signal to tumor cells.

To recapitulate tumor-mimicking fluid dynamics, the use of bioreactors to include perfusion in 3D culture systems has been demonstrated. A perfused 3D cell culture system refers to the continuous flow of media through a construct for the supply of nutrients. The development of perfused 3D tumor models can better recapitulate drug transport and overcome diffusional limitation in static culture systems. Perfusion flow rate is regulated to control shear stress and drug transport within 3D constructs[233]. Santoro and colleagues have demonstrated the utility of flow perfusion bioreactor for culturing Ewing sarcoma cells on electrospun PCL 3D scaffolds[233]. Cancer cells that were exposed to mechanical stimulation via flow-derived shear stress produced more insulin-like growth factor (IGF-1) when compared with 3D tumor constructs under static conditions. The effect of IGF-1R inhibitor dalotuzumab on cells cultured in perfused 3D constructs was compared with cells under static conditions. Increase in flow rate from 0.04 to 40 mL/min resulted in high shear stress and increase in drug transport within the construct. Despite increase in drug transport, the Ewing sarcoma cells cultured in perfused 3D PCL constructs displayed more resistance to IGF-1R inhibitor dalotuzumab. This effect could be due to the higher levels of IGF-1 produced by cells under mechanical stimulation counteracting the effects of the IGF-1R inhibitor dalotuzumab. The same effect was not observed in the control group with cells cultured under static conditions[233]. Additionally, perfused 3D tumor models have been demonstrated to

mimic cellular behavior and proliferation more closely to the *in vivo* tumor microenvironment. In a study conducted by Hirt *et al*., colorectal cancer (CRC) HT-29 cells were cultured in 2D, in collagen sponges in static conditions, or in perfused bioreactors (Figure 43), or injected subcutaneously in mice[231].

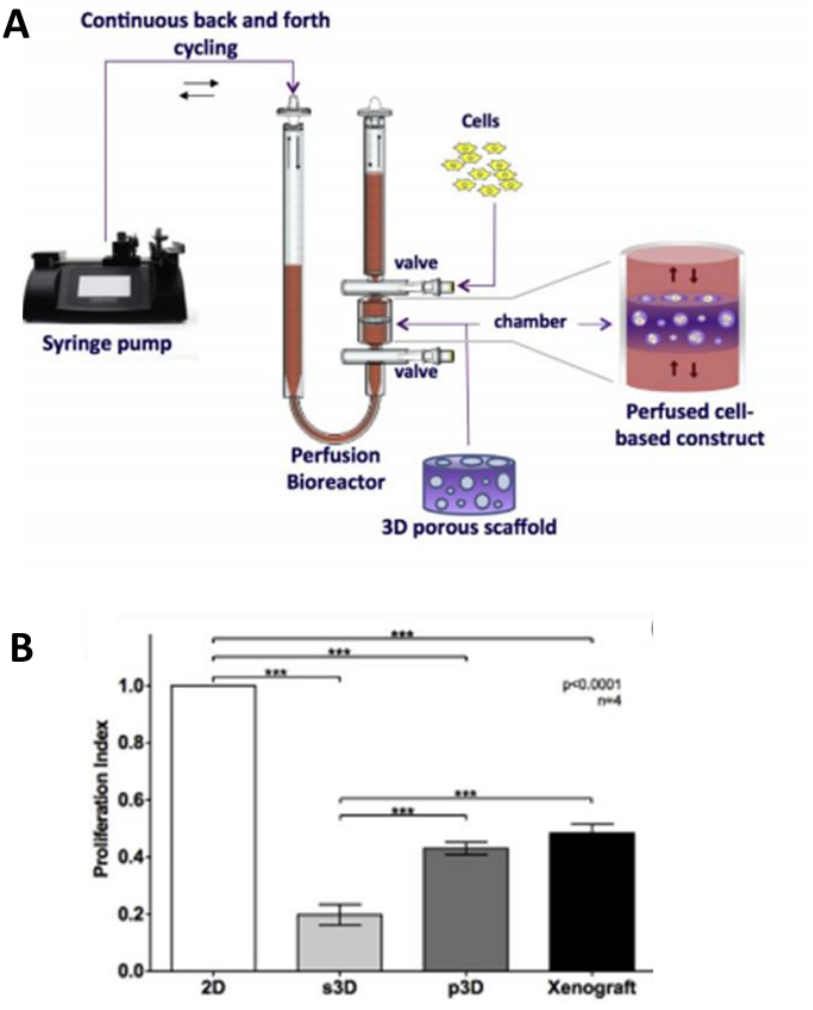


**Figure 43: Schematic of the bioreactor utilized in studies conducted by Hirt *et al*. for the culture of for (CRC) HT-29 cells in perfused 3D constructs. The bioreactor includes a perfusion chamber with a 3D porous scaffold and fluid flow dynamics is controlled by a pump connected with the bioreactor. B) Perfused 3D (p3D) cultures**

**resulted in significantly higher cell proliferation than static 3D (s3D) cultures with proliferation in p3D cultures similar to *in vivo* xenografts. From Hirt *et al*[231].**

Perfused 3D (p3D) cultures resulted in significantly higher cell proliferation than static 3D (s3D) cultures with cellular morphology and proliferation similar to *in vivo* xenografts. Cells in 2D treated with the chemotherapeutic drug, 5-Fluorouracil (5-FU), underwent apoptosis post treatment whereas no significant change in apoptotic cell numbers was evident in cells in p3D cultures and xenografts upon drug treatment[231]. Studies conducted by Santoro *et al.* and Hirt *et al.* highlight how incorporating fluid flow in 3D tumor model can accurately represent mechanical influences in the cancer environment and affect the efficacy of potential drug therapies. Incorporating fluid flow in degradable PEG hydrogels has been demonstrated and accomplished previously with the use of a microfluidic system shown in Figure 44.

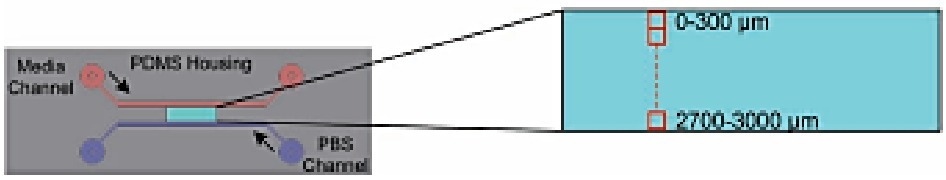


**Figure 44: Schematic of microfluidic system which consists of a PDMS housing with molded microchannels for perfused media (red) and buffer (blue) to provide fluid flow to PEG hydrogels (cyan) placed in the middle of the microchannels. From Cuchiara *et al*[234].**

Cuchiara *et al.* integrated a degradable PEG hydrogel with encapsulated HUVECs and 10T1/2 cells in a microfluidic hydrogel fabricated by soft lithographic and photolithographic techniques (Figure 44). The system was used to perfuse self-assembled microvascular networks. Cuchiara *et al*. showed that incorporating flow through cell-laden hydrogels via microfluidic channels maintained high cell viability for cells near the media channels. However, cell viability decreased significantly with increased distance from the media channels. Similar to the studies conducted by Cuchiara *et al*., future studies could involve incorporating a 3D tumor microenvironment mimicking model (described in chapter 4) to investigate changes in cancer cell survival with perfused vessel networks in 3D hydrogels.

# References


(1) Jemal, A.; Siegel, R. Cancer Facts & Figures 2013 http://www.cancer.org/research/cancerfactsstatistics/global.

(2) Siegel, R. L.; Miller, K. D.; Jemal, A. Cancer statistics, 2015. *CA. Cancer J. Clin.* **2015**, *65* (1), 5–29.

(3) Bremnes, R. M.; Donnem, T.; Al-Saad, S.; Al-Shibli, K.; Anderson, S.; Sirera, R.; Camps, C.; Marines, I.; Busund, L.-T. The Role of Tumor Stroma in Cancer Progression and. *J. Thorac. Oncol.* **2011**, *6*, 209–217.

(4) Kalluri, R. Basement membranes: structure, assembly and role in tumour angiogenesis. *Nat. Rev. Cancer* **2003**, *3* (6), 422–433 DOI: 10.1038/nrc1094.

(5) Mueller, M. M.; Fusenig, N. E. Friends or foes - bipolar effects of the tumour stroma in cancer. *Nat. Rev. Cancer* **2004**, *4* (11), 839–849 DOI: 10.1038/nrc1477.

(6) Koontongkaew, S. The tumor microenvironment contribution to development, growth, invasion and metastasis of head and neck squamous cell carcinomas. *J. Cancer* **2013**, *4* (1), 66–83 DOI: 10.7150/jca.5112.

(7) Kalluri, R.; Zeisberg, M. Fibroblasts in cancer. *Nat. Rev. Cancer* **2006**, *6* (5), 392–401 DOI: 10.1038/nrc1877.

(8) Tlsty, T. D.; Hein, P. W. Know thy neighbor: stromal cells can contribute oncogenic signals. *Curr. Opin. Genet. Dev.* **2001**, *11*, 54–59.

(9) Rodemann, H. P.; Muller, G. A. Characterization of human renal fibroblasts in health and disease: In vitro growth, differentiation, and collagen synthesis of fibroblasts from kidneys with interstitial fibrosis. *Am. J. Kidney Dis.* **1991**, *17*, 684–686.

(10) Liotta, L. A.; Stetler-stevenson, W. G. Tumor Invasion and Metastasis : An Imbalance of Positive and Negative Regulation. *Cancer Res.* **1991**, *51*, 5054a – 5059a.

(11) Liotta, L. A.; Kohn, E. C. The microenvironment of the tumour–host interface. **2001**, 380–384.

(12) Mueller, L.; Goumas, F. a; Affeldt, M.; Sandtner, S.; Gehling, U. M.; Brilloff, S.; Walter, J.; Karnatz, N.; Lamszus, K.; Rogiers, X.; et al. Stromal fibroblasts in colorectal liver metastases originate from resident fibroblasts and generate an inflammatory microenvironment. *Am. J. Pathol.* **2007**, *171* (5), 1608–1618 DOI: 10.2353/ajpath.2007.060661.

(13) Orimo, A.; Gupta, P. B.; Sgroi, D. C.; Arenzana-Seisdedos, F.; Delaunay, T.;

Naeem, R.; Carey, V. J.; Richardson, A. L.; Weinberg, R. a. Stromal fibroblasts present in invasive human breast carcinomas promote tumor growth and angiogenesis through elevated SDF-1/CXCL12 secretion. *Cell* **2005**, *121* (3), 335–348 DOI: 10.1016/j.cell.2005.02.034.

(14) Zeisberg, E. M.; Potenta, S.; Xie, L.; Zeisberg, M.; Kalluri, R. Discovery of endothelial to mesenchymal transition as a source for carcinoma-associated fibroblasts. *Cancer Res.* **2007**, *67* (21), 10123–10128 DOI: 10.1158/0008-5472.CAN-07-3127.

(15) Yayon, a; Klagsbrun, M.; Esko, J. D.; Leder, P.; Ornitz, D. M. Cell surface, heparin-like molecules are required for binding of basic fibroblast growth factor to its high affinity receptor. *Cell* **1991**, *64*, 841–848 DOI: 10.1016/0092-8674(91)90512-W.

(16) Renehan, A. G.; Zwahlen, M.; Minder, C.; O'Dwyer, S. T.; Shalet, S. M.; Egger, M. Insulin-like growth factor (IGF)-I, IGF binding protein-3, and cancer risk: Systematic review and meta-regression analysis. *Lancet* **2004**, *363* (9418), 1346–1353 DOI: 10.1016/S0140-6736(04)16044-3.

(17) Derksen, P. W. B.; Keehnen, R. M. J.; Evers, L. M.; Van Oers, M. H. J.; Spaargaren, M.; Pals, S. T. Cell surface proteoglycan syndecan-1 mediates hepatocyte growth factor binding and promotes Met signaling in multiple myeloma. *Blood* **2002**, *99* (4), 1405–1410 DOI: 10.1182/blood.V99.4.1405.

(18) Bhowmick, N. A.; Neilson, E. G.; Moses, H. L. Stromal fibroblasts in cancer initiation and progression. *Nature* **2004**, *432*, 332–337.

(19) Pietras, K.; Pahler, J.; Bergers, G.; Hanahan, D. Functions of paracrine PDGF signaling in the proangiogenic tumor stroma revealed by pharmacological targeting. *PLoS Med.* **2008**, *5* (1), e19 DOI: 10.1371/journal.pmed.0050019.

(20) Pietras, K.; Sjöblom, T.; Rubin, K.; Heldin, C. H.; Östman, A. PDGF receptors as cancer drug targets. *Cancer Cell* **2003**, *3*, 439–443 DOI: 10.1016/S1535-6108(03)00089-8.

(21) Lu, P.; Weaver, V. M.; Werb, Z. The extracellular matrix: a dynamic niche in cancer progression. *J. Cell Biol.* **2012**, *196* (4), 395–406 DOI: 10.1083/jcb.201102147.

(22) Kim, S.-H.; Turnbull, J.; Guimond, S. Extracellular matrix and cell signalling: the dynamic cooperation of integrin, proteoglycan and growth factor receptor. *J. Endocrinol.* **2011**, *209* (2), 139–151 DOI: 10.1530/JOE-10-0377.

(23) Hynes, R. O. The extracellular matrix: not just pretty fibrils. *Science* **2009**, *326* (5957), 1216–1219 DOI: 10.1126/science.1176009.

(24) Ozbek, S.; Balasubramanian, P. G.; Chiquet-Ehrismann, R.; Tucker, R. P.; Adams, J. C. The evolution of extracellular matrix. *Mol. Biol. Cell* **2010**, *21* (24), 4300–4305 DOI: 10.1091/mbc.E10-03-0251.

(25) Davis, G. E.; Senger, D. R. Endothelial extracellular matrix: biosynthesis, remodeling, and functions during vascular morphogenesis and neovessel stabilization. *Circ. Res.* **2005**, *97* (11), 1093–1107 DOI: 10.1161/01.RES.0000191547.64391.e3.

(26) Kanematsu, A.; Marui, A.; Yamamoto, S.; Ozeki, M.; Hirano, Y.; Yamamoto, M.; Ogawa, O.; Komeda, M.; Tabata, Y. Type I collagen can function as a reservoir of basic fibroblast growth factor. *J. Control. Release* **2004**, *99* (2), 281–292 DOI: 10.1016/j.jconrel.2004.07.008.

(27) Hardingham, T.; Fosang, A. Proteoglycans: many forms and many functions. *FASEB J.* **1992**, *6*, 861–870.

(28) Stupack, D. G.; Cheresh, D. a. ECM Remodeling Regulates Angiogenesis: Endothelial Integrins Look for New Ligands. *Sci. Signal.* **2002**, *2002* (119), pe7–pe7 DOI: 10.1126/stke.2002.119.pe7.

(29) Roycik, M. D. A fresh prospect of extracellular matrix hydrolytic enzymes and their substrates. *Curr. Pharm. Des.* **2009**, *15* (12), 1295.

(30) Lu, P.; Takai, K.; Weaver, V. M.; Werb, Z. Extracellular matrix degradation and remodeling in development and disease. *Cold Spring Harb. Perspect. Biol.* **2011**, *3* (12) DOI: 10.1101/cshperspect.a005058.

(31) Mitra, S. K.; Schlaepfer, D. D. Integrin-regulated FAK–Src signaling in normal and cancer cells. *Curr. Opin. Cell Biol.* **2006**, *18* (5), 516–523 DOI: 10.1016/j.ceb.2006.08.011.

(32) Giancotti, F. G.; Ruoslahti, E. Integrin Signaling. **1999**, *285* (August), 1028–1032.

(33) Marie, P. J.; Hay, E.; Saidak, Z. Integrin and cadherin signaling in bone : role and potential therapeutic targets. **2014**, *25* (11), 567–575 DOI: 10.1016/j.tem.2014.06.009.

(34) Baird, B. N.; Schliekelman, M. J.; Ahn, Y.-H.; Chen, Y.; Roybal, J. D.; Gill, B. J.; Mishra, D. K.; Erez, B.; O'Reilly, M.; Yang, Y.; et al. Fibulin-2 is a driver of malignant progression in lung adenocarcinoma. *PLoS One* **2013**, *8* (6), e67054 DOI: 10.1371/journal.pone.0067054.

(35) Bignon, M.; Pichol-Thievend, C.; Hardouin, J.; Malbouyres, M.; Bréchot, N.; Nasciutti, L.; Barret, A.; Teillon, J.; Guillon, E.; Etienne, E.; et al. Lysyl oxidase-like protein-2 regulates sprouting angiogenesis and type IV collagen assembly in the endothelial basement membrane. *Blood* **2011**, *118* (14), 3979–3989 DOI:

10.1182/blood-2010-10-313296.

(36) Barker, H. E.; Chang, J.; Cox, T. R.; Lang, G.; Bird, D.; Nicolau, M.; Evans, H. R.; Gartland, A.; Erler, J. T. LOXL2-mediated matrix remodeling in metastasis and mammary gland involution. *Cancer Res.* **2011**, *71* (5), 1561–1572 DOI: 10.1158/0008-5472.CAN-10-2868.

(37) Stetler-stevenson, W. G.; Aznavoorian, S.; Liotta, A. Tumor Cell Interaction with the extracellular matrix during invasion and metastasis. *Annu. Rev. Cell Biol.* **1993**, *9*, 541–573.

(38) Psaila, B.; Lyden, D. The metastatic niche: adapting the foreign soil. **2009**, *9* (APrIl), 285–293.

(39) van Hinsbergh, V. W. M.; Koolwijk, P. Endothelial sprouting and angiogenesis: matrix metalloproteinases in the lead. *Cardiovasc. Res.* **2008**, *78* (2), 203–212 DOI: 10.1093/cvr/cvm102.

(40) Page-McCaw, A.; Ewald, A. J.; Werb, Z. Matrix metalloproteinases and the regulation of tissue remodelling. *Nat. Rev. Mol. Cell Biol.* **2007**, *8* (3), 221–233 DOI: 10.1038/nrm2125.

(41) Coussens, L. M.; Fingleton, B.; Matrisian, L. M. Matrix metalloproteinase inhibitors and cancer: trials and tribulations. *Science* **2002**, *295* (5564), 2387–2392 DOI: 10.1126/science.1067100.

(42) Egeblad, M.; Werb, Z. New functions for the matrix metalloproteinases in cancer progression. *Nat. Rev. Cancer* **2002**, *2* (3), 161–174 DOI: 10.1038/nrc745.

(43) Newman, A. C.; Nakatsu, M. N.; Chou, W.; Gershon, P. D.; Hughes, C. C. W. The requirement for fibroblasts in angiogenesis: fibroblast-derived matrix proteins are essential for endothelial cell lumen formation. *Mol. Biol. Cell* **2011**, *22* (20), 3791–3800 DOI: 10.1091/mbc.E11-05-0393.

(44) Mott, J. D.; Werb, Z. Regulation of matrix biology by matrix metalloproteinases. *Curr. Opin. Cell Biol.* **2004**, *16* (5), 558–564 DOI: 10.1016/j.ceb.2004.07.010.

(45) Madar, S.; Goldstein, I.; Rotter, V. "Cancer associated fibroblasts"--more than meets the eye. *Trends Mol. Med.* **2013**, *19* (8), 447–453 DOI: 10.1016/j.molmed.2013.05.004.

(46) Chen, W.-J.; Ho, C.-C.; Chang, Y.-L.; Chen, H.-Y.; Lin, C.-A.; Ling, T.-Y.; Yu, S.-L.; Yuan, S.-S.; Chen, Y.-J. L.; Lin, C.-Y.; et al. Cancer-associated fibroblasts regulate the plasticity of lung cancer stemness via paracrine signalling. *Nat. Commun.* **2014**, *5*, 3472 DOI: 10.1038/ncomms4472.

(47) Roybal, J. D.; Zang, Y.; Ahn, Y.-H.; Yang, Y.; Gibbons, D. L.; Baird, B. N.; Alvarez,

C.; Thilaganathan, N.; Liu, D. D.; Saintigny, P.; et al. miR-200 Inhibits lung adenocarcinoma cell invasion and metastasis by targeting Flt1/VEGFR1. *Mol. Cancer Res.* **2011**, *9* (1), 25–35 DOI: 10.1158/1541-7786.MCR-10-0497.

(48) Orimo, A.; Weinberg, R. a. Stromal Fibroblasts in Cancer: A Novel Tumor-Promoting Cell Type. *Cell Cycle* **2006**, *5* (15), 1597–1601 DOI: 10.4161/cc.5.15.3112.

(49) Xing, F.; Saidou, J.; Watabe, K. Cancer Associated Fibroblasts (CAFs) in tumor microenvironment. **2011**, No. 2, 166–179.

(50) Ungefroren, H.; Sebens, S.; Seidl, D.; Lehnert, H.; Hass, R. Interaction of tumor cells with the microenvironment. *Cell Commun. Signal.* **2011**, *9* (1), 18 DOI: 10.1186/1478-811X-9-18.

(51) Jodele, S.; Blavier, L.; Yoon, J. M.; DeClerck, Y. a. Modifying the soil to affect the seed: role of stromal-derived matrix metalloproteinases in cancer progression. *Cancer Metastasis Rev.* **2006**, *25* (1), 35–43 DOI: 10.1007/s10555-006-7887-8.

(52) Chaffer, C. L.; Weinberg, R. a. A perspective on cancer cell metastasis. *Science* **2011**, *331* (6024), 1559–1564 DOI: 10.1126/science.1203543.

(53) Geevarghese, A.; Herman, I. M. Pericyte-endothelial crosstalk: implications and opportunities for advanced cellular therapies. *Transl. Res.* **2014**, 1–11 DOI: 10.1016/j.trsl.2014.01.011.

(54) Gerhardt, H.; Betsholtz, C. Endothelial-pericyte interactions in angiogenesis. *Cell Tissue Res.* **2003**, *314* (1), 15–23 DOI: 10.1007/s00441-003-0745-x.

(55) Moon, J. J.; West, J. L. Vascularization of engineered tissues: approaches to promote angio-genesis in biomaterials. *Curr. Top. Med. Chem.* **2008**, *8* (4), 300–310.

(56) Patan, S. Vasculogenesis and angiogenesis as mechanisms of vascular network formation, growth and remodeling. *J. Neurooncol.* **2001**, *50* (1-2), 1–15.

(57) Phelps, Edward A. & Garcia, A. J. Update on therapeutic vascularization strategies. **2009**, *4* (1), 65–80 DOI: 10.2217/17460751.4.1.65.Update.

(58) Bergers, G. The role of pericytes in blood-vessel formation and maintenance. *Neuro. Oncol.* **2005**, *7* (4), 452–464 DOI: 10.1215/S1152851705000232.

(59) Eberhard, A.; Kahlert, S.; Goede, V.; Hemmerlein, B.; Plate, K. H.; Augustin, H. G. Heterogeneity of Angiogenesis and Blood Vessel Maturation in Human Tumors : Implications for Antiangiogenic Tumor Therapies Heterogeneity of Angiogenesis and Blood Vessel Maturation in Human Tumors : Implications for Antiangiogenic Tumor Therapies 1. *Cancer Res.* **2000**, *60*, 1388–1393.

(60) Jain, R. K. Normalization of tumor vasculature: an emerging concept in

antiangiogenic therapy. *Science* **2005**, *307* (5706), 58–62 DOI: 10.1126/science.1104819.

(61) Morikawa, S.; Baluk, P.; Kaidoh, T.; Haskell, A.; Jain, R. K.; McDonald, D. M. Abnormalities in pericytes on blood vessels and endothelial sprouts in tumors. *Am. J. Pathol.* **2002**, *160* (3), 985–1000 DOI: 10.1016/S0002-9440(10)64920-6.

(62) Carmeliet, P., Ferreira, V., Breier, G., Polleyfeyt, S., Kieckens, L., Gertsenstein, M., Fahrig, M., Vandenhoeck, A., Harpal, K., Harpal, C., E. C. Abnormal blood vessel development and lethality in embryos lacking a single VEGF allele. *Nature* **1996**, *380*, 435–439.

(63) Hutmacher, D. W.; Loessner, D.; Rizzi, S.; Kaplan, D. L.; Mooney, D. J.; Clements, J. a. Can tissue engineering concepts advance tumor biology research? *Trends Biotechnol.* **2010**, *28* (3), 125–133 DOI: 10.1016/j.tibtech.2009.12.001.

(64) Grabowska, I.; Szeliga, A.; Moraczewski, J.; Czaplicka, I.; Brzóska, E. Comparison of satellite cell-derived myoblasts and C2C12 differentiation in two- and three-dimensional cultures: changes in adhesion protein expression. *Cell Biol. Int.* **2011**, *35* (2), 125–133 DOI: 10.1042/CBI20090335.

(65) Weaver, V. M.; Petersen, O. W.; Wang, F.; Larabell, C. a; Briand, P.; Damsky, C.; Bissell, M. J. Reversion of the malignant penotype of human breast cells in three-dimensional cutlure and in vivo by integrin blocking antibodies. *J.Cell Biol.* **1997**, *137* (1), 231–245 DOI: 10.1083/jcb.137.1.231.

(66) Jeanes, A. I.; Maya-Mendoza, A.; Streuli, C. H. Cellular microenvironment influences the ability of mammary epithelia to undergo cell cycle. *PLoS One* **2011**, *6* (3), e18144 DOI: 10.1371/journal.pone.0018144.

(67) Tung, Y.-C.; Hsiao, A. Y.; Allen, S. G.; Torisawa, Y.; Ho, M.; Takayama, S. High-throughput 3D spheroid culture and drug testing using a 384 hanging drop array. *Analyst* **2011**, *136* (3), 473–478 DOI: 10.1039/C0AN00609B.

(68) Drury, J. L.; Mooney, D. J. Hydrogels for tissue engineering: scaffold design variables and applications. *Biomaterials* **2003**, *24* (24), 4337–4351 DOI: 10.1016/S0142-9612(03)00340-5.

(69) Li, M. L.; Aggeler, J.; Farson, D. A.; Hatier, C.; Hassell, J.; Bissell, M. J. Influence of a reconstituted basement membrane and its components on casein gene expression and secretion in mouse mammary epithelial cells. *Proc. Natl. Acad. Sci.* **1987**, *84* (1), 136–140 DOI: 10.1073/pnas.84.1.136.

(70) Weigelt, B.; Ghajar, C. M.; Bissell, M. J. The need for complex 3D culture models to unravel novel pathways and identify accurate biomarkers in breast cancer. *Adv. Drug Deliv. Rev.* **2014**, *69-70*, 42–51 DOI: 10.1016/j.addr.2014.01.001.

(71) Mukai, N.; Akahori, T.; Komaki, M.; Li, Q.; Kanayasu-Toyoda, T.; Ishii-Watabe, A.; Kobayashi, A.; Yamaguchi, T.; Abe, M.; Amagasa, T.; et al. A comparison of the tube forming potentials of early and late endothelial progenitor cells. *Exp. Cell Res.* **2008**, *314* (3), 430–440 DOI: 10.1016/j.yexcr.2007.11.016.

(72) Haralabopoulos, G. C.; Grant, D. S.; Kleinman, H. K.; Maragoudakis, M. E. Thrombin promotes endothelial cell alignment in Matrigel in vitro and angiogenesis in vivo. *Am. J. Physiol.* **1997**, *273* (1 Pt 1), C239–C245.

(73) Khoo, C. P.; Micklem, K.; Watt, S. M. A comparison of methods for quantifying angiogenesis in the Matrigel assay in vitro. *Tissue Eng. Part C. Methods* **2011**, *17* (9), 895–906 DOI: 10.1089/ten.TEC.2011.0150.

(74) Delacoux, F.; Fichard, a; Geourjon, C.; Garrone, R.; Ruggiero, F. Molecular features of the collagen V heparin binding site. *J. Biol. Chem.* **1998**, *273* (24), 15069–15076.

(75) Montesano, R.; Orci, L.; Vassalli, P. In vitro rapid organization of endothelial cells into capillary-like networks is promoted by collagen matrices. *J. Cell Biol.* **1983**, *97* (5 Pt 1), 1648–1652.

(76) Califano, J. P.; Reinhart-King, C. a. The effects of substrate elasticity on endothelial cell network formation and traction force generation. *Proc. 31st Annu. Int. Conf. IEEE Eng. Med. Biol. Soc. Eng. Futur. Biomed. EMBC 2009* **2009**, *8491*, 3343–3345 DOI: 10.1109/IEMBS.2009.5333194.

(77) Szot, C. S.; Buchanan, C. F.; Freeman, J. W.; Rylander, M. N. 3D in vitro bioengineered tumors based on collagen I hydrogels. *Biomaterials* **2011**, *32* (31), 7905–7912 DOI: 10.1016/j.biomaterials.2011.07.001.

(78) Lee, K. Y.; Mooney, D. J. Hydrogels for Tissue Engineering. *Chem. Rev.* **2001**, *101* (7), 1869–1880 DOI: 10.1021/cr000108x.

(79) Roeder, B. a.; Kokini, K.; Sturgis, J. E.; Robinson, J. P.; Voytik-Harbin, S. L. Tensile Mechanical Properties of Three-Dimensional Type I Collagen Extracellular Matrices With Varied Microstructure. *J. Biomech. Eng.* **2002**, *124* (2), 214 DOI: 10.1115/1.1449904.

(80) Achilli, M.; Mantovani, D. Tailoring Mechanical Properties of Collagen-Based Scaffolds for Vascular Tissue Engineering: The Effects of pH, Temperature and Ionic Strength on Gelation. *Polymers (Basel).* **2010**, *2* (4), 664–680 DOI: 10.3390/polym2040664.

(81) Pankajakshan, D.; Agrawal, D. K. Scaffolds in tissue engineering of blood vessels. **2010**, *873*, 855–873 DOI: 10.1139/Y10-073.

(82) Ratliff, B. B.; Ghaly, T.; Brudnicki, P.; Yasuda, K.; Rajdev, M.; Bank, M.; Mares, J.; Hatzopoulos, A. K.; Goligorsky, M. S. Endothelial progenitors encapsulated in bioartifical niches are insulated from systemic cytotoxicity and are angiogenesis competent. *Am J Physiol Ren. Physiol* **2010**, *299*, 178–186.

(83) Gurski, L. a; Jha, A. K.; Zhang, C.; Jia, X.; Farach-Carson, M. C. Hyaluronic acid-based hydrogels as 3D matrices for in vitro evaluation of chemotherapeutic drugs using poorly adherent prostate cancer cells. *Biomaterials* **2009**, *30* (30), 6076–6085 DOI: 10.1016/j.biomaterials.2009.07.054.

(84) Liu, J.; Tan, Y.; Zhang, H.; Zhang, Y.; Xu, P.; Chen, J.; Poh, Y.-C.; Tang, K.; Wang, N.; Huang, B. Soft fibrin gels promote selection and growth of tumorigenic cells. *Nat. Mater.* **2012**, *11* (8), 734–741 DOI: 10.1038/nmat3361.

(85) Hall, H.; Hubbell, J. a. Matrix-bound sixth Ig-like domain of cell adhesion molecule L1 acts as an angiogenic factor by ligating alphavbeta3-integrin and activating VEGF-R2. *Microvasc. Res.* **2004**, *68* (3), 169–178 DOI: 10.1016/j.mvr.2004.07.001.

(86) Wu, X.; Rabkin-Aikawa, E.; Guleserian, K. J.; Perry, T. E.; Masuda, Y.; Sutherland, F. W. H.; Schoen, F. J.; Mayer, J. E.; Bischoff, J. Tissue-engineered microvessels on three-dimensional biodegradable scaffolds using human endothelial progenitor cells. *Am. J. Physiol. Circ. Physiol.* **2004**, *287* (2), H480–H487.

(87) Chung, T. W.; Yang, M. .; Liu, D. .; Chen, W. P.; Pan, C. I.; Wang, S. . Enhancing growth human endothelial cells on Arg-Gly-Asp (RGD) embedded poly(ε-caprolactone) (PCL) surface with nanometer scale of surface disturbance. *J. Biomed. Mater. Res.* **2005**, *72* (2), 213–219.

(88) Leung, L.; Chan, C.; Baek, S.; Naguib, H. Comparison of morphology and mechanical properties of PLGA bioscaffolds. *Biomed. Mater.* **2008**, *3* (2), 025006 DOI: 10.1088/1748-6041/3/2/025006.

(89) Griffith, L. G.; Swartz, M. a. Capturing complex 3D tissue physiology in vitro. *Nat. Rev. Mol. Cell Biol.* **2006**, *7* (3), 211–224 DOI: 10.1038/nrm1858.

(90) Luu, Y. K.; Kim, K.; Hsiao, B. S.; Chu, B.; Hadjiargyrou, M. Development of a nanostructured DNA delivery scaffold via electrospinning of PLGA and PLA-PEG block copolymers. *J. Control. Release* **2003**, *89* (2), 341–353 DOI: 10.1016/S0168-3659(03)00097-X.

(91) Moon, J. J.; Saik, J. E.; Poché, R. a; Leslie-Barbick, J. E.; Lee, S.-H.; Smith, A. a; Dickinson, M. E.; West, J. L. Biomimetic hydrogels with pro-angiogenic properties. *Biomaterials* **2010**, *31* (14), 3840–3847 DOI: 10.1016/j.biomaterials.2010.01.104.

(92) Saik, J. E.; Gould, D. J.; Watkins, E. M.; Dickinson, M. E.; West, J. L. Covalently immobilized platelet-derived growth factor-BB promotes angiogenesis in biomimetic poly(ethylene glycol) hydrogels. *Acta Biomater.* **2011**, *7* (1), 133–143 DOI: 10.1016/j.actbio.2010.08.018.

(93) Saik, J. E.; Gould, D. J.; Keswani, A. H.; Dickinson, M. E.; West, J. L. Biomimetic hydrogels with immobilized ephrinA1 for therapeutic angiogenesis. *Biomacromolecules* **2011**, *12* (7), 2715–2722 DOI: 10.1021/bm200492h.

(94) Ali, S.; Saik, J. E.; Gould, D. J.; Dickinson, M. E.; West, J. L. Immobilization of Cell-Adhesive Laminin Peptides in Degradable PEGDA Hydrogels Influences Endothelial Cell Tubulogenesis. *Biores. Open Access* **2013**, *2* (4), 241–249 DOI: 10.1089/biores.2013.0021.

(95) Hern, D. L.; Hubbell, J. a. Incorporation of adhesion peptides into nonadhesive hydrogels useful for tissue resurfacing. *J. Biomed. Mater. Res.* **1998**, *39* (2), 266–276 DOI: 10.1002/(SICI)1097-4636(199802)39:2<266::AID-JBM14>3.0.CO;2-B.

(96) Harbers, G. M.; Emoto, K.; Greef, C.; Metzger, S. W.; Woodward, H. N.; Mascali, J. J.; Grainger, D. W.; Lochhead, M. J. Functionalized poly(ethylene glycol)-based bioassay surface chemistry that facilitates bio-immobilization and inhibits nonspecific protein, bacterial, and mammalian cell adhesion. *Chem. Mater.* **2007**, *19* (1), 4405–4414 DOI: 10.1021/cm070509u.

(97) Nguyen, K. T.; West, J. L. Photopolymerizable hydrogels for tissue engineering applications. *Biomaterials* **2002**, *23* (22), 4307–4314.

(98) Valdes-Aguilera, O.; Pathak, C. P.; Shi, J.; Watson, D.; Neckers, D. C. Photopolymerization studies using visible light photoinitiators. *Macromolecules* **1992**, *25*, 541–547 DOI: 10.1021/ma00028a008.

(99) Nicodemus, G. D.; Bryant, S. J. Cell encapsulation in biodegradable hydrogels for tissue engineering applications. *Tissue Eng. Part B. Rev.* **2008**, *14* (2), 149–165 DOI: 10.1089/ten.teb.2007.0332.

(100) West, J. L.; Hubbell, J. A. Polymeric Biomaterials with Degradation Sites for Proteases Involved in Cell Migration. *Macromolecules* **1999**, *32* (1), 241–244 DOI: 10.1021/ma981296k.

(101) Lutolf, M. P.; Hubbell, J. a. Synthetic biomaterials as instructive extracellular microenvironments for morphogenesis in tissue engineering. *Nat. Biotechnol.* **2005**, *23* (1), 47–55 DOI: 10.1038/nbt1055.

(102) Raeber, G. P.; Lutolf, M. P.; Hubbell, J. a. Molecularly Engineered PEG Hydrogels: A Novel Model System for Proteolytically Mediated Cell Migration. *Biophys. J.* **2005**, *89* (2), 1374–1388 DOI: 10.1529/biophysj.104.050682.

(103) Nemir, S.; Hayenga, H. N.; West, J. L. PEGDA hydrogels with patterned elasticity: Novel tools for the study of cell response to substrate rigidity. *Biotechnol. Bioeng.* **2010**, *105* (3), 636–644 DOI: 10.1002/bit.22574.

(104) Marsh, T.; Pietras, K.; McAllister, S. S. Fibroblasts as architects of cancer pathogenesis. *Biochim. Biophys. Acta* **2013**, *1832* (7), 1070–1078 DOI: 10.1016/j.bbadis.2012.10.013.

(105) Micke, P.; Arne, O. Tumour – stroma interaction : cancer-associated fibroblasts as novel targets in anti-cancer therapy ? **2004**, *2* DOI: 10.1016/j.lungcan.2004.07.000.

(106) Räsänen, K.; Vaheri, A. Activation of fibroblasts in cancer stroma. *Exp. Cell Res.* **2010**, *316* (17), 2713–2722 DOI: 10.1016/j.yexcr.2010.04.032.

(107) Gibbons, D. L.; Lin, W.; Creighton, C. J.; Rizvi, Z. H.; Gregory, P. a; Goodall, G. J.; Thilaganathan, N.; Du, L.; Zhang, Y.; Pertsemlidis, A.; et al. Contextual extracellular cues promote tumor cell EMT and metastasis by regulating miR-200 family expression. *Genes Dev.* **2009**, *23* (18), 2140–2151 DOI: 10.1101/gad.1820209.

(108) Gibbons, D. L.; Lin, W.; Creighton, C. J.; Zheng, S.; Berel, D.; Yang, Y.; Raso, M. G.; Liu, D. D.; Wistuba, I. I.; Lozano, G.; et al. Expression signatures of metastatic capacity in a genetic mouse model of lung adenocarcinoma. *PLoS One* **2009**, *4* (4), e5401 DOI: 10.1371/journal.pone.0005401.

(109) Fromigué, O.; Louis, K.; Dayem, M.; Milanini, J.; Pages, G.; Tartare-Deckert, S.; Ponzio, G.; Hofman, P.; Barbry, P.; Auberger, P.; et al. Gene expression profiling of normal human pulmonary fibroblasts following coculture with non-small-cell lung cancer cells reveals alterations related to matrix degradation, angiogenesis, cell growth and survival. *Oncogene* **2003**, *22* (52), 8487–8497 DOI: 10.1038/sj.onc.1206918.

(110) Anderson, I. C.; Mari, S. E.; Broderick, R. J.; Cocultures, P. F.; Mari, B. P.; Shipp, M. A. The Angiogenic Factor Interleukin 8 Is Induced in Non-Small Cell Lung Cancer / Pulmonary Fibroblast Cocultures Advances in Brief The Angiogenic Factor Interleukin 8 Is Induced in Non-Small Cell Lung Cancer /. **2000**, 269–272.

(111) Koumas, L.; Smith, T. J.; Feldon, S.; Blumberg, N.; Phipps, R. P. Thy-1 Expression in Human Fibroblast Subsets Defines Myofibroblastic or Lipofibroblastic Phenotypes. **2003**, *163* (4), 1291–1300.

(112) Davies, M.; Rudland, P.; Robertson, L.; EW, P.; Jolicoeur, P.; Barraclough, R. Expression of the calcium-binding protein S100A4 (p9Ka) in MMTV-neu transgenic mice induces metastasis of mammary tumours. *Oncogene* **1996**, *13* (8), 1631–1637.

(113) Gould, D. J.; Vadakkan, T. J.; Poché, R. A.; Dickinson, M. E. Multifractal and

lacunarity analysis of microvascular morphology and remodeling. *Microcirculation* **2011**, *18* (2), 136–151 DOI: 10.1111/j.1549-8719.2010.00075.x.

(114) Jones, M.; Wang, H.; Peskar, B.; Levin, E.; Itani, R. M.; Sarfeh, J.; Tarnawski, A. S. Inhibition of angiogenesis by nonsteroidal anti-inflammatory drugs : Insight into mechanisms and implications for cancer growth and ulcer healing. **1999**, *5* (12), 1–6.

(115) Kanda, S. Fibroblast Growth Factor-2-mediated Capillary Morphogenesis of Endothelial Cells Requires Signals via Flt-1/Vascular Endothelial Growth Factor Receptor-1: POSSIBLE INVOLVEMENT OF c-Akt. *J. Biol. Chem.* **2003**, *279* (6), 4007–4016 DOI: 10.1074/jbc.M307569200.

(116) Yamamoto, S.; Fukumoto, E.; Yoshizaki, K.; Iwamoto, T.; Yamada, A.; Tanaka, K.; Suzuki, H.; Aizawa, S.; Arakaki, M.; Yuasa, K.; et al. Platelet-derived growth factor receptor regulates salivary gland morphogenesis via fibroblast growth factor expression. *J. Biol. Chem.* **2008**, *283* (34), 23139–23149 DOI: 10.1074/jbc.M710308200.

(117) Yancopoulos, G. D.; Davis, S.; Gale, N. W.; Rudge, J. S.; Wiegand, S. J.; Holash, J. Vascular-specific growth factors and blood vessel formation. *Nature* **2000**, *407* (6801), 242–248 DOI: 10.1038/35025215.

(118) Garrett, S. C.; Varney, K. M.; Weber, D. J.; Bresnick, A. R. S100A4, a mediator of metastasis. *J. Biol. Chem.* **2006**, *281* (2), 677–680 DOI: 10.1074/jbc.R500017200.

(119) Fontanini, G.; Bigini, D.; Vignati, S.; Basolo, F.; Mussi, a; Lucchi, M.; Chine, S.; Angeletti, C. a; Harris, a L.; Bevilacqua, G. Microvessel count predicts metastatic disease and survival in non-small cell lung cancer. *J. Pathol.* **1995**, *177* (1), 57–63 DOI: 10.1002/path.1711770110.

(120) Levental, K. R.; Yu, H.; Kass, L.; Lakins, J. N.; Egeblad, M.; Erler, J. T.; Fong, S. F. T.; Csiszar, K.; Giaccia, A.; Weninger, W.; et al. Matrix crosslinking forces tumor progression by enhancing integrin signaling. *Cell* **2009**, *139* (5), 891–906 DOI: 10.1016/j.cell.2009.10.027.

(121) Thyboll, J.; Kortesmaa, J.; Cao, R.; Soininen, R.; Wang, L.; Iivanainen, A.; Sorokin, L.; Risling, M.; Cao, Y.; Tryggvason, K. Deletion of the laminin alpha4 chain leads to impaired microvessel maturation. *Mol. Cell. Biol.* **2002**, *22* (4), 1194–1202 DOI: 10.1128/MCB.22.4.1194.

(122) Gelse, K. Collagens—structure, function, and biosynthesis. *Adv. Drug Deliv. Rev.* **2003**, *55* (12), 1531–1546 DOI: 10.1016/j.addr.2003.08.002.

(123) Lo, C. M.; Wang, H. B.; Dembo, M.; Wang, Y. L. Cell movement is guided by the rigidity of the substrate. *Biophys. J.* **2000**, *79* (1), 144–152 DOI: 10.1016/S0006-

3495(00)76279-5.

(124) Samuel, M. S.; Lopez, J. I.; McGhee, E. J.; Croft, D. R.; Strachan, D.; Timpson, P.; Munro, J.; Schröder, E.; Zhou, J.; Brunton, V. G.; et al. Actomyosin-mediated cellular tension drives increased tissue stiffness and β-catenin activation to induce epidermal hyperplasia and tumor growth. *Cancer Cell* **2011**, *19* (6), 776–791 DOI: 10.1016/j.ccr.2011.05.008.

(125) Karagiannis, G. S.; Poutahidis, T.; Erdman, S. E.; Kirsch, R.; Riddell, R. H.; Diamandis, E. P. Cancer-associated fibroblasts drive the progression of metastasis through both paracrine and mechanical pressure on cancer tissue. *Mol. Cancer Res.* **2012**, *10* (11), 1403–1418 DOI: 10.1158/1541-7786.MCR-12-0307.

(126) Ilan, N.; Mahooti, S.; Rimm, D. L.; Madri, J. a. PECAM-1 (CD31) functions as a reservoir for and a modulator of tyrosine-phosphorylated beta-catenin. *J. Cell Sci.* **1999**, *112 Pt 18*, 3005–3014.

(127) Saaristo, a; Karpanen, T.; Alitalo, K. Mechanisms of angiogenesis and their use in the inhibition of tumor growth and metastasis. *Oncogene* **2000**, *19* (53), 6122–6129 DOI: 10.1038/sj.onc.1203969.

(128) Sikora, J. Tumor angiogenesis in human lung adenocarcinoma. *Cancer* **1995**, *76* (5), 915–916.

(129) Lindner, V.; Reidy, M. a. Proliferation of smooth muscle cells after vascular injury is inhibited by an antibody against basic fibroblast growth factor. *Proc. Natl. Acad. Sci. U. S. A.* **1991**, *88* (9), 3739–3743.

(130) Montesano, R.; Vassalli, J. D.; Baird, a; Guillemin, R.; Orci, L. Basic fibroblast growth factor induces angiogenesis in vitro. *Proc. Natl. Acad. Sci. U. S. A.* **1986**, *83* (19), 7297–7301.

(131) Dirix, L. Y.; Vermeulen, P. B.; Pawinski, a; Prové, a; Benoy, I.; De Pooter, C.; Martin, M.; Van Oosterom, a T. Elevated levels of the angiogenic cytokines basic fibroblast growth factor and vascular endothelial growth factor in sera of cancer patients. *Br. J. Cancer* **1997**, *76* (2), 238–243.

(132) Fukumura, D.; Xavier, R.; Sugiura, T.; Chen, Y.; Park, E.; Lu, N.; Selig, M.; Nielsen, G.; Taksir, T.; Jain, R. K.; et al. Tumor Induction of VEGF Promoter Activity in Stromal Cells. **1998**, *94*, 715–725.

(133) Hirschi, K. K.; Rohovsky, S. a.; Beck, L. H.; Smith, S. R.; D'Amore, P. a. Endothelial Cells Modulate the Proliferation of Mural Cell Precursors via Platelet-Derived Growth Factor-BB and Heterotypic Cell Contact. *Circ. Res.* **1999**, *84* (3), 298–305 DOI: 10.1161/01.RES.84.3.298.

(134) Laurence Beck, J. and P. A. D. Vascular development : cellular and molecular regulation. *FASEB J.* **1997**, *11* (5), 365–373.

(135) Cao, R.; Bråkenhielm, E.; Pawliuk, R.; Wariaro, D.; Post, M. J.; Wahlberg, E.; Leboulch, P.; Cao, Y. Angiogenic synergism, vascular stability and improvement of hind-limb ischemia by a combination of PDGF-BB and FGF-2. *Nat. Med.* **2003**, *9* (5), 604–613 DOI: 10.1038/nm848.

(136) Hellström, M.; Kalén, M.; Lindahl, P.; Abramsson, a; Betsholtz, C. Role of PDGF-B and PDGFR-beta in recruitment of vascular smooth muscle cells and pericytes during embryonic blood vessel formation in the mouse. *Development* **1999**, *126* (14), 3047–3055.

(137) Lindahl, P. Pericyte Loss and Microaneurysm Formation in PDGF-B-Deficient Mice. *Science (80-. ).* **1997**, *277* (5323), 242–245 DOI: 10.1126/science.277.5323.242.

(138) Davis, G. E.; Senger, D. R. Extracellular matrix mediates a molecular balance between vascular morphogenesis and regression. *Curr. Opin. Hematol.* **2008**, *15* (3), 197–203 DOI: 10.1097/MOH.0b013e3282fcc321.

(139) Al, F. E. T. Endothelial Cell – Matrix Interactions in Neovascularization. *Tissue Eng.* **2008**, *14* (1) DOI: 10.1089/teb.2007.0115.

(140) Nicosia, R. F.; Madri, J. A. The microvascular extracellular matrix. Developmental changes during angiogenesis in the aortic ring-plasma clot model. *Am. J. Pathol.* **1987**, *128* (1), 78–90.

(141) Miner, J. H. Laminins and Their Roles in Mammals. *Microsc. Res. Tech.* **2008**, *356* (May 2004), 349–356 DOI: 10.1002/jemt.20563.

(142) Hamill, K. J.; Kligys, K.; Hopkinson, S. B.; Jones, J. C. R. Laminin deposition in the extracellular matrix : a complex picture emerges. *J. Cell Sci.* **2009** DOI: 10.1242/jcs.041095.

(143) Barczyk, M.; Carracedo, S. At-a-glance article. *Cell Tissue Res.* **2010**, 269–280 DOI: 10.1007/s00441-009-0834-6.

(144) Sreejalekshmi, K. G.; Nair, P. D. Review Biomimeticity in tissue engineering scaffolds through synthetic peptide modifications — Altering chemistry for enhanced biological response. **2010**, 477–491 DOI: 10.1002/jbm.a.32980.

(145) Xi, I.; Ranieri, J. P.; Bellamkonda, R.; Bekos, E. J.; Vargo, T. G.; Gardella, J. A.; Aebischer, P. Neuronal cell attachment to fluorinated ethylene propylene films with covalently immobilized laminin oligopeptides. *Biomed. Mater.* **1995**, *29*, 779–785.

(146) Miller, J. S.; Shen, C. J.; Legant, W. R.; Baranski, J. D.; Blakely, B. L.; Chen, C. S.

Bioactive hydrogels made from step-growth derived PEG-peptide macromers. *Biomaterials* **2010**, *31* (13), 3736–3743 DOI: 10.1016/j.biomaterials.2010.01.058.

(147) Massia, S.; Hubbell, J. A. An RGD spacing of 440nm is sufficient for integrin a4b3-mediated fibroblast spreading and 140nm for focal contact and stress fiber formation. *J. Cell Biol.* **1991**, *114*, 1089–1100.

(148) Massia, S. P.; Hubbell, J. A. Human endothelial cell interactions with surface-coupled adhesion peptides on a nonadhesive glass substrate and two polymeric biomaterials. *Biomed. Mater.* **1991**, *25*, 223–242.

(149) Lin, X.; Takahashi, K.; Liu, Y.; Zamora, P. O. Enhancement of cell attachment and tissue integration by a IKVAV containing multi-domain peptide. *Engineering* **2006**, *1760*, 1403–1410 DOI: 10.1016/j.bbagen.2006.05.010.

(150) Grant, D. S.; Kinsella, J. L.; Fridman, R.; Auerbach, R.; Piasecki, B. A.; Yamada, Y.; Zain, M.; Kleinman, H. K. Interaction of endothelial cells with a laminin A chain peptide (SIKVAV) in vitro and induction of angiogenic behavior in vivo. *J. Cell. Physiol.* **1992**, *153* (3), 614–625 DOI: 10.1002/jcp.1041530324.

(151) Nakamura, M.; Mie, M.; Mihara, H.; Nakamura, M.; Kobatake, E. Construction of multi-functional extracellular matrix proteins that promote tube formation of endothelial cells. *Biomaterials* **2008**, *29* (20), 2977–2986 DOI: 10.1016/j.biomaterials.2008.04.006.

(152) Grant, D. S.; Zukowska, Z. Revascularization of ischemic tissues with SIKVAV and neuropeptide Y (NPY). *Adv. Exp. Med. Biol.* **2000**, *476*, 139–154.

(153) Massia, S. P.; Rao, S. S.; Hubbell, J. A. Covalently immobilized laminin peptide Tyr-Ile-Gly-Ser-Arg (YIGSR) supports cell spreading and co-localization of the 67-kilodalton laminin receptor with alphaactinin and vinculin. *J. Biol. Chem.* **1993**, *268*, 8053–8059.

(154) Dee, K. C.; Andersen, T. T.; Bizios, R. Cell Function on Substrates Containing Immobilized Bioactive Peptides. *MRS Proc.* **1993**, *331* (-1).

(155) S Grant, D.; Tashiro, K.; Segui-Real, B.; Yamada, Y.; R Martin, G.; K Kleinman, H. Two different laminin domains mediate the differentiation of human endothelial cells into capillary-like structures in vitro. *Cell* **1989**, *58* (5), 933–943.

(156) Jun, H.; West, J. L. Development of a YIGSR peptide-modified polyurethaneurea to enhance endothelialization. *J. Biomater. Sci. Polym.* **2004**, No. 15, 73–94.

(157) Massia, S.; Rao, S.; Hubbell, J. Covalently immobilized laminin peptide Tyr-Ile-Gly-Ser-Arg (YIGSR) supports cell spreading and co-localization of the 67-kilodalton laminin receptor with alpha-actinin and vinculin. *J. Biol. Chem.* **1993**,

*268* (11), 8053–8059.

(158) Jun, H.; West, J. L. Modification of Polyurethaneurea with PEG and YIGSR Peptide to Enhance Endothelialization Without Platelet Adhesion. *J. Biomed. Mater. Res.* **2004**, No. April, 131–139 DOI: 10.1002/jbm.b.30135.

(159) Adighibe, O.; Micklem, K.; Campo, L.; Ferguson, M.; Harris, A.; Pozos, R.; Gatter, K.; Pezzella, F. Is nonangiogenesis a novel pathway for cancer progression? A study using 3-dimensional tumour reconstructions. *Br. J. Cancer* **2006**, *94* (8), 1176–1179 DOI: 10.1038/sj.bjc.6603039.

(160) Poché, R. A.; Larina, I. V; Scott, M. L.; Saik, J. E.; West, J. L.; Dickinson, M. E. The Flk1-myr::mCherry mouse as a useful reporter to characterize multiple aspects of ocular blood vessel development and disease. *Dev. Dyn.* **2009**, *238* (9), 2318–2326 DOI: 10.1002/dvdy.21886.

(161) Larina, I. V; Shen, W.; Kelly, O. G.; Hadjantonakis, A.-K.; Baron, M. H.; Dickinson, M. E. A membrane associated mCherry fluorescent reporter line for studying vascular remodeling and cardiac function during murine embryonic development. *Anat. Rec. (Hoboken).* **2009**, *292* (3), 333–341 DOI: 10.1002/ar.20821.

(162) Terranova, V. P.; Llotta, L. a; Russo, R. G.; Liotta, L. a; Martin, G. R. Role of Laminin in the Attachment and Metastasis of Murine Tumor Cells Role of Laminin in the Attachment and Metastasis of Murine Tumor Cells. *Cancer Res.* **1982**, *42* (June), 2265–2269.

(163) McCarthy, J. B.; Furcht, L. T. Laminin and fibronectin promote the haptotactic migration of B16 mouse melanoma cells in vitro. *J. Cell Biol.* **1984**, *98* (4), 1474–1480 DOI: 10.1083/jcb.98.4.1474.

(164) Terranova, V. P.; Rao, C. N.; Kalebic, T.; Margulies, I. M.; Liotta, L. a. Laminin receptor on human breast carcinoma cells. *Proc. Natl. Acad. Sci. U. S. A.* **1983**, *80* (2), 444–448 DOI: 10.1073/pnas.80.2.444.

(165) Givant-Horwitz, V.; Davidson, B.; Reich, R. Laminin-induced signaling in tumor cells. *Cancer Lett.* **2005**, *223* (1), 1–10 DOI: 10.1016/j.canlet.2004.08.030.

(166) Yannariello-Brown, J.; Wewer, U.; Liotta, L.; Madri, J. a. Distribution of a 69-kD laminin-binding protein in aortic and microvascular endothelial cells: modulation during cell attachment, spreading, and migration. *J. Cell Biol.* **1988**, *106* (5), 1773–1786.

(167) Davidson, B.; Givant-Horwitz, V.; Lazarovici, P.; Risberg, B.; Nesland, J. M.; Trope, C. G.; Schaefer, E.; Reich, R. Matrix metalloproteinases (MMP), EMMPRIN (extracellular matrix metalloproteinase inducer) and mitogen-activated protein kinases (MAPK): co-expression in metastatic serous ovarian carcinoma. *Clin. Exp.*

*Metastasis* **2003**, *20* (7), 621–631 DOI: 10.1023/A:1027347932543.

(168) Kouvroukoglou, S. Endothelial cell migration on surfaces modified with immobilized adhesive peptides. *Biomaterials* **2000**, *21* (17), 1725–1733 DOI: 10.1016/S0142-9612(99)00205-7.

(169) Merrett, K.; Griffith, C. M.; Deslandes, Y.; Pleizier, G.; Dubé, M. A.; Sheardown, H. Interactions of corneal cells with transforming growth factor beta 2-modified poly dimethyl siloxane surfaces. *J. Biomed. Mater. Res. A* **2003**, *67* (3), 981–993 DOI: 10.1002/jbm.a.10165.

(170) Sharma, S.; Sharma, M. C.; Sarkar, C. Morphology of angiogenesis in human cancer: A conceptual overview, histoprognostic perspective and significance of neoangiogenesis. *Histopathology* **2005**, *46* (5), 481–489 DOI: 10.1111/j.1365-2559.2005.02142.x.

(171) Weidner, N.; Semple, J. P.; Welch, W. R.; Folkman, J. Tumor angiogenesis and metastasis--correlation in invasive breast carcinoma. *N. Engl. J. Med.* **1991**, *324* (1), 1–8.

(172) Korkolopoulou, P.; Patsouris, E.; Kavantzas, N.; Konstantinidou, a. E.; Christodoulou, P.; Thomas-Tsagli, E.; Pananikolaou, a.; Eftychiadis, C.; Pavlopoulos, P. M.; Angelidakis, D.; et al. Prognostic implications of microvessel morphometry in diffuse astrocytic neoplasms. *Neuropathol. Appl. Neurobiol.* **2002**, *28*, 57–66 DOI: 10.1046/j.1365-2990.2002.00367.x.

(173) Davis, G. E.; Senger, D. R. Endothelial extracellular matrix: biosynthesis, remodeling, and functions during vascular morphogenesis and neovessel stabilization. *Circ. Res.* **2005**, *97* (11), 1093–1107 DOI: 10.1161/01.RES.0000191547.64391.e3.

(174) Hamill, K. J.; Kligys, K.; Hopkinson, S. B.; Jones, J. C. R. Laminin deposition in the extracellular matrix: a complex picture emerges. *J. Cell Sci.* **2009**, *122* (Pt 24), 4409–4417 DOI: 10.1242/jcs.041095.

(175) Risau, W.; Lemmon, V. Changes in the vascular extracellular matrix during embryonic vasculogenesis and angiogenesis. *Dev. Biol.* **1988**, *125* (2), 441–450 DOI: 10.1016/0012-1606(88)90225-4.

(176) Khoshnoodi, J.; Pedchenko, V.; Hudson, B. G. Mammalian collagen IV. *Microsc. Res. Tech.* **2008**, *71* (5), 357–370 DOI: 10.1002/jemt.20564.

(177) Kruegel, J.; Miosge, N. Basement membrane components are key players in specialized extracellular matrices. *Cell. Mol. Life Sci.* **2010**, *67* (17), 2879–2895 DOI: 10.1007/s00018-010-0367-x.

(178) Hodivala-Dilke, K. M.; Reynolds, A. R.; Reynolds, L. E. Integrins in angiogenesis: multitalented molecules in a balancing act. *Cell Tissue Res.* **2003**, *314* (1), 131–144 DOI: 10.1007/s00441-003-0774-5.

(179) Ghosh, S.; Stack, M. S. Proteolytic modification of laminins: functional consequences. *Microsc. Res. Tech.* **2000**, *51* (3), 238–246 DOI: 10.1002/1097-0029(20001101)51:3<238::AID-JEMT4>3.0.CO;2-3.

(180) Kuratomi, Y.; Nomizu, M.; Tanaka, K.; Ponce, M. L.; Komiyama, S.; Kleinman, H. K.; Yamada, Y. Laminin g1 chain peptide , C-16 ( KAFDITYVRLKF ), promotes migration , MMP-9 secretion , and pulmonary metastasis of B16 – F10 mouse melanoma cells. **2002**, *16*, 1169–1173 DOI: 10.1038/sj/bjc/6600187.

(181) Brooks, P. C.; Strömblad, S.; Sanders, L. C.; Von Schalscha, T. L.; Aimes, R. T.; Stetler-Stevenson, W. G.; Quigley, J. P.; Cheresh, D. a. Localization of matrix metalloproteinase MMP-2 to the surface of invasive cells by interaction with integrin $\alpha v\beta 3$. *Cell* **1996**, *85* (5), 683–693 DOI: 10.1016/S0092-8674(00)81235-0.

(182) Yu, Q.; Stamenkovic, I. Cell surface-localized matrix metalloproteinase-9 proteolytically activates TGF-beta and promotes tumor invasion and angiogenesis. *Genes Dev.* **2000**, *14* (2), 163–176 DOI: 10.1101/gad.14.2.163.

(183) Margadant, C.; Sonnenberg, A. Integrin-TGF-beta crosstalk in fibrosis, cancer and wound healing. *EMBO Rep.* **2010**, *11* (2), 97–105 DOI: 10.1038/embor.2009.276.

(184) Zips, D.; Thames, H. D.; Baumann, M. New Anticancer Agents : In Vitro and In Vivo Evaluation. **2005**, *8*, 1–7.

(185) Hande, K. R. Etoposide: Four decades of development of a topoisomerase II inhibitor. *Eur. J. Cancer* **1998**, *34* (10), 1514–1521 DOI: 10.1016/S0959-8049(98)00228-7.

(186) Llovet, J. M.; Di Bisceglie, A. M.; Bruix, J.; Kramer, B. S.; Lencioni, R.; Zhu, A. X.; Sherman, M.; Schwartz, M.; Lotze, M.; Talwalkar, J.; et al. Design and Endpoints of Clinical Trials in Hepatocellular Carcinoma. *JNCI J. Natl. Cancer Inst.* **2008**, *100* (10), 698–711 DOI: 10.1093/jnci/djn134.

(187) Lin, Y.-C.; Shun, C.-T.; Wu, M.-S.; Chen, C.-C. A novel anticancer effect of thalidomide: inhibition of intercellular adhesion molecule-1-mediated cell invasion and metastasis through suppression of nuclear factor-kappaB. *Clin. Cancer Res.* **2006**, *12* (23), 7165–7173 DOI: 10.1158/1078-0432.CCR-06-1393.

(188) Adams, C. P.; Brantner, V. V. Estimating The Cost Of New Drug Development: Is It Really $802 Million? *Health Aff.* **2006**, *25* (2), 420–428 DOI: 10.1377/hlthaff.25.2.420.

(189) Nyga, A.; Cheema, U.; Loizidou, M. 3D tumour models: novel in vitro approaches to cancer studies. *J. Cell Commun. Signal.* **2011**, *5* (3), 239–248 DOI: 10.1007/s12079-011-0132-4.

(190) Richmond, A.; Su, Y. Mouse xenograft models vs GEM models for human cancer therapeutics. *Dis. Model. Mech.* **2008**, *1*, 78–82.

(191) Sausville, E. A.; Burger, A. M.; Becher, O. J.; Holland, E. C. Contributions of Human Tumor Xenografts to Anticancer Drug Development. *Cancer Res.* **2006**, *66* (7), 3351–3354 DOI: 10.1158/0008-5472.CAN-05-3627.

(192) Beecken, W. C.; Joussen, A. M.; Achilles, E.; Flynn, E.; Lo, K.; Gillies, S. D.; Javaherian, K.; Folkman, J.; Inst, J. N. C. Effect of Antiangiogenic Therapy on Slowly Growing , Poorly Vascularized Tumors in Mice Background : Angiogenesis is essential for tumor growth and progression . Therefore , inhibition of angiogenesis is being studied as a new anticancer therapy . Because. **2001**, *93* (5).

(193) Bonine-summers, A. R.; Aakre, M. E.; Brown, K. A.; Arteaga, C. L.; Pietenpol, J. A.; Moses, H. L.; Cheng, N. Epidermal Growth Factor Receptor Plays a Significant Role in Hepatocyte Growth Factor Mediated Biological Responses in Mammary Epithelial Cells ND Key words RIB ND ES SC RIB. **2007**, No. April.

(194) Castoldi, R.; Ecker, V.; Wiehle, L.; Majety, M.; Busl-Schuller, R.; Asmussen, M.; Nopora, a; Jucknischke, U.; Osl, F.; Kobold, S.; et al. A novel bispecific EGFR/Met antibody blocks tumor-promoting phenotypic effects induced by resistance to EGFR inhibition and has potent antitumor activity. *Oncogene* **2013**, *32* (50), 5593–5601 DOI: 10.1038/onc.2013.245.

(195) Pampaloni, F.; Reynaud, E. G.; Stelzer, E. H. K. Most of the cell-based data-harvesting efforts that drive the integration of cell biology. *Nat. Rev. Mol. Cell Biol.* **2007**, *8* (10), 839–845 DOI: 10.1038/nrm2236.

(196) Breslin, S.; O'Driscoll, L. Three-dimensional cell culture: the missing link in drug discovery. *Drug Discov. Today* **2013**, *18* (5-6), 240–249 DOI: 10.1016/j.drudis.2012.10.003.

(197) Godugu, C.; Patel, A. R.; Desai, U.; Andey, T.; Sams, A.; Singh, M. AlgiMatrix™ based 3D cell culture system as an in-vitro tumor model for anticancer studies. *PLoS One* **2013**, *8* (1), e53708 DOI: 10.1371/journal.pone.0053708.

(198) Fischbach, C.; Chen, R.; Matsumoto, T.; Schmelzle, T.; Brugge, J. S.; Polverini, P. J.; Mooney, D. J. Engineering tumors with 3D scaffolds. *Nat. Methods* **2007**, *4* (10), 855–860 DOI: 10.1038/nmeth1085.

(199) Fischbach, C.; Kong, H. J.; Hsiong, S. X.; Evangelista, M. B.; Yuen, W.; Mooney, D.

J. Cancer cell angiogenic capability is regulated by 3D culture and integrin engagement. *Proc. Natl. Acad. Sci. U. S. A.* **2009**, *106* (2), 399–404 DOI: 10.1073/pnas.0808932106.

(200) Yamada, K. M.; Cukierman, E. Modeling tissue morphogenesis and cancer in 3D. *Cell* **2007**, *130* (4), 601–610 DOI: 10.1016/j.cell.2007.08.006.

(201) van de Stolpe, A.; den Toonder, J. Workshop meeting report Organs-on-Chips: human disease models. *Lab Chip* **2013**, *13* (18), 3449–3470 DOI: 10.1039/c3lc50248a.

(202) Oliveira-Ferrer, L.; Hauschild, J.; Fiedler, W.; Bokemeyer, C.; Nippgen, J.; Celik, I.; Schuch, G. Cilengitide induces cellular detachment and apoptosis in endothelial and glioma cells mediated by inhibition of FAK/src/AKT pathway. *J. Exp. Clin. Cancer Res.* **2008**, *27*, 86 DOI: 10.1186/1756-9966-27-86.

(203) Filyak, Y.; Filyak, O.; Stoika, R. Transforming growth factor beta-1 enhances cytotoxic effect of doxorubicin in human lung adenocarcinoma cells of A549 line. *Cell Biol. Int.* **2007**, *31* (8), 851–855 DOI: 10.1016/j.cellbi.2007.02.008.

(204) Chen, P.-N.; Hsieh, Y.-S.; Chiou, H.-L.; Chu, S.-C. Silibinin inhibits cell invasion through inactivation of both PI3K-Akt and MAPK signaling pathways. *Chem. Biol. Interact.* **2005**, *156* (2-3), 141–150 DOI: 10.1016/j.cbi.2005.08.005.

(205) Singh, R. P.; Mallikarjuna, G. U.; Sharma, G.; Dhanalakshmi, S.; Tyagi, A. K.; Chan, D. C. F.; Agarwal, C.; Agarwal, R. Oral silibinin inhibits lung tumor growth in athymic nude mice and forms a novel chemocombination with doxorubicin targeting nuclear factor kappaB-mediated inducible chemoresistance. *Clin. Cancer Res.* **2004**, *10* (24), 8641–8647 DOI: 10.1158/1078-0432.CCR-04-1435.

(206) Maschek, G.; Savaraj, N.; Priebe, W.; Braunschweiger, P.; Hamilton, K.; Tidmarsh, G. F.; Young, L. R. De; Lampidis, T. J. 2-Deoxy-d-glucose Increases the Efficacy of Adriamycin and Paclitaxel in Human Osteosarcoma and Non-Small Cell Lung Cancers In Vivo Osteosarcoma and Non-Small Cell Lung Cancers In Vivo. **2004**, 31–34.

(207) Abdollahi, A.; Lipson, K. E.; Han, X.; Krempien, R.; Trinh, T.; Weber, K. J.; Hahnfeldt, P.; Hlatky, L.; Debus, J.; Howlett, A. R.; et al. SU5416 and SU6668 Attenuate the Angiogenic Effects of Radiation-induced Tumor Cell Growth Factor Production and Amplify the Direct Anti-endothelial Action of Radiation in Vitro SU5416 and SU6668 Attenuate the Angiogenic Effects of Radiation-induced Tumor . **2003**.

(208) Abdollahi, A.; Lipson, K. E.; Sckell, A.; Zieher, H.; Klenke, F.; Poerschke, D.; Roth, A.; Han, X.; Krix, M.; Bischof, M.; et al. Combined Therapy with Direct and Indirect Angiogenesis Inhibition Results in Enhanced Antiangiogenic and

Antitumor Effects Combined Therapy with Direct and Indirect Angiogenesis Inhibition Results in Enhanced Antiangiogenic and Antitumor Effects. **2003**, 8890–8898.

(209) Temming, K.; Schiffelers, R. M.; Molema, G.; Kok, R. J. RGD-based strategies for selective delivery of therapeutics and imaging agents to the tumour vasculature. *Drug Resist. Updat.* **2005**, *8* (6), 381–402 DOI: 10.1016/j.drup.2005.10.002.

(210) Zhang, Y.; Song, S.; Yang, F.; Au, J. L.; Wientjes, M. G. Nontoxic doses of suramin enhance activity of doxorubicin in prostate tumors. *J. Pharmacol. Exp. Ther.* **2001**, *299* (2), 426–433.

(211) Hardman, W.; Moyer, M.; Cameron, I. Efficacy of treatment of colon, lung and breast human carcinoma xenografts with: doxorubicin, cisplatin, irinotecan or topotecan. *Anticancer Res.* **1999**, *3B*, 2269–2274.

(212) Dubrovska, A.; Elliott, J.; Salamone, R. J.; Kim, S.; Aimone, L. J.; Walker, J. R.; Watson, J.; Sauveur-Michel, M.; Garcia-Echeverria, C.; Cho, C. Y.; et al. Combination Therapy Targeting Both Tumor-Initiating and Differentiated Cell Populations in Prostate Carcinoma. *Clin. Cancer Res.* **2010**, *16* (23), 5692–5702 DOI: 10.1158/1078-0432.CCR-10-1601.

(213) Loessner, D.; Stok, K. S.; Lutolf, M. P.; Hutmacher, D. W.; Clements, J. A.; Rizzi, S. C. Bioengineered 3D platform to explore cell–ECM interactions and drug resistance of epithelial ovarian cancer cells. *Biomaterials* **2010**, *31* (32), 8494–8506 DOI: 10.1016/j.biomaterials.2010.07.064.

(214) Cichona, M.; Gainullinb, V.; Zhanga, Y.; Radiskya, D. C. Growth of lung cancer cells in three-dimensional microenvironments reveals key features of tumor malignancy. *Integr. Biol.* **2012**, *4* (4), 440–448 DOI: 10.1039/c1ib00090j.Growth.

(215) Kim, H.; Phung, Y.; Ho, M. Changes in global gene expression associated with 3D structure of tumors: an ex vivo matrix-free mesothelioma spheroid model. *PLoS One* **2012**, *7* (6), e39556 DOI: 10.1371/journal.pone.0039556.

(216) Bezler, M.; Hengstler, J. G.; Ullrich, A. Inhibition of doxorubicin-induced HER3-PI3K-AKT signalling enhances apoptosis of ovarian cancer cells. *Mol. Oncol.* **2012**, *6* (5), 516–529 DOI: 10.1016/j.molonc.2012.07.001.

(217) Mendel, D. B.; Schreck, R. E.; West, D. C.; Li, G.; Strawn, L. M.; Tanciongco, S. S.; Vasile, S.; Shawver, L. K.; Cherrington, J. M. The angiogenesis inhibitor SU5416 has long-lasting effects on vascular endothelial growth factor receptor phosphorylation and function. *Clin. Cancer Res.* **2000**, *6* (December), 4848–4858.

(218) Horning, J. L.; Sahoo, S. K.; Vijayaraghavalu, S.; Dimitrijevic, S.; Vasir, J. K.; Jain, T. K.; Panda, A. K.; Labhasetwar, V. 3-D tumor model for in vitro evaluation of

anticancer drugs. *Mol. Pharm.* **2008**, *5* (5), 849–862 DOI: 10.1021/mp800047v.

(219) Fukumura, D.; Jain, R. K. Tumor microvasculature and microenvironment: targets for anti-angiogenesis and normalization. *Microvasc. Res.* **2007**, *74* (2-3), 72–84 DOI: 10.1016/j.mvr.2007.05.003.

(220) Devor, A.; Sakadzic, S.; Saisan, P. A.; Yaseen, M. A.; Roussakis, E.; Srinivasan, V. J.; Vinogradov, S. A.; Rosen, B. R.; Buxton, R. B.; Dale, A. M.; et al. "Overshoot" of O2 Is Required to Maintain Baseline Tissue Oxygenation at Locations Distal to Blood Vessels. *J. Neurosci.* **2011**, *31* (38), 13676–13681 DOI: 10.1523/JNEUROSCI.1968-11.2011.

(221) O'Donnell, a; Padhani, a; Hayes, C.; Kakkar, a J.; Leach, M.; Trigo, J. M.; Scurr, M.; Raynaud, F.; Phillips, S.; Aherne, W.; et al. A Phase I study of the angiogenesis inhibitor SU5416 (semaxanib) in solid tumours, incorporating dynamic contrast MR pharmacodynamic end points. *Br. J. Cancer* **2005**, *93*, 876–883 DOI: 10.1038/sj.bjc.6602797.

(222) Reynolds, A. R.; Hart, I. R.; Watson, A. R.; Welti, J. C.; Silva, R. G.; Robinson, S. D.; Da Violante, G.; Gourlaouen, M.; Salih, M.; Jones, M. C.; et al. Stimulation of tumor growth and angiogenesis by low concentrations of RGD-mimetic integrin inhibitors. *Nat. Med.* **2009**, *15* (4), 392–400 DOI: 10.1038/nm.1941.

(223) Yamada, S.; Bu, X.; Khankaldyyan, V.; Gonzales-Gomez, I.; McComb, J.; Laug, W. No Effect of the angiogenesis inhibitor Cilengitide (EMD 121974) on glioblastoma growth in nude mice. *Neurosurgery* **2006**, *59* (6), 1304–1312.

(224) Muraoka, R. S.; Dumont, N.; Ritter, C. a.; Dugger, T. C.; Brantley, D. M.; Chen, J.; Easterly, E.; Renee Roebuck, L.; Ryan, S.; Gotwals, P. J.; et al. Blockade of TGF-?? inhibits mammary tumor cell viability, migration, and metastases. *J. Clin. Invest.* **2002**, *109* (12), 1551–1559 DOI: 10.1172/JCI200215234.Introduction.

(225) Balkwill, F.; Mantovani, A. Inflammation and cancer: Back to Virchow? *Lancet* **2001**, *357* (9255), 539–545 DOI: 10.1016/S0140-6736(00)04046-0.

(226) Grivennikov, S. I.; Greten, F. R.; Karin, M. Immunity, Inflammation, and Cancer. *Cell* **2010**, *140* (6), 883–899 DOI: 10.1016/j.cell.2010.01.025.

(227) Oster, W.; Lindemann, A.; Horn, S.; Mertelsmann; R.Herrmann. Tumor Necrosis Factor (TNF)-alpha but not TNF-beta Induces Secretion of Colony Stimulating Factor for Macrophages (CSF-I) by Human Monocytes. **2014**, *70* (5), 1700–1703.

(228) Bingle, L.; Brown, N. J.; Lewis, C. E. The role of tumour-associated macrophages in tumour progression: implications for new anticancer therapies. *J. Pathol.* **2002**, *196* (3), 254–265 DOI: 10.1002/path.1027.

(229) Hsu, C.-W.; Poché, R. a.; Saik, J. E.; Ali, S.; Wang, S.; Yosef, N.; Calderon, G. a.; Scott, L.; Vadakkan, T. J.; Larina, I. V.; et al. Improved Angiogenesis in Response to Localized Delivery of Macrophage-Recruiting Molecules. *PLoS One* **2015**, *10* (7), e0131643 DOI: 10.1371/journal.pone.0131643.

(230) Polacheck, W. J.; Charest, J. L.; Kamm, R. D. Interstitial flow influences direction of tumor cell migration through competing mechanisms. *Proc. Natl. Acad. Sci.* **2011**, *108* (27), 11115–11120 DOI: 10.1073/pnas.1103581108.

(231) Hirt, C.; Papadimitropoulos, A.; Muraro, M. G.; Mele, V.; Panopoulos, E.; Cremonesi, E.; Ivanek, R.; Schultz-Thater, E.; Droeser, R. a.; Mengus, C.; et al. Bioreactor-engineered cancer tissue-like structures mimic phenotypes, gene expression profiles and drug resistance patterns observed "in vivo." *Biomaterials* **2015**, *62*, 138–146 DOI: 10.1016/j.biomaterials.2015.05.037.

(232) Shields, J. D.; Fleury, M. E.; Yong, C.; Tomei, A. a.; Randolph, G. J.; Swartz, M. a. Autologous Chemotaxis as a Mechanism of Tumor Cell Homing to Lymphatics via Interstitial Flow and Autocrine CCR7 Signaling. *Cancer Cell* **2007**, *11* (6), 526–538 DOI: 10.1016/j.ccr.2007.04.020.

(233) Santoro, M.; Lamhamedi-Cherradi, S.-E.; Menegaz, B. a.; Ludwig, J. a.; Mikos, A. G. Flow perfusion effects on three-dimensional culture and drug sensitivity of Ewing sarcoma. *Proc. Natl. Acad. Sci.* **2015**, *112* (33), 10304–10309 DOI: 10.1073/pnas.1506684112.

(234) Cuchiara, M. P.; Gould, D. J.; McHale, M. K.; Dickinson, M. E.; West, J. L. Integration of Self-Assembled Microvascular Networks with Microfabricated PEG-Based Hydrogels. *Adv. Funct. Mater.* **2012**, *22* (21), 4511–4518 DOI: 10.1002/adfm.201200976.

# Biography

Saniya Ali received the Bachelor of Science in biomedical engineering from Texas A&M University in 2004 and the Master of Science in biomedical engineering from Texas A&M University in 2008. She has been awarded numerous research and academic awards, some of which include the Center for Biomolecular Tissue Engineering fellowship and National Science Foundation GK-12 fellowship. She has served as a Research Assistant in the Department of Biomedical Engineering at Texas A&M University, Rice University, and Duke University.